DIRECT QUANTITATIVE ANALYSIS OF MULTIPLE MICRORNAS

DAVID WILLEM WEGMAN

A DISSERTATION SUBMITTED TO

THE FACULTY OF GRADUATE STUDIES

IN PARTIAL FULFILLMENT OF THE REQUIREMENTS

FOR THE DEGREE OF

DOCTOR OF PHILOSOPHY

GRADUATE PROGRAM IN BIOLOGY

YORK UNIVERSITY

TORONTO, ONTARIO

March 2016

ABSTRACT

MicroRNAs (miRNAs) play a significant role in gene regulation and have been shown to be deregulated in various diseases. Specific sets of deregulated miRNAs, termed "miRNA fingerprints", can distinguish diseased from healthy samples. Detecting disease-specific fingerprints could be used in diagnostics, and there are significant efforts toward developing miRNA-detection methods for this purpose. These methods would require the ability to detect multiple miRNAs in a direct, quantitative, specific and timely manner with a low limit of detection. Most of the common methods used today are indirect, requiring chemical or enzymatic modifications of the miRNAs prior to analysis. These modifications increase the overall assay time and decrease the quantitative accuracy of the method by creating sequence-specific biases. In my project, I developed the first direct quantitative analysis of multiple miRNAs (DQAMmiR) which does not require any modifications to the target miRNAs. DQAMmiR is a hybridization assay which utilizes the separative abilities of capillary electrophoresis to analyze multiple miRNAs. I used two well-known separation-enhancement approaches: 1) drag tags on the DNA probes to separate multiple hybrids and 2) single-strand DNA binding protein (SSB) in the run buffer to separate any excess, unbound DNA probes from the hybrids. In the proof-of-principle work, I detected three miRNAs directly from a cell lysate with a limit of detection of 100 pM and a total assay time of 90 min. My goal was to develop a miRNA detection method that could be used in clinical assays, which required significant improvements to the proof-of-principle DQAMmiR work in terms of increasing the number of detectable miRNAs, reducing overall assay time, improving limit of detection and improving specificity. I was able to increase the number of detectable miRNAs by conjugating short peptides of varying length to the DNA probes. These peptides acted as drag tags which allowed for the separation and detection of 5

miRNAs. To reduce overall assay time I devised an efficient purification procedure for the DNA probes, significantly reducing impurities. This allowed me to use a higher probe concentration, decreasing the hybridization time from 60 min down to 10 min. To lower the limit of detection I combined DQAMmiR with isotachophoresis (ITP), an in-capillary pre-concentration technique. The limit of detection improved by two orders of magnitude (from 100 pM down to 1 pM), allowing the detection of low abundance miRNAs. To improve the specificity of DQAMmiR I incorporated locked nucleic acid (LNA) bases into the probes to normalize the melting temperature of all target miRNA hybrids. This allowed me to use a single hybridization temperature, at which all target miRNA hybrids remained intact while single-nucleotide mismatches melted. Also, a dual capillary temperature technique was developed in which separation started with a high capillary temperature, required for proper hybridization, and continued at a low capillary temperature required for quality electrophoretic separation of the hybrids. I was able to combine all of these improvements to DQAMmiR while using an automated, commercially available instrument, making it an accurate, quantitative, specific, sensitive, time and cost efficient method for the analysis of multiple miRNAs. I believe, with all of these improvements, DQAMmiR can be used for the analysis of miRNAs in a clinical setting.

DEDICATION

Mom and Dad: for encouraging and supporting me always

&

Katelyn and Lucas: for being my inspiration and motivation in life

ACKNOWLEDGEMENTS

First and foremost, I would like thank Prof. Sergey Krylov. He has been there every step of the way and I wouldn't be here if not for him. His patience allowed me to finish every project I started (even if it took 2 years longer than expected). His knowledge gave me an answer for every one of my questions. His work ethic was an inspiration and motivator to keep going. Finally, he instilled a confidence in me that I could accomplish anything in both science and in life.

From our laboratory, I would like to acknowledge several people. First off, Mirzo and Fletch, who have both been here with me since day 1. It has been great growing up together and being a part of so many special events (manuscripts, weddings, and babies). Also Natasha, Ruchi, Jiayin and Roman, it has been a blast, motivating each other, whether in the lab or training for a marathon, I couldn't have done it without you. Also Farhad, I have never seen such a motivated and intelligent undergrad. Your work made a huge impact on my research and I wish you nothing but the best in med school and in life.

The rest of the Krylov members, both present and past, thank you so much for your collaborations and your friendships. You made it such an enjoyable experience coming to the lab every day.

Profs. Dasantila Golemi-Kotra and Kathi Hudak, thank you for your time and guidance. You always gave such insightful questions and comments on my research every time we met.

Thanks, as always, to our Canadian funding agencies, NSERC and OGS.

TABLE OF CONTENTS

LIST OF TABLES

LIST OF FIGURES

COMMONLY USED ABBREVIATIONS

1-nt: single nucleotide
A: Area of peak
aa: Amino acid
C: Celsius
CE: Capillary electrophoresis
DQAMmiR: Direct quantitative analysis of multiple microRNAs
EOF: Electroosmotic flow
f: Fraction
FFPE: Formalin-fixed paraffin embedded
HPLC: High performance liquid chromatography
IB: Incubation buffer
ITP: Isotachophoresis
LE: Leading electrolyte
LNA: Locked nucleic acid
LOD: Limit of detection
miRNA: MicroRNA
mRNA: Messenger RNA
nt: Nucleotide
P: Probe
PCR: Polymerase Chain Reaction
pre-miRNA: Precursor microRNA
pri-miRNA: Primary microRNA
q: Quantum yield
qRT-PCR: quantitative reverse transcriptase polymerase chain reaction
R: Resolution
RISC: RNA-induced silencing complex
SSB: Single strand DNA binding protein
ssDNA: single stranded DNA
T: Target microRNA
t: Time
t_{cr}: Critical time-point
TE: Trailing electrolyte
TP: Target-probe hybrid
UTR: Untranslated region

CHAPTER 1: INTRODUCTION TO THE DETECTION OF MIRNA

1.1 Introduction to miRNA

MicroRNAs (miRNAs) are 18 – 25-nucleotide non-coding RNA molecules that play a significant role in the regulation of gene expression. MiRNAs were first discovered in 1993 in *C. Elegans* by the Ambros lab when it described them as small endogenous regulatory RNA.**[1]** These small RNAs were later discovered to be important post-transcriptional regulators of gene expression in humans as well. Potentially targeting up to 60% of all human genes, miRNAs have a widespread influence on gene expression, showing why they are such an emerging area in research.**[2]**

The biogenesis of miRNAs starts with the transcription of a long primary miRNA strand (pri-miRNA) by RNA polymerase II. Pri-miRNAs are 100s – 1000s of bases long, contain a long double-stranded stem with a hairpin loop (**Fig. 1.1.1**) and can be located in the intronic, exonic or intergenic regions of the chromosome.**[3]** Once the pri-miRNA is transcribed it is cleaved within the nucleus by the enzyme Drosha to form a shorter, ~70 base stem and hairpin loop called the precursor-miRNA (pre-miRNA). The pre-miRNA is exported to the cytoplasm by Exportin-5 and is further cleaved by the enzyme, Dicer, to form a double-stranded 18 – 25 oligonucleotide. The duplex binds to an argonaute (Ago) protein, where one of the strands is selected as the guide strand (mature miRNA) and the other strand (referred to as miRNA*) is released from the complex. Several other proteins then bind to the complex to form the finished RNA-induced silencing complex (RISC).**[4]**

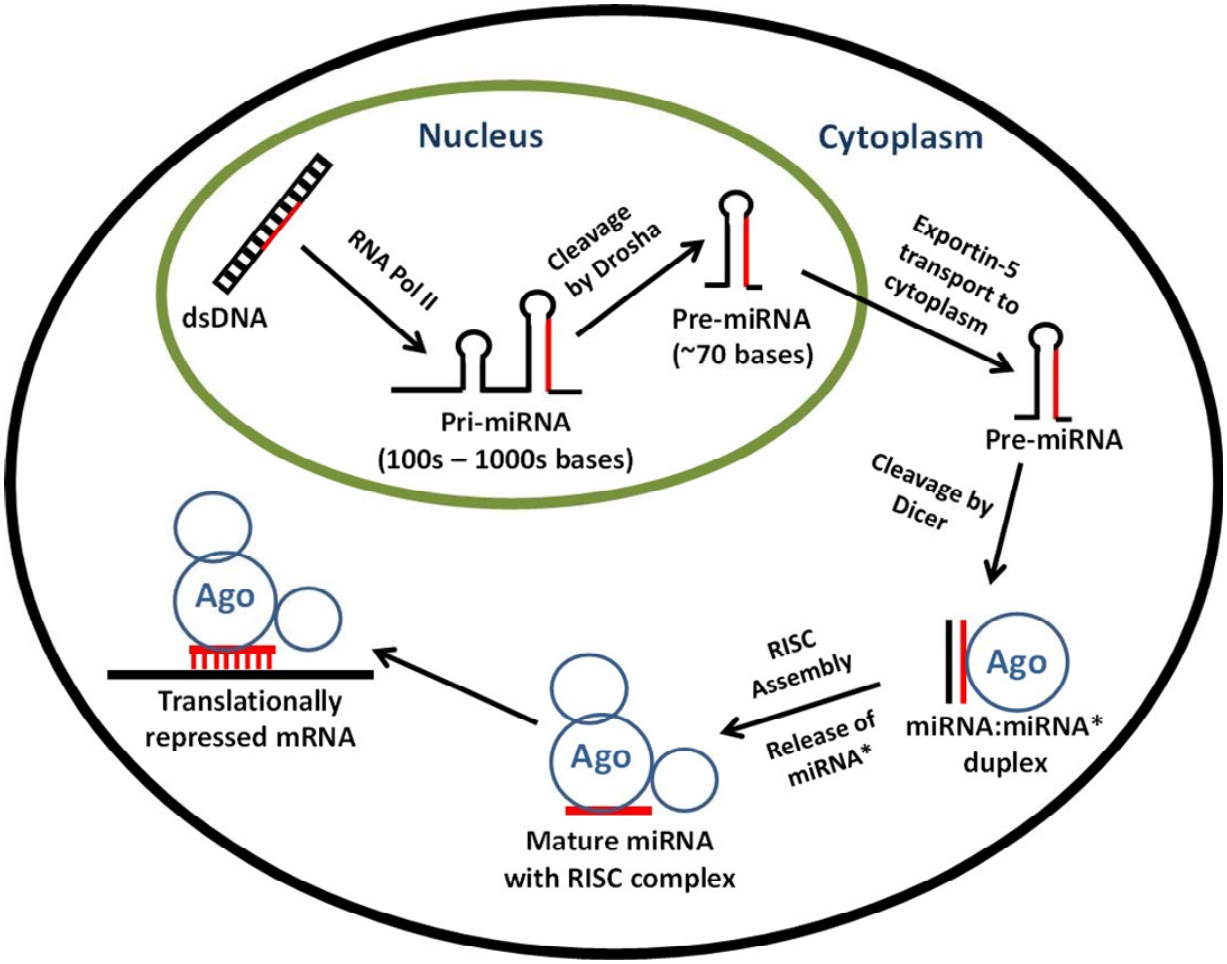

Figure 1.1.1. Biogenesis of microRNA and translational repression of target mRNA. See text for details.

The mature miRNA "guides" the RISC complex to a target mRNA, binding with complementarity. Typically the "seed" region of the miRNA, nucleotides 2 – 8 from the 5' end, bind to the 3' untranslated region (UTR) of the target mRNA, commonly without perfect complementarity. This lack of perfect complementarity allows for a single miRNA to bind to multiple target mRNAs, with some miRNAs potentially having hundreds of target mRNAs.**[5]** Commonly a single miRNA targets specific signalling pathways, targeting multiple mRNAs on the same pathway. One example is mir21 which effects the expression of multiple proteins in the

caspase activation pathway leading to inhibition of cellular apoptosis.**[6, 7]** When miRNAs bind to mRNA two outcomes can occur for the mRNA depending on complementarity. In general, if there is a perfect complementarity between the miRNA and mRNA (rare in human miRNAs) the mRNA is signalled for degradation. Imperfect complementarity results in the inhibition of translation, with no degradation occurring. There are several theories on how miRNAs prevent translation with the most common theory being that the binding of the RISC complex to the 3' UTR of the mRNA prevents the localization of translation initiation factors to the initiation start site, a process known to involve the 3' UTR.

Recently there have been alternative mechanisms suggested on how miRNAs affect gene regulation. It has been discovered that seed region-binding is just one of multiple ways in which a miRNA can bind to mRNA.**[5]** MiRNAs have also been shown to bind to the open-reading frame, 5' UTR, and promoter of target mRNAs.**[8-10]** One study showed that mir373 binds to a promoter, competing with a repressor and causing an upregulation in gene expression.**[9]** Though this variety in binding sites makes it difficult to predict targets, it shows that miRNAs may have an even larger influence on gene expression than we thought and that there is still much to be discovered.

The majority of known miRNAs are involved in biological processes such as cell differentiation, proliferation, tissue formation, metabolism, apoptosis, and stem cell division.**[11-15]** Diseases that affect these processes are often accompanied by a change in cellular miRNA content.**[16-20]** The associated up- or down-regulation of miRNAs with such diseases means that miRNAs have great potential as a diagnostic and prognostic biomarker for many human diseases.

There are significant efforts directed towards combining sets of such deregulated miRNAs into fingerprints that can be used for disease diagnosis. Cancer-specific miRNA fingerprints have been found for multiple forms of cancer and even cancer subtype-specific fingerprints have been discovered.**[18, 21, 22]** In one example, miRNA fingerprints (of 7 miRNAs or fewer) have reliably been able to distinguish all 5 intrinsic subtypes associated with breast cancer.**[21]**

Another advantage in the use of miRNAs as disease biomarkers is their remarkable stability in biological samples. Formalin-fixed paraffin embedded (FFPE) tissues are one of the more commonly used methods for long-term sample storage. One of the issues with FFPE is the preparation process which can potentially cause the degradation of cancer biomarkers.**[23-25]** It has been shown recently that the FFPE preparation process has a very minimal effect on miRNA stability.**[26, 27]** MiRNAs have also been found circulating in blood plasma, and even when tested under adverse conditions plasma miRNAs remained stable. **[[28, 29]** This led researchers to believe that miRNAs are stored in vesicles, termed exosomes, which are released from cells and help prevent miRNAs degradation in the blood. Circulating miRNA fingerprints have been found to be correlated with several cancer types, showing that they have potential to be non-invasive cancer biomarkers. Excitingly, Liu *et al.* found circulating miRNA fingerprints associated with early stage pancreatic cancer.**[30]** Typically, pancreatic cancer is diagnosed in its later stages due to the lack of symptoms resulting in poor prognoses, showing that such work on the detection of circulating miRNA fingerprints could have a significant impact in the future of cancer diagnosis.

MiRNA fingerprints can distinguish healthy from cancerous cells, can identify specific cancer subtypes, and are stable in bodily fluids showing they have potential to be very effective cancer biomarkers. There is a need for a miRNA detection technique that can detect such fingerprints in a clinical setting.

1.2 MiRNA Hybridization Assays and Their Potential in Diagnostics

The presented material was published previously and reprinted with permission from "Wegman, D.W.; Krylov, S.N. Direct miRNA-hybridization assays and their potential in diagnostics. *TrAC* **2013**, *44*, 121 – 130". Copyright 2013 Elsevier. My contribution to the article was: (i) preparation of all classification schematics, (ii) writing first draft of manuscript.

For miRNA fingerprints to be used in diagnostics a suitable detection method is required. Such a method should be able to sense multiple miRNAs with low LOD and high specificity. In addition it should be robust, rugged, and financially feasible. However, the most important aspect of this method lies in its ability to detect miRNAs in a highly quantitative manner. A detection method with high quantitative accuracy would allow for the analysis of fingerprints that are based on slight deregulations in miRNA levels, rather than the presence or absence of particular miRNA species. Furthermore, because disease fingerprints always consist of more than one miRNA species, these detection methods must avoid sequence-related biases in quantitation. Such biases are present in the majority of indirect detection methods, in which pre-amplification of miRNAs or enzymatic/chemical modification to the miRNAs is required.**[31-33]** These additional steps also often result in the loss of miRNA sample and increase assay time. For this reason the use of direct methods, which do not involve amplification/modification of miRNAs, is advantageous.

Currently, the two main methods for practical miRNAs analysis are microarrays and quantitative reverse transcriptase PCR (qRT-PCR). Microarrays allow simultaneous detection of several hundred miRNAs and qRT-PCR allows detection of low abundance miRNA species.**[34, 35]** These methods have been essential in identifying candidates of disease-specific miRNA fingerprints; however, due to their indirect nature and the associated lack of robustness in quantitation, their usefulness in the validation of miRNA fingerprints and miRNAs-based diagnostics is limited. We must look for other potential methods that best meet the criteria for use in diagnostics.

1.2.1. Classification

To ensure specificity, any detection method must be able to sense a target miRNA based on its unique nucleotide sequence. Thus, it is useful to classify miRNA detection methods based on the degree at which their sequence is exploited for their detection. All detection methods can then be classified into 3 main groups: sequencing-based methods, signature-based methods, and hybridization-based methods (**Fig 1.2.1**).

1.2.1.1. Sequencing-based methods

Sequencing-based methods identify the nucleotide sequence of miRNAs by transcribing them into their respective cDNA and analyzing them base-by-base using a DNA-sequencing method. The classical Sanger method uses DNA chain-terminating dideoxynucleotide bases that terminate DNA strand elongation. The four dideoxynucleotide bases are each labeled with a

different fluorophore allowing for identification of each sequential base. Next-generation sequencing is a much more high-throughput technique that parallelizes this process, lowering the cost of sequencing. There are several different forms of next-generation sequencing; however most of them still use the four dye-labeled terminating bases, allowing detection of each individual base in the sequence. Sequencing-based miRNAs detection methods allow higher confidence in target specificity due to the larger set of information provided for each miRNA species. These methods are, thus, less prone to false positive results. Current sequencing methods, however, require the ligation of adaptor sequences to both ends of the target miRNA followed by reverse transcription and PCR amplification.**[36-38]** Thus, sequencing-based methods do not meet our requirement of being direct. Nanopore-based sequencing techniques have the potential to be direct; however, this technology is not yet sufficiently developed to be feasible in any practical application.**[39, 40]**

1.2.1.2. Signature-based methods

Signature-based methods detect target miRNAs *via* information retrieved by different kinds of spectroscopic techniques. These methods do not specifically identify the nucleotide sequence, but rather associate the target miRNAs with a physical characteristic such as mass, charge, or structure of a molecule. For example, Driskell *et al.* used surface-enhanced Raman scattering (SERS) to create sequence-specific spectra of miRNAs.**[41]** Even though there are efforts underway to adopt other spectroscopic techniques, such as mass spectrometry **[42]** and circular dichroism **[43]**, for miRNAs detection, none are yet feasible in diagnostics.

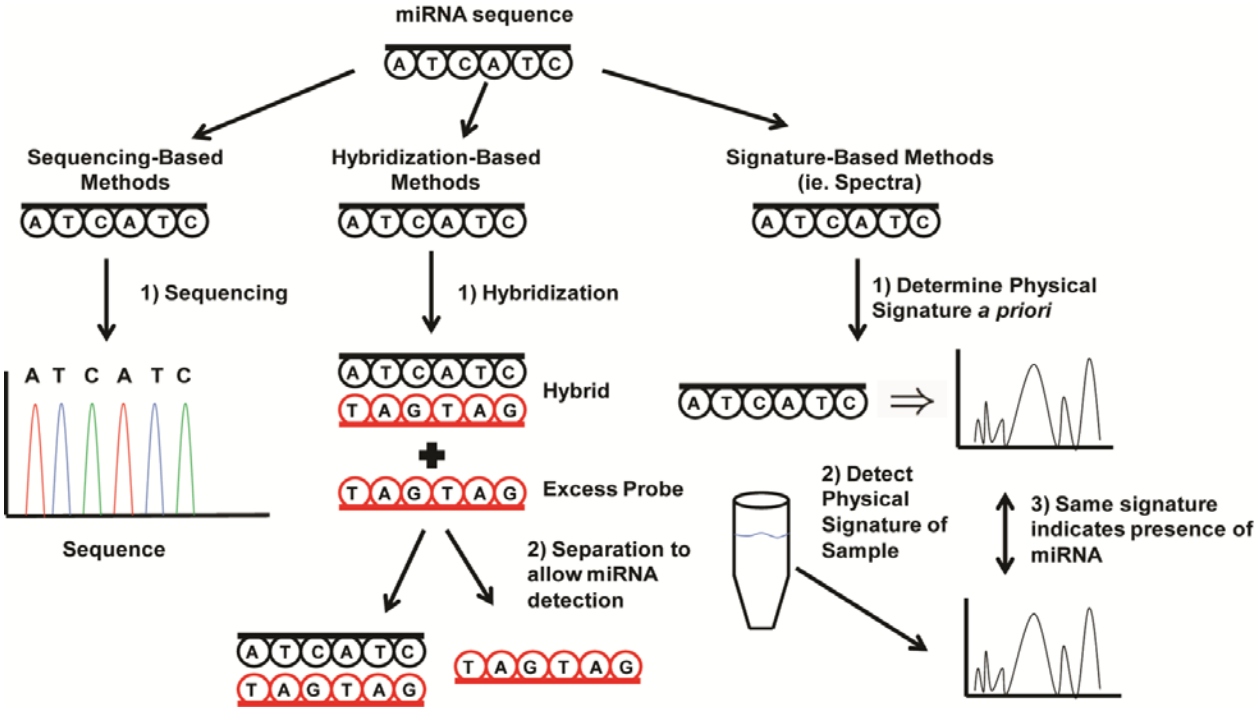

Figure 1.2.1. Classification of all miRNAs detection techniques based on how the miRNAs sequences are exploited in the analysis.

Unfortunately, all of these methods have an inherent limitation of being prone to false positive results, due to the fact that non-identical miRNAs with some similarities can produce indistinguishable signatures. Furthermore, as various classes of molecules can potentially mimic miRNA signatures, this limitation becomes even more detrimental when working with complex biological samples. In these cases, a significant effort would have to be made to validate the specificity of each individual signature. This currently prevents these methods from being used for practical miRNA analysis.

1.2.1.3. Hybridization-based methods

Hybridization-based methods employ a complementary probe to detect specific miRNAs. Designing hybridization (typically DNA) probes requires *a priori* knowledge of the target miRNA sequence. Also, careful consideration of melting temperatures and chemical composition of the probes is required to prevent hybridization to miRNAs that differ by 1 – 2 nt. It is desirable to keep such false positives to a minimum as there are families of miRNAs that differ by only a single base. It has been shown that the use of a varying number of locked nucleic acid (LNA) bases in DNA probes can equalize melting temperatures of multiple miRNA hybrids, allowing for increased specificity of the assay.**[44,45]** Furthermore, current hybridization assays can be direct and have low LODs. There are techniques available that allow for simultaneous analysis of multiple miRNAs in a robust and efficient manner, which will be discussed in this chapter. As long as certain considerations are taken into account, hybridization assays can meet all of the established criteria: (i) quantitativeness, (ii) low LOD, (iii) high specificity (iv) ability to simultaneously analyze multiple miRNAs, and (v) robustness, ruggedness, and financial feasibility. As sequencing- and signature-based methods do not meet these chosen criteria, they will not be further reviewed. This review will focus instead on direct hybridization-based assays that are currently feasible for use in diagnostics.

Every hybridization assay requires the binding of the target miRNA to a complementary probe, composed of DNA, RNA, LNA or PNA (peptide nucleic acid). The presence and quantity of miRNAs are inferred from the detection of such hybrids. There are two basic ways of detecting the presence of probe-miRNA hybrids; they can be distinguished from the unbound

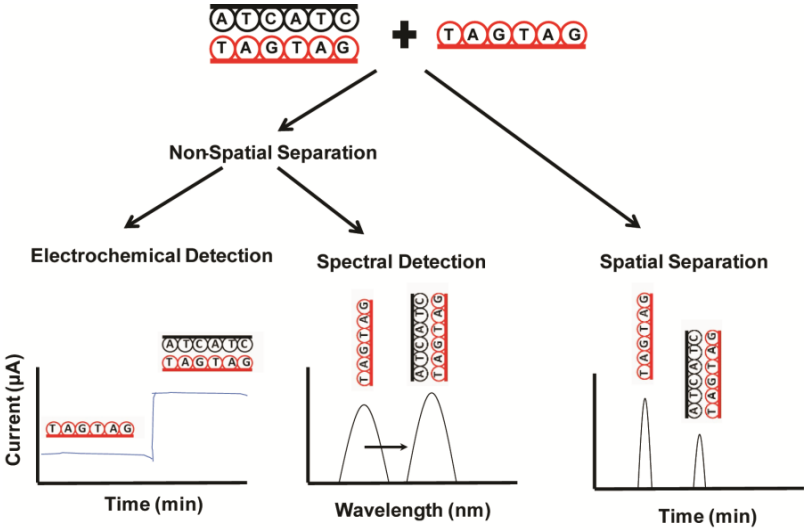

Figure 1.2.2. Hybridization assays classified based on how the signals from the hybrid and excess unbound probe are separated.

probe either by detecting hybridization-dependent signal changes or through spatial separation of hybrids from the unbound probes. This allows us to categorize all hybridization-based assays into two basic groups: detection that requires no spatial separation and spatial separation-based detection (**Fig. 1.2.2**). In the former category, hybrids are detected by measuring changes in hybridization-dependent parameters, such as fluorescence or electrical conductivity of the sample. In the latter category, hybrids can be spatially separated using techniques such as immobilization or electrophoresis. We will focus on the advantages and limitations of each of these categories, highlighting methods with the most potential for diagnostics.

1.2.2. Non-spatial separation methods

1.2.2.1. Electrochemical detection

The use of electrochemical detection in hybridization assays is a relatively recent technique that takes advantage of a change in circuit properties upon miRNAs hybridization. In all electrochemical techniques, miRNAs hybridize to a complementary probe that is immobilized on either an electrode or a nanowire. Depending on which technique is used, miRNA-binding causes either the promotion of oxidation on an electrode or a change in the conductance of a nanowire.

Though indirect, the first electrochemical miRNAs detection method was developed in 2006 by Gao *et al.*, which took advantage of a catalyzed oxidation reaction.**[44]** In this initial design, a ligation reaction was required between an oxidation reagent and the target miRNA (**Fig. 1.2.3**). In 2009, Yang *et al.* designed a direct electrochemical detection method by constructing microelectrodes decorated with immobilized PNA probes.**[45]** In PNA, the negative sugar-phosphate backbone is replaced with a neutral peptide backbone. Binding of miRNAs to these PNA probes resulted in an accumulation of negative charge on the electrode, which in turn,

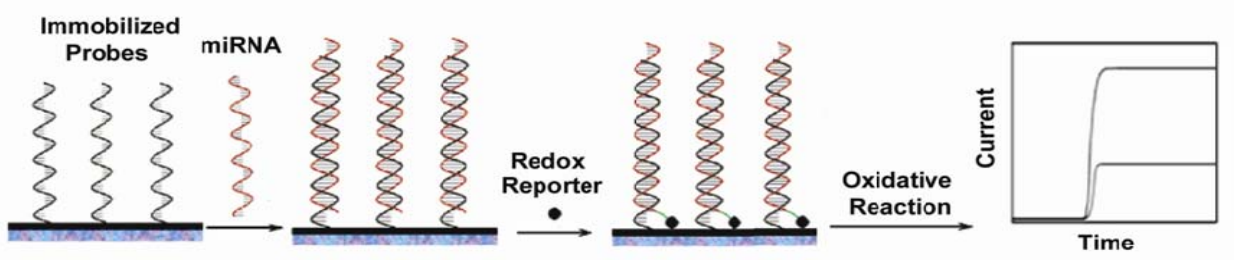

Figure 1.2.3. Schematic of an electrochemical detection technique, miRNAs are hybridized to immobilized probe, allowing for accumulation of redox reporter, causing a detectable change in circuit properties. (Adapted from **[46]**. Copyright [2006] American Chemical Society).

attracted Ru^{3+} redox reporter. Electrochemical reduction of Ru^{3+} to Ru^{2+} resulted in a detectable change in electrical current. With the use of a signal amplification technique, an impressive LOD of 10 aM (attomolar) was achieved. The signal amplification technique involved the addition of ferricyanide, which oxidizes the Ru^{2+} back to $Ru^{3+}$and allows for a single ruthenium atom to interact with miRNAs multiple times. Yang *et al.* were able to measure the quantity of mir21 and mir205 from total RNA extracts of various cell lines.**[45]** Unfortunately, signal amplification techniques often achieve improvement in LOD at the expense of quantitative accuracy, as it is difficult to precisely control the number of amplification events per each signal event. Furthermore, in this particular method, the great sensitivity was also accompanied by a relatively narrow dynamic range of 2 orders of magnitude. Since miRNA levels can potentially range over 4 orders of magnitude, this method in its current format is hardly suitable for practical measurement of deregulated miRNAs in tissue samples.

Other forms of electrochemical detection **[46, 47]** involve the use of nanowires to sense target miRNAs. Fan *et al.* designed an electronic circuit where a conducting polyaniline nanowire was interrupted by nanometre-sized gaps.**[46]** These gaps were decorated with neutral PNA hybridization probes. The negatively-charged target miRNAs, upon hybridization with the probes, interacted with cationic anilines and increased the conductance of the electronic circuit. Electrical conductance of the nanowire directly correlated with the amount of hybridized miRNAs. This allowed the authors to detect miRNAs at concentrations as low as 5 fM (femtomolar). Zhang *et al.* developed a similar method, where a PNA decorated silicon nanowire was used.**[47]** In this technique, hybridization of negatively-charged miRNAs affected the semi-

conductor properties of the silicon nanowire, resulting in an increased resistance of the circuit in a miRNA concentration-dependent manner. This method also showed great sensitivity, with an LOD of 1 fM. Unfortunately, the complicated manufacturing process of these nanocircuits has, so far, prevented them from being used for simultaneous detection of multiple miRNAs. However, the authors did express an interest in developing nanocircuit-based miRNA arrays and reports on their progress are anticipated with interest.

The main advantage of electrochemical methods lies in their impressive LODs, which can be as low as 10 aM of miRNAs. In general, detection limits of these methods are better than the limits of all other types of miRNAs hybridization assays. This allows for electrochemical methods to avoid the use of miRNA amplification by PCR. The electrochemical methods also possess high specificity, as they are able to distinguish miRNAs with 1-nt accuracy.

Unfortunately, the use of electrochemical methods in diagnostics will require researchers to overcome some major limitations. In most of the described examples, only a single miRNA was detected. Currently efforts in multiplexing miRNA targets are hindered by either narrow dynamic range of detection or complicated manufacturing process of the chips. Also, all of the electrochemical methods are currently not compatible with crude biological samples. Various components of cell lysate may interact with the nanostructures in unforeseen ways and cause either false positive or false negative readings. Thus, the use of miRNAs extraction kits is required, which can introduce different quantitation biases and increase overall assay time. This makes electrochemical detection methods less rugged, as strict control over clinical standards will have to be implemented. Lastly, as the chips have a limited lifespan, their complex

manufacturing process still presents itself as a major limitation in terms of cost associated with analysis.

1.2.2.2. Spectral detection

Spectral detection methods require a change in absorbance, fluorescence, refractive index or reflectivity of the sample to occur upon binding of target miRNA to its complementary probe. The most common spectral detection technique involves the use of molecular beacons (MBs). MBs are constructs that take advantage of such phenomena as quenching or fluorescence resonance energy transfer (FRET). MBs consist of four functional parts: (i) target miRNA hybridization sequence (similar to a hybridization probe); (ii) complementary sequences at the 5' and 3' ends; (iii) a terminal fluorophore, and (iv) a terminal quencher/acceptor (**Fig. 1.2.4**). When the target miRNAs are absent, a stem-loop is formed through the hybridization of the 5 – 6 nucleotide-long complementary components at the ends of the construct. In this conformation, the fluorophore and the quencher are brought into close proximity and, thus, the absence of target

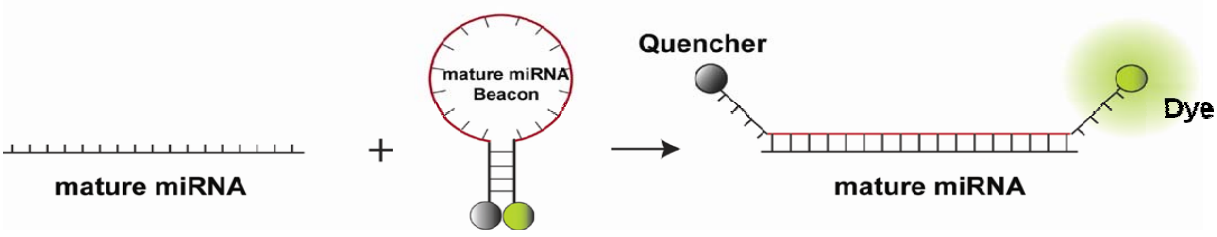

Figure 1.2.4. Schematic diagram of a molecular beacon which consists of four parts, target miRNA hybridization sequence, complementary 5-6 DNA bases at 5' and 3' ends, a fluorophore and a quencher. Upon hybridization, MB structure opens, allowing for fluorescence to occur. (Adapted from **[50]** by permission of Oxford University Press).

miRNAs results in the absence of fluorescence signal. However, when a target miRNAs hybridizes to the MB, it interferes with the stem-loop structure and results in a spatial separation of the fluorophore and quencher. Thus, the presence of target miRNAs results in an increase in fluorescence signal (**Fig. 1.2.4**).

MBs have been used extensively with miRNAs in recent years.**[48-51]** Unfortunately, MB methods suffer from an inherent lack of dynamic range and poor LOD due to incomplete quenching in the absence of target miRNAs. Several protocols were developed to improve the LOD of molecular beacon techniques. Hartig, in 2004, used a signal amplifying ribozyme instead of the typical molecular beacon.**[52]** The target miRNA binds to the ribozyme and causes its structural change, activating the cleavage of a fluorophore/quencher-labeled substrate. This cleavage releases the fluorophore, which, in turn, produces a detectable signal. Signal amplification was achieved by multiple substrates being cleaved by a single activated ribozyme. They were able to achieve an LOD of 5 nM though the dynamic range was only 2 orders of magnitude.

Kang *et al.* showed the versatility of MBs by detecting two miRNA species within single live cells.**[49]** Mir26a and mir206 were detected from individual mouse myoblast cells simultaneously using two differently labeled fluorophores. Confocal microscopy was used to monitor the two miRNA species through myogenesis. Thus, MBs can be used to detect miRNAs *in vivo*, which, in turn, can help understand the role of miRNAs in cellular processes.

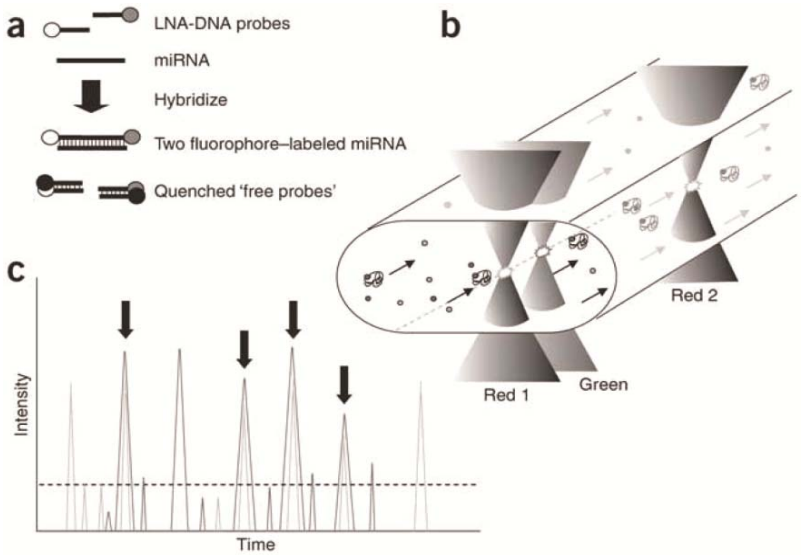

Figure 1.2.5. Single molecule quantitation of miRNAs using dual fluorophores. Two labeled probes, each with a different fluorophore, hybridize to target miRNAs. Sample is run through capillary and synchronized detection of both fluorophores indicates presence of target miRNAs. (Reprinted from **[55]** by permission from Macmillan Publishers Ltd. Copyright [2011])

There are also examples of spectral techniques that do not require the use of MBs. Neely *et al.* used a single molecule detector, LNA-DNA probes, and dual fluorophores to achieve an LOD of 500 fM and a dynamic range of 3 orders of magnitude.**[53]** Two short hybridization probes were hybridized to a single target with each of the two probes decorated with a different fluorophore (**Fig. 1.2.5**). After hybridization, the fluorescence of excess non-bound probes was deactivated by a quencher-labeled complement. The sample was then put through a capillary and analyzed in flow. Two detectors were placed along the length of the capillary, one for each fluorophore. To decrease background fluorescence in miRNAs detection, only coincident signals from both detectors were recorded. Unfortunately, this elaborate instrument design, requiring

multiple lasers and complex detector synchronization, poses a large limitation for the ruggedness of the method.

Yin *et al*. developed a signal amplification technique with the use of a Taqman probe and a duplex specific nuclease (DSN).**[54]** A Taqman probe is a short DNA oligo with a fluorophore and quencher at either end that requires cleavage to fluoresce. Upon hybridization with target miRNAs, the DSN cleaves the Taqman probe, thus breaking the energy transfer connection between the fluorophore and quencher. Thus the presence of Taqman-miRNA hybrids results in an increased fluorescence signal. Furthermore, cleavage of Taqman releases the target miRNAs undamaged, allowing for hybridization to a new Taqman probe to occur. This signal amplification technique yielded an LOD of 100 fM and had a dynamic range of over 4 orders of magnitude.

Thus, spectral techniques that do not use typical MBs have a dynamic range of up to four orders of magnitude, which make them suitable for detecting multiple miRNAs at different expression levels in practical assays. The use of multiple fluorophores or microarray format allows for simultaneous analysis of multiple miRNA targets. Also, some spectral methods are less prone to non-specific effects of crude biological samples and as a result require fewer preparative steps (e.g., RNA extraction). The fact that spectral methods can be applied directly to cell lysates, and even used directly in living cells, increases their versatility. Spectral methods can usually be performed with relatively inexpensive commercial equipment making them especially attractive for clinical use.

Spectral methods do not have many limitations, but, unfortunately, the ones they do have significantly affect their potential for use in diagnostics. Due to the high background signal that accompanies fluorophore-quencher systems, the current limits of detection of classical spectral methods make them not suitable for analysis of such low abundance miRNA samples as from fine-needle biopsies or blood. While there are efforts to improve these LODs, they typically result in either decreased quantitative accuracy or significantly more complex and cost-inefficient instrumentation.

1.2.3. Spatial separation

1.2.3.1. Hybridization Assays

There are two basic ways to physically separate the miRNA-probe hybrid from the excess probe. In the first category of methods, miRNAs are immobilized on a surface through various techniques and are then hybridized with labeled probes. In the second category, the hybrids are separated from the excess probe based on their inherent physical properties, such as mass or charge. For nucleic acids, one of the most efficient ways to achieve this separation is through use of electrophoretic techniques.

Northern blotting is a gold-standard immobilization technique in miRNAs detection. In this technique, the components of total RNA extracts from biological samples are separated based on size using gel electrophoresis. Afterwards, bands of separated RNA are blotted onto a nitrocellulose membrane. Labeled target-specific DNA probes are then washed over the membrane, allowing them to become immobilized through hybridization. While very popular

among biologists, Northern blotting has several limitations when it comes to clinical applications, including long assay time (~24 h), large sample requirements, high LODs and dependence on radioactive probes. Variations of Northern blotting were developed to address some of these issues. For example, Varallyay was able to reduce the overall assay time down to 4 h through various improvements, including the use of LNA hybridization probes.**[55]** Kim *et al.* developed a non-radioactive technique through use of LNA probes, a digoxigenin (DIG) label and an improved cross-linking reagent to achieve an LOD of 0.8 pM.**[56]** DIG-labeling allowed for non-radioactive detection of miRNAs by using alkaline-phosphatase (AP)-labeled anti-DIG antibodies. The activity of the enzyme, AP, could then be measured to detect the presence of target miRNAs. Though LNA probes, DIG labels, and the cross-linking reagent had been used previously, the combination of the three techniques allowed for the improved LOD. The authors applied this technique to detect low abundance miRNAs from a breast cancer cell line. Unfortunately, these improved methods still require an initial sample (5 – 20 μg total RNA per lane) that is too large to be feasible for most diagnostic applications.

Sandwich assays are another form of immobilization techniques that take advantage of two different functional probes: capture and labeled probes. The capture probe typically includes regions of complementarity to both target and labeled probe. Hybridization of the labeled probe depends on the hybridization status of the target-specific region of the capture probe, through exploitation of the base-stacking phenomenon. In base-stacking, the presence of an adjacent hybrid region stabilizes hybridization of a very short nucleotide that otherwise would have been too weak to remain bound. Yang *et al.* combined the use of a sandwich assay design with gold

nanoparticle labeling, and were able to achieve a 10 fM LOD through signal amplification by silver enhancement.**[57]**

Roy *et al*. further improved the LOD of the sandwich assays by introducing an exonuclease processing step.**[58]** In their design, after the capture probe had a chance to hybridize with the target miRNAs, exonuclease was added to degrade any unbound capture probe. This decreased the probability of non-specific interactions between the capture and labeled probes and resulted in a lower background signal. Employing the differential interference contrast method for detection of gold nanoparticle labels, the authors were able to detect as few as 300 copies of miRNA (1 fM) without the use of any signal amplification.

Physical separation between excess probe and miRNA-probe hybrids via immobilization significantly reduces possibilities of detecting non-specific interactions, giving immobilization-based methods excellent quantitative accuracy. Similar to other hybridization assays, immobilization techniques are capable of 1-nt specificity. Furthermore, the dynamic range of these methods spans up to 4 orders of magnitude, making them well-suited for simultaneous analysis of deregulated miRNAs. There have been some recently introduced immobilization techniques that have great potential for use in diagnostic assays.**[59-61]** The limitations of such immobilization techniques used for physical separation are that they require the use of microarrays for detection of multiple miRNAs and their hybridization times can be quite long with most commercially available microarrays requiring 16 – 18 h.**[58]**

Powerful separation techniques have all the similar advantages of immobilization techniques without the requirement of lengthy hybridization times. There are, however, only a

few physical separation techniques that do not require miRNAs immobilization. Even with the use of a powerful separation technique such as capillary electrophoresis (CE), it is difficult to separate excess probes from hybrids due to their inherently similar physical properties. Chang *et al.* were the first to use CE to separate excess DNA probe from the miRNA-probe hybrid. They did not achieve sufficient separation to accurately quantitate the miRNA showing that CE alone is not sufficient for separation.**[62]** To overcome this problem Khan *et al.* used various separation enhancers which altered the size to charge ratio of either the excess probe or the miRNA-probe hybrid allowing for sufficient separation of the hybrid and probe to be achieved.**[63]** This showed that the use of CE with separation enhancers has potential for the quantitation of miRNAs.

In the next section I will go into more detail on the use of CE for hybridization assays, specifically I will focus on how I can make CE quantitative with the use of separation enhancers.

1.3 Making Hybridization Assays in Capillary Electrophoresis Quantitative

The presented material was published previously and reprinted with permission from "Krylova, S.M.; Wegman, D.W.; Krylov, S.N. Making DNA Hybridization Assays in Capillary Electrophoresis Quantitative. *Anal Chem*, **2010**, *82*, 4428 – 4433". Copyright 2010 American Chemical Society. My contribution to the article was: (i) planning all experiments, (ii) performing all experiments, (iii) interpreting results, (iv) preparing all experimental figures, (v) writing first draft of experimental section, (vi) assisted in writing theoretical section. Fraction of bound probe mathematically determined by Prof. Krylov.

1.3.1. Hybridization Assays and Capillary Electrophoresis

Hybridization assays, which detect DNA or RNA targets using labeled DNA probes with sequences complementary to those of the targets, are a key tool in molecular biology.**[64-66] Fig. 1.3.1** shows the general concept of such assays. In step 1, an excess of labeled probe (P*) is added to a target (T)-containing sample to bind the majority of the target, resulting in a mix of

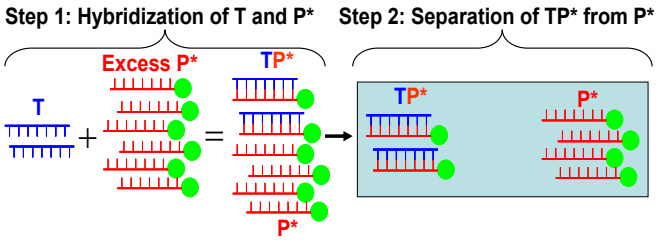

Figure 1.3.1. Schematic illustration of hybridization analysis. In Step 1, the target sequence T is hybridized with a labeled probe P* to form the target-probe hybrid, TP*, through mixing the target with the excess of the probe. In Step 2, the unreacted probe is separated from the target-probe hybrid to facilitate the quantitation of the hybrid.

TP* hybrid and any unreacted P*. In step 2, TP* is separated from P* to facilitate the quantitation of TP* using the label on P* for detection. Ideally, in a hybridization assay, the fast hybridization reaction between the target and labeled probe would be followed by their efficient and fast separation, which, in turn would be accompanied by real-time quantitation of both the hybrid and the unbound probe. CE provides an instrumental platform for fast hybridization assays with real-time detection. A number of CE-based hybridization assays have been developed including gel and gel-free assays.**[67-70]** One of gel-free hybridization analyses is based on separation of the unbound probe from the target-probe hybrid by affinity capillary electrophoresis mediated by a separation enhancer, single-strand DNA binding protein (SSB).**[68]** Both the probe and the hybrid were quantified with a fluorescent label on the probe. In this approach, SSB is added to the electrophoresis run buffer where it binds the single-stranded probe but does not bind the double-stranded hybrid. By binding the probe, SSB drags ssDNA away from the hybrid, whose mobility is not affected by SSB **(Fig. 1.3.2)**. If the probe is labeled fluorescently, real-time sensitive detection can be facilitated. While the concept of SSB-mediated hybridization analysis has been experimentally demonstrated,**[67, 68]** the question of how to make such analysis quantitative remains open. To address this question, here I propose a general approach for making SSB-mediated analysis quantitative. The quantity of the target is determined taking into consideration: (i) the potential influence of the probe-target hybridization and probe-SSB binding on the quantum yield of the fluorescent label and (ii) potential dissociation of the hybrid by SSB. The proposed approach was used to study the quenching and the dissociation phenomena for an experimental model which included a 22-nt long ssDNA

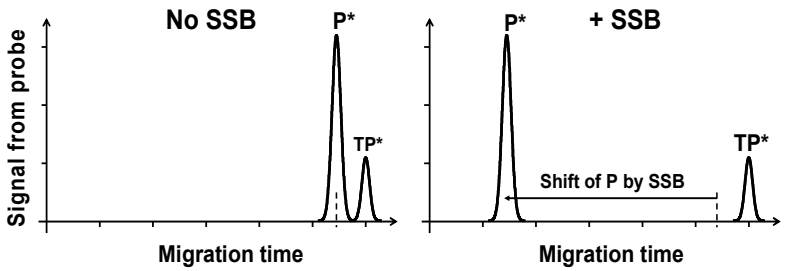

Figure 1.3.2. Conceptual illustration of the effect of SSB present in the run buffer on the capillary-electrophoresis separation of target-probe hybrid, TP*, form the excess of free probe, P*.

target and the same-length fluorescently-labeled DNA probe. I showed that the binding of the probe to either the target or SSB reduces the quantum yield of fluorescence. On the other hand, SSB was proved not to detectably dissociate the hybrid. Finally, I proved that when the probe quenching is taken into account, the SSB-mediated hybridization analysis is quantitative without the requirement of building a calibration curve.

1.3.2. Theoretical Considerations

1.3.2.1. Target amount

It is assumed that the fluorescently-labeled probe, P* (asterisk designates the label), is in excess to the target, T, and that the hybridization proceeds to completion:

$$\mathrm{T+P^*(excess)} \rightarrow \mathrm{TP^* + P^*} \qquad (1\text{–}1)$$

Where TP* is the target-probe hybrid. In such a case, the initial amounts of the probe and target, $\mathbf{P^*}_0$ and $\mathbf{T}_0$, are linked with the amounts of the remaining probe, **P***, and formed hybrid, **TP***, as:

$$\mathbf{P^*}_0 = \mathbf{TP^* + P^*} \qquad (1\text{–}2)$$

$$\mathbf{T}_0 = \mathbf{TP^*} \qquad (1\text{–}3)$$

In the rest of this work, symbols A with corresponding indexes denote measurable areas of peaks in electropherograms, which are equivalent to integrated fluorescent signals. To compensate for differences in the residence time in the detector, these areas should be divided by corresponding migration times if on-column detection is used. To be proportional to the amount of the fluorophore, the areas should be divided by the absolute quantum yield of fluorescence, Q.

Using **eq. (1–2)** I can express the known initial amount of probe through: (i) fluorescence signals from the hybrid, A_{TP*}, and remaining free probe, A_{P*}, (ii) corresponding absolute quantum yields of the target-bound probe, Q_{TP*}, and free probe, Q_{P*}, and (iii) a proportionality coefficient a, which is constant for the same fluorophore and the same detector:

$$\mathbf{P*}_0 = a(A_{TP*} / Q_{TP*} + A_{P*} / Q_{P*}) \tag{1–4}$$

Using **eq. (1–3)** I can express the sought initial amount of the target through A_{TP*}, Q_{TP*}, and a:

$$\mathbf{T}_0 = aA_{TP*} / Q_{TP*} \tag{1–5}$$

To eliminate the unknown coefficient a I divide **eq. (1–5)** by **eq. (1–4)** and obtain the following equation for finding the unknown amount of the target:

$$\mathbf{T}_0 = \mathbf{P*}_0 \frac{A_{TP*} / Q_{TP*}}{A_{TP*} / Q_{TP*} + A_{P*} / Q_{P*}} \tag{1–6}$$

To simplify the analysis, both the numerator and denominator in **eq. (1–6)** are multiplied by Q_{P*} to lead to:

$$\mathbf{T}_0 = \mathbf{P*}_0 \frac{A_{TP*} / q_{TP*}}{A_{TP*} / q_{TP*} + A_{P*}} \tag{1–7}$$

Where q_{TP*} is the relative quantum yield of the target-bound probe with respect to that of the free probe: $q_{TP*} = Q_{TP*}/Q_{P*}$.

I will now consider the case of SSB being present in the run buffer under an assumption of fast equilibration between SSB-bound and SSB-unbound probe. In the presence of SSB, a fraction, f, of target-unbound probe is bound to SSB and another fraction, $1 - f$, is SSB-unbound. The effective relative quantum yield of the probe "fractionally" bound to SSB, q_{P*}^{SSB}, is a sum of two terms corresponding to the SSB-unbound and SSB-bound fractions:

$$q_{P*}^{SSB} = q_{P*}(1-f) + q_{SSB\bullet P*} f = 1 - f(1 - q_{SSB\bullet P*}) \qquad (1\text{–}8)$$

where the relative quantum yield of the unbound probe, q_{P*}, is equal to one because I define all quantum yields relative to that of unbound probe. To compensate for the potential quenching of fluorescence by SSB, the fluorescence signal of the probe in the presence of SSB, A_{P*}^{SSB}, should be divided by the effective quantum yield defined in **eq. (1–8),** and, accordingly, **eq. (1–7)** will have the form:

$$\mathbf{T}_0^{SSB} = \mathbf{P*}_0 \frac{A_{TP*} / q_{TP*}}{A_{TP*} / q_{TP*} + A_{P*}^{SSB} / q_{P*}^{SSB}} \qquad (1\text{–}9)$$

In addition to quenching probe fluorescence, SSB may potentially destabilize the hybrid and promote its dissociation into free probe and target. The target-probe hybrid is typically very stable at non-denaturing conditions. However, SSB can potentially bind the stable hybrid with low but finite affinity and potentially break the complex by competitively replacing one of the strands in the hybrid. Although, to the best of my knowledge, the effect of SSB on hybrid stability has never been investigated, it is conceivable to suggest that such an effect can be

significant under certain conditions, such as higher temperature, shorter probe, low salt concentration, etc. Therefore, in theoretical consideration, I take the potential effect of SSB on complex stability into account.

If SSB, which is present in the run buffer, accelerates hybrid dissociation, then such accelerated dissociation will be a continuous process during the entire separation. The dissociated probe will be bound by SSB and will start migrating with a velocity different from that of the hybrid. It will be separated from the free target and will be unable to reform the hybrid. Hybrid dissociation will follow the monomolecular decay pattern with a pseudo-first-order rate constant k, which is a function of concentration of SSB:

$$\mathrm{TP^*} \xrightarrow{k \sim [\mathrm{SSB}]} \mathrm{T} + \mathrm{P^*} \qquad (1\text{–}10)$$

This kind of separation is termed Non-Equilibrium Capillary Electrophoresis of Equilibrium Mixtures (NECEEM).**[71]** If hybrid dissociation is significant, the area of the intact hybrid in the NECEEM electropherogram will decrease and an exponential decay area between the peaks of the hybrid and SSB-shifted probe will appear (**Fig. 1.3.3**). The probe formed by hybrid dissociation is bound to SSB with the same fraction coefficient f that characterizes binding of free probe to SSB (see above). The same f allows us to use for this area the same effective quantum yield $q_{\mathrm{P}^*}{}^{\mathrm{SSB}}$ defined in **eq. (1–8)**. In order to generalize **eq. (1–9)** for the case of hybrid dissociation, I should replace the term $A_{\mathrm{TP}^*}/q_{\mathrm{TP}^*}$ with a sum of two terms corresponding to the remaining intact hybrid, $A_{\mathrm{TP}^*}{}^{\mathrm{int}}/q_{\mathrm{TP}^*}$, and the dissociated hybrid, $A_{\mathrm{TP}^*}{}^{\mathrm{dis}}/q_{\mathrm{P}^*}{}^{\mathrm{SSB}}$:

$$\mathbf{T}_0^{\mathrm{SSB}} = \mathbf{P^*}_0 \frac{A_{\mathrm{TP}^*}{}^{\mathrm{int}} / q_{\mathrm{TP}^*} + A_{\mathrm{TP}^*}{}^{\mathrm{dis}} / q_{\mathrm{P}^*}{}^{\mathrm{SSB}}}{A_{\mathrm{TP}^*}{}^{\mathrm{int}} / q_{\mathrm{TP}^*} + \left(A_{\mathrm{TP}^*}{}^{\mathrm{dis}} + A_{\mathrm{P}^*} \right) / q_{\mathrm{P}^*}{}^{\mathrm{SSB}}} \qquad (1\text{–}11)$$

If SSB-induced hybrid dissociation is significant (that is if A_{TP*}^{int}/q_{TP*} is not much greater than $A_{TP*}^{dis}/q_{P*}^{SSB}$), then **eq. (1–11)** should be used instead of **eq. (1–9)** to calculate the unknown amount of the target in the hybridization analysis.

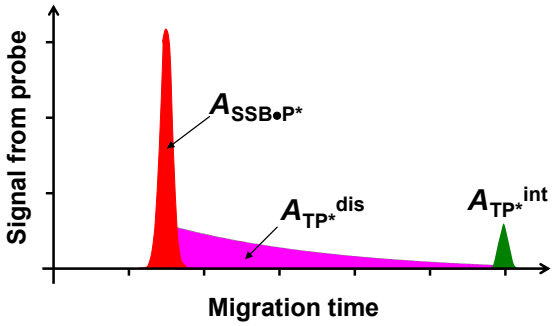

Figure 1.3.3. A conceptual illustration of a NECEEM electropherogram if SSB present in the electrophoresis run buffer dissociates the hybrid, TP*, into free probe, P*, and free target, T*. Area $A_{SSB•P*}$ corresponds to the SSB-bound excess of probe. Area A_{TP*}^{int} corresponds to the target-probe hybrid intact by the time of reaching the detector. A_{TP*}^{dis} corresponds to the target-probe hybrid dissociated by SSB during electrophoresis and bound to SSB after that.

1.3.2.2. Fraction of bound probe.

The fraction of SSB-bound probe can be found using the apparent migration time of the probe, t, for the concentration of SSB chosen for the assay as well as the migration times of the SSB-unbound probe, t_{P*}, and SSB-bound probe, $t_{SSB•P*}$:

$$f = \frac{t_{SSB•P*}}{t} \frac{t_{P*} - t}{t_{P*} - t_{SSB•P*}} \qquad (1–12)$$

The value of $t_{SSB•P*}$ can be measured experimentally at a saturating concentration of SSB. The saturating concentration of SSB should be higher than the equilibrium dissociation constant, K_d, of SSB-probe complex, thus ensuring that most of the probe is SSB-bound.

1.3.2.3. Quantum yields.

Assuming that the probe can be baseline-separated from the hybrid in the absence of SSB, the relative quantum yields of the target-bound probe, q_{TP*}, can be found from two sets of data obtained for the same amount of the probe with and without the target, respectively:

$$q_{TP*} = \frac{A_{TP*}}{A_{P*}^{[T]=0} - A_{P*}^{[T]\neq 0}} \tag{1–13}$$

where $A_{P*}^{[T]=0}$ is the fluorescent signal of the probe for no target and $A_{P*}^{[T]=0}$ and A_{TP*} are fluorescent signals of the remaining target-unbound probe and target-bound probe, respectively, for a non-zero target concentration.

The relative quantum yield of SSB-bound probe, $q_{SSB•P*}$, can be found from two areas of target-unbound probe obtained in the absence of SSB, A_{P*}, and at a saturating concentration of SSB, $A_{P*}^{[SSB]sat}$:

$$q_{SSB•P*} = \frac{A_{P*}^{[SSB]_{sat}}}{A_{P*}} \tag{1–14}$$

The above theoretical consideration was then tested experimentally.

1.3.3. Materials and Methods

1.3.3.1. Oligonucleotides

All DNA for hybridization assays were custom-synthesized by IDT (Coralville, IA). The hybridization probe was 5'-Alexa$_{488}$-TCACAAGTTAGGGTCTCAGGGA-3'. The hybridization target was 5'-TCCCTGAGACCCTAACTTGTGA-3'. SSB (Single-Stranded DNA Binding Protein), from *E. coli* was from Epicentre Biotechnologies (Madison, WI). All other materials were obtained from Sigma-Aldrich (Oakville, ON, Canada) unless otherwise stated.

1.3.3.2. Hybridization Conditions

All hybridizations were carried out in a Mastercycler 5332 thermocycler (Eppendorf, Hamburg, Germany). Working-stock solutions of DNA were kept at 37°C to reduce the sticking of the DNA to the test tube walls. Varying concentrations of DNA probe and DNA target were incubated with 100 nM of fluorescein in the incubation buffer (50 mM Tris-Ac, 50 mM NaCl, 10 mM EDTA, pH 8.2). Temperature was increased to a denaturing 80°C and lowered to 20°C in decremental steps of 1°C every three seconds and finally kept at 20°C for 1 h to allow complete hybridization.

1.3.3.3. Capillary Electrophoresis with Laser Induced Fluorescence (CE-LIF)

A P/ACE MDQ capillary electrophoresis system (Beckman-Coulter, Fullerton, CA) was used with laser-induced fluorescence detection. The fluorescence was excited with a 488-nm line argon-ion laser. Uncoated fused-silica capillaries were used with an inner diameter of 75 μm and

an outer diameter of 365 μm. The total length of the capillary was 50 cm with a distance of 40 cm to the detector. The running buffer was 25 mM sodium tetraborate, pH 9.3, with or without 50 nM SSB. The capillary was rinsed prior to each run with a sequence of 100 mM HCl, 100 mM NaOH, double-distilled water and 25 mM sodium tetraborate, pH 9.3 for one minute each. Samples were injected by a pressure pulse of 0.5 psi (3.45 kPa) for 5 s, the volume of the injected sample plug was ~14 nL. Electrophoresis was driven by an electric field of 500 V/cm. The capillary temperature was maintained at 20°C. After every run the capillary was washed with fluorescence detector turned on to monitor potential adsorption of fluorescently-labeled DNA to capillary walls. Electropherograms were analyzed using 32 Karat software. Peak areas were divided by the corresponding migration times to compensate for the dependence of the residence time in the detector on the electrophoretic velocity of species. All areas were normalized by dividing them by the area of the internal standard, fluorescein.

1.3.3.4. Spectrophotometric Determination of Target Concentration

DNA target concentration was determined by light absorption at 260 nm using the Nano-Drop ND-1000 Spectrophotometer (Thermo-Fisher Scientific). The stock concentration of the target was too high to measure directly, therefore, a small sample of the stock solution was serially diluted and absorbance of each sample at 260 nm was measured 3 times. The concentration of each sample was determined as $absorbance/\varepsilon l$ where ε is the molar extinction coefficient of the DNA target at 260 nm (provided by IDT) and l is the optical path-length. Using the concentrations of the serial dilutions, the original stock concentration was extrapolated.

1.3.4. Results and Discussion

1.3.4.1. Binding of the Probe to SSB

To demonstrate the applicability of my quantitative approach to SSB-mediated hybridization analysis, I used SSB from *E. coli* which is known to bind a minimum of 8-mer ssDNA. A 22-mer DNA of a random sequence was used as a target and a 22-mer DNA with a sequence complementary to that of the target was used as a probe. The probe was labeled with an Alexa fluoro 488 dye through an ester linker at the N' end.

The influence of SSB on probe migration and fluorescence was studied by varying the concentration of SSB in the run buffer. I found that with increasing concentration of SSB the peak of the probe was shifting to the left and reaching its leftmost position when the

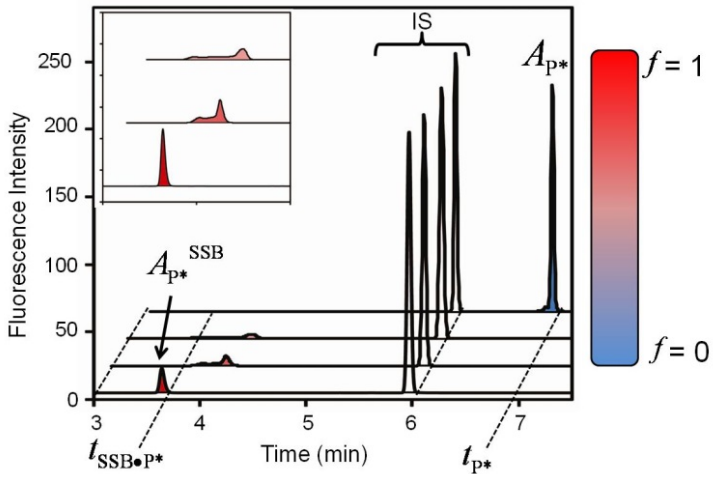

Figure 1.3.4. Quenching of probe, P*, fluorescence upon binding to SSB. The study was conducted by CE with the run buffer containing SSB at varying concentrations: in descending order 0 (top trace), 5, 10 and 50 nM (bottom trace). The injected amount of the probe was 14×10^{-16} mol: 100 nM in an injected plug of 14 nL. The inset shows the peaks corresponding to the SSB-bound probe enlarged in the vertical direction. The internal standard (IS) was 100 nM fluorescein.

concentration of SSB exceeded 50 nM (**Fig. 1.3.4**). At these high concentrations, the fraction of SSB-bound probe was approaching unity. For my set of conditions, I defined the saturating concentration of SSB as $[SSB]_{sat}$ = 50 nM. It should be noted that the decrease of the fluorescence peak in the presence of SSB could not be attributed to the binding of the SSB-DNA complex to capillary walls; no fluorescence material was washed from the capillary after separation.

If the working concentration of SSB chosen for the hybridization assay is below the saturating one, then the fraction of SSB-bound probe is not equal to unity and it should be calculated using **eq. (1–12)** with experimentally determined times. As an example, I calculated the fraction of SSB-bound probe for [SSB] = 10 nM using the time data in **Fig. 1.3.4**; the fraction was $f = 0.63$.

To determine the quantum yield, $q_{SSB \bullet P*}$, of SSB-bound probe, I increased the concentration of SSB to the saturating one (see **Fig. 1.3.4**). The fraction of SSB-bound probe was equal to unity and the quantum yield could be determined with **eq. (1–14)** using the two areas, $A_{P*}^{[SSB]sat}$ and A_{P*}, found from **Fig. 1.3.4**. My calculations showed that the quantum yield was significantly less than 1: $q_{SSB \bullet P*} = 0.24$.

It should be emphasized, that the quantum yields measured depend on the nature of the probe and target as well as the buffer composition. Therefore, the quantum yields have to be measured for every new set of conditions.

1.3.4.2. Binding of the Probe to the Target

The influence of the target on probe migration and fluorescence was studied by hybridizing the target to an excess of the probe. The amounts of the target and probe were chosen such that the areas of their corresponding peaks in CE would be comparable and could be accurately measured. To study the influence of the target on probe fluorescence in SSB-free solution, P* should be baseline separated from TP*. While such separation is challenging, I was able to achieve it through carefully selecting the separation conditions (**Fig. 1.3.5**). It should be noted, that while the resolution of SSB-free separation, $R_S^{[SSB]=0} = 7.2$, is suitable for my goal of calculating the quantum yield, it is much less than that of SSB-mediated separation, $R_S^{[SSB]sat} = 35.6$. To calculate the quantum yield of the target-bound probe, q_{TP*}, I conducted two

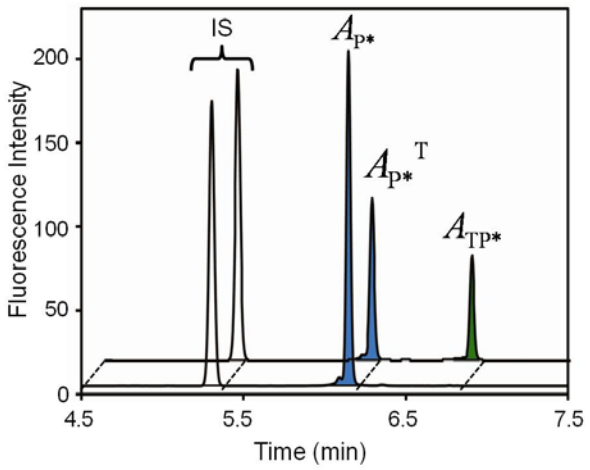

Figure 1.3.5. Quenching of probe, P*, fluorescence upon its binding to the target, T. The study was conducted with CE by injecting identical 14 nL samples containing identical amounts of the probe, 14×10^{-16} mol, but different amounts of the target: 0 (bottom trace) and 3.5×10^{-16} mol (top trace). The concentration of the probe was 100 nM while the concentrations of the target were 0 and 25 nM for the bottom and top traces, respectively. The internal standard (IS) was 100 nM fluorescein.

CE experiments with two amounts of the target – one of which was zero – and the same amount of the probe. From CE electropherograms presented in **Fig. 1.3.5** I determined the three areas, $A_{P*}^{[T]=0}$, $A_{P*}^{[T]\neq 0}$ and A_{TP*}, required for the calculation of the quantum yield of the target-bound probe using **eq. (1–13)**. I found that this quantum yield was also significantly different from unity: $q_{TP*} = 0.60$. The different from unity quantum yields require that **eq. (1–9)** be used for finding T_0.

1.3.4.3. Influence of SSB on Hybrid Stability

To answer the question of whether or not SSB causes target dissociation, I conducted an experiment identical to those used in an actual hybridization analysis. The target-probe mixture with an excess of the probe was injected into the capillary and run in an electrophoresis buffer containing the saturating concentration of SSB. The obtained electropherograms (**Fig. 1.3.6**) show no detectable difference between the A_{TP*} and A_{TP*}^{SSB} (within the N% experimental error of area calculation) and, accordingly, no detectable signal from the dissociated hybrid. These results suggest that SSB does not appreciably bind and dissociate the hybrid under these conditions. As a result, **eq. (1–9)** can be used instead of **eq. (1–11)** for finding the unknown amount of the target.

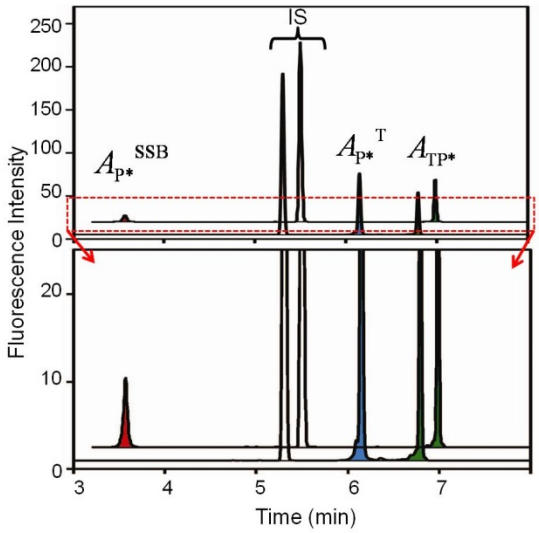

Figure 1.3.6. The influence of SSB on the hybridization assay conducted by CE. The injected 14 nL sample contained 14×10^{-16} mol of the probe, P*, and 3.5×10^{-16} mol of the target, T, resulting in final concentrations of 100 nM and 25 nM for the probe and target respectively. The concentration of SSB in the run buffer was either 0 (bottom trace) or 50 nM (top trace). The bottom panel is identical to the top one except for a different scale of the y-axis. The internal standard (IS) was 100 nM fluorescein.

1.3.4.4. Quantitative Hybridization Analysis

To demonstrate the correctness of the approach developed above, I conducted a hybridization analysis with a constant 100 nM concentration of the probe and target concentrations varying within 0 – 50 nM. The saturating concentration of SSB was used to ensure that $f = 1$. The areas determined from the electropherograms (**Fig. 1.3.7**) and the quantum yields, $q_{TP*} = 0.61$ and $q_{SSB \bullet P*} = 0.24$, determined above were used for calculations of $\mathbf{T}_0$ with **eq. (1–9)**. I found that the calculated amounts were identical to the loaded amounts measured spectrophotometrically within the limits of experimental error (**Fig. 1.3.8A**), thus confirming that the analysis was quantitative without building a calibration curve.

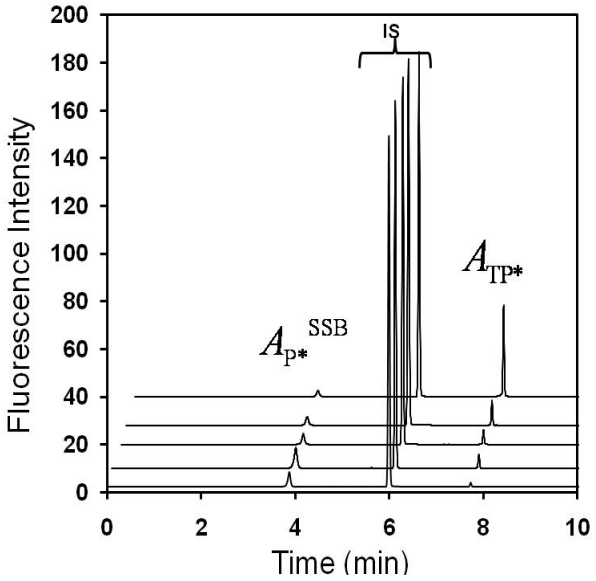

Figure 1.3.7. Electropherograms used for calculation of target, T, concentration in. **Fig 1.3.8A.** The areas of the peaks, along with calculated quantum yields were used in determining target concentration. 100 nM DNA probe was incubated with (from bottom): 3.125, 6.25, 12.5, 25, and 50 nM target, respectively. The mixture was spiked with 100 nM fluorescein used as an internal standard (IS) and the components of the mixture were separated in the run buffer containing 50 nM SSB.

To demonstrate the inaccuracies that could be caused by ignoring the quenching of fluorescence it is instructive to calculate the target amount for three assumptions: (i) no quenching by SSB ($q_{SSB•P*} = 1$), (ii) no quenching by T ($q_{TP*} = 1$), and (iii) no quenching by both SSB and T ($q_{SSB•P*} = q_{TP*} = 1$). The results plotted in **Fig. 1.3.8B** show that the deviation of the incorrectly calculated $\mathbf{T}_0$ from the loaded $\mathbf{T}_0$ is as high as 2.5 times.

1.3.5. Conclusions

With the approach developed in this work, SSB-mediated hybridization analysis can now be made quantitative without building a calibration curve. To accurately quantitate a target one

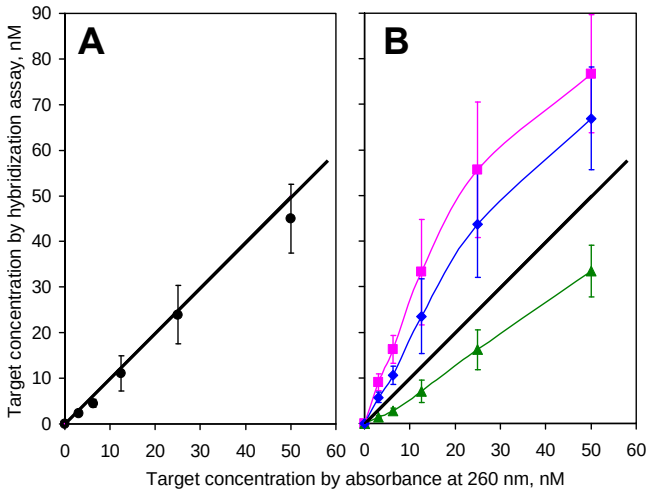

Figure 1.3.8. Target recovery in SSB-mediated hybridization assay with different ways of correction for quenching of probe fluorescence. Panel A: $q_{SSB•P*} = 0.24$ and $q_{TP*} = 0.60$. Panel B: $q_{SSB•P*} = 1$ and $q_{TP*} = 0.60$ (squares), $q_{SSB•P*} = 0.24$ and $q_{TP*} = 1$ (triangles), and $q_{SSB•P*} = q_{TP*} = 1$ (diamonds). The black line is a theoretically expected dependence. Each experimental point is an average and standard deviation obtained from 4 experiments. The concentrations of probe and SSB were 100 and 50 nM, respectively, in all experiments.

needs to measure the relative quantum yields of the hybrid, q_{TP*}, and SSB-bound probe, $q_{SSB•P*}$, and determine whether or not SSB dissociates the hybrid. It is also essential to find and use the saturating concentration of SSB which guarantees that most of the target-unbound probe is bound to SSB creating a large separation window. The wide separation window has an important advantage. It allows us to use a large excess of the probe to the target without the interference between the corresponding peaks of the probe and hybrid. Using a high concentration of the probe is beneficial as it shortens the hybridization time and can be used for a wider range of target concentrations. Furthermore, the large window also creates enough "space" for multiple peaks and, thus, can potentially facilitate simultaneous detection of multiple targets.

CHAPTER 2: DIRECT QUANTITATIVE ANALYSIS OF MULTIPLE MIRNAS (DQAMmiR)

The presented material was published previously and reprinted with permission from "Wegman, D.W.; and Krylov, S.N. Direct Quantitative Analysis of Multiple miRNAs (DQAMmiR). *Angew Chem Int Ed*, **2011**, *50*, 10335 – 10339". Copyright 2011 John Wiley and Sons. My contribution to the article was: (i) planning all experiments, (ii) performing all experiments, (iii) interpreting results, (iv) preparing all figures, (v) writing first draft of manuscript. Mathematic derivations performed by Victor Okhonin.

2.1. Introduction to DQAMmiR

Not only did my previous work in **section 1.3** make CE-based hybridizations assays quantitative but also, as mentioned, the large window between the SSB-DNA probe peak and the hybrid peak allowed for me to potentially detect multiple targets. I applied this CE technique to the detection of multiple miRNAs and here I report the first direct quantitative analysis of multiple miRNAs (DQAMmiR). In **section 1.2** I showed the growing need for a method capable of detecting multiple miRNAs in a quantitative fashion. DQAMmiR uses miRNAs directly, without any modification, and accurately determines concentrations of multiple miRNAs without the need to build calibration curves. This was achieved by a CE-based hybridization assay with an ideologically-simple combination of two well-known separation-enhancement approaches: (i) drag tags on the DNA probes,**[72]** and (ii) single-strand DNA binding protein (SSB) in the run

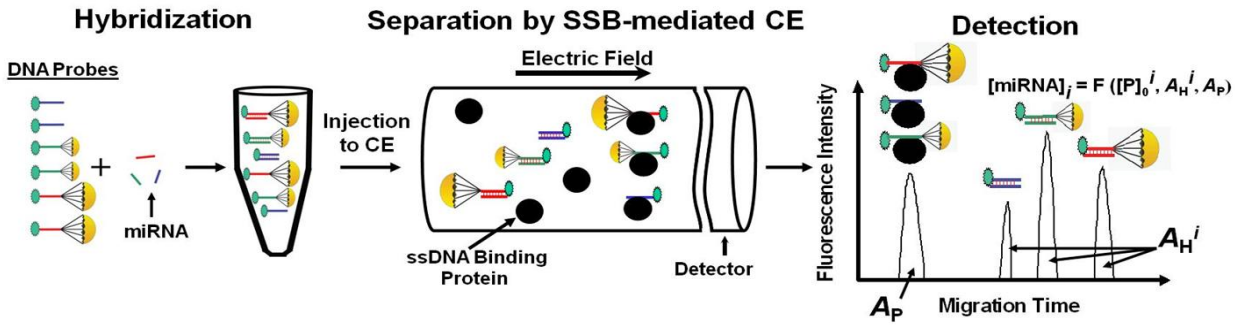

Figure 2.1. Schematic representation of the direct quantitative analysis of miRNAs. See text for details.

buffer.**[67] Fig. 2.1** illustrates this hypothetical approach where the miRNAs and their complementary ssDNA probes are shown as short lines of the same color, drag tags are shown as parachutes, a fluorescent label is shown as small green circles and SSB is shown as large black circles. In the hybridization step, the excess of the probes is mixed with the miRNAs which leads to all miRNAs' being hybridized but with some probes left unbound to miRNAs. A short plug of the hybridization mixture is introduced into a capillary prefilled with an SSB-containing run buffer. SSB binds all ssDNA probes but does not bind the double stranded miRNA-DNA hybrid. When an electric field is applied, all SSB-bound probes move faster than all the hybrids (SSB works as a propellant).**[67]** Different drag tags make different hybrids move with different velocities. SSB-bound probes, however, can move even with similar velocities if the drag tags are small with respect to SSB. In such a case, a fluorescent detector at the end of the capillary generates separate signals for the hybrids and a cumulative signal (one peak or multiple peaks) for the excess of the probes. The amounts of miRNAs are finally determined with a simple mathematical approach that uses the integrated signals (peak areas in the graph). I reserve the

term of direct quantitative analysis of multiple miRNAs and its abbreviation of DQAMmiR for the specific approach described above.

2.2. Materials and Methods

2.2.1. Oligonucleotides

To experimentally test the viability of our hypothetical DQAMmiR, I decided to use three miRNAs known to be deregulated in breast cancer: mir21 (5'-UAGCUUAUCAGA CUGAUGUUGA-3'), mir125b (5'-UCCCUGAGACCCUAACUU GUGA-3'), and mir145 (5'-GUCCAGUUUUCCCAGGAAUCCC U-3'). Three ssDNA probes were designed all labeled with Alexa 488 at the 5' end; the 3' end was reserved for drag tags. To separate the three hybrids I needed only two probes modified with drag tags; one probe could be without a drag tag. In the proof-of-principle work, I chose to use the two simplest available drag tags: a hairpin formed by a DNA extension at the 3' end of the probe and biotin covalently attached to the 3' end. The probe for mir21 was the one with the hairpin formed by the italicized extension: 5'-Alexa488-TCAACATCAGTCTGATAAGCTA*GCGCGCTTTGCGCGC*-3'. The probe for mir125b was the one with no tag: 5'-Alexa488-TCACAAGTTAGGGTCTCAGGGA-3'. The probe for mir145 was the one with biotin: 5'-Alexa488-AGGGATTCCTGGGAAAACTGGAC-Biotin-3'. All DNA and RNA for hybridization assays were custom-synthesized by IDT (Coralville, IA).

2.2.2. Hybridization Conditions

Using a Mastercycler 5332 thermocycler (Eppendorf, Hamburg, Germany) the miRNAs were hybridized with the probes in incubation buffer (50 mM Tris-Ac, 50 mM NaCl, 10 mM EDTA, pH 7.8) containing fluorescein as an internal standard. The temperature was increased to a denaturing 80°C, then lowered to 37°C at a rate of 20°C/min and finally kept at 37°C for 1 h to allow complete hybridization. Working-stock solutions of DNA and miRNA were kept at 37°C to reduce sticking to the test tube walls. The structures of the three hybrids formed are schematically depicted in **Fig. 2.2A**.

2.2.3. CE-LIF

A P/ACE MDQ capillary electrophoresis system (Beckman-Coulter, Fullerton, CA) was used with laser-induced fluorescence detection. The fluorescence was excited with a 488-nm line argon-ion laser. Uncoated fused-silica capillaries were used with an inner diameter of 75 μm and an outer diameter of 365 μm. The total length of the capillary was 50 cm with a distance of 40 cm to the detector. The capillary was rinsed prior to each run with a sequence of 100 mM HCl, 100 mM NaOH, double-distilled water and 25 mM sodium tetraborate, pH 9.3 for one minute each. The capillary was pre-filled with the SSB-containing run buffer: 25 mM sodium tetraborate at pH 9.3 supplemented with 50 nM SSB. Under such conditions, an electroosmotic flow occurred and moved negatively charged hybrids and probes to the detection end of the capillary where the negative electrode was situated. Samples were injected by a pressure pulse of 0.5 psi (3.45 kPa) for 5 s, the volume of the injected sample was ~14 nL. Electrophoresis was

driven by an electric field of 500 V/cm with a capillary coolant temperature set at 20ºC. Electropherograms were analyzed using 32 Karat software. Peak areas were divided by the corresponding migration times to compensate for the dependence of the residence time in the detector on the electrophoretic velocity of species. All areas were normalized by dividing them by the area of the internal standard, fluorescein. Concentrations of miRNAs were determined using **eq. (2–8)**.

2.2.4. DQAMmiR in Cell Lysate

An *E.coli* BL21 cell culture was grown to an OD600 of 1.6, harvested by centrifugation at 5,000 × g for 10 min at 4 °C and resuspended in sonication buffer: 50 mM Tris-HCl, 2.5 mM $MgCl_2$, 5 mM KCl at pH 8.3. They were lysed by sonication on ice with 5 s ‘‘on’’/15 s ‘‘off’’ intervals for a total of 10 min. Cell lysates were aliquoted and stored at –80 °C. A 10× dilution of the lysed cells was spiked with 5 nM the 3 miRNAs with 50 nM of their respective DNA probes, along with 20 nM fluorescein, 1 μM of mask RNA and 2.5 μM masking DNA. The masking RNA was a tRNA library from baker’s yeast from Sigma-Aldrich (Oakville, ON, Canada). Masking DNA was a 20-nt DNA strand, with the sequence of 5’-CAAAAAATGAGTCATCCGGA-3’.

MCF-7 cells were purchased from ATCC and grown in an incubator at 37°C in the atmosphere of 5% CO_2. Cells were grown in DMEM media (Invitrogen) with FBS and 10,000 μg/mL penicillin, streptomycin in a 100 mm Petri dish. When cells covered roughly 90% of the plate they were washed with PBS, trypsinized to detach them from bottom of dish and

centrifuged at 300 × g for 5 min. Pellet was washed twice with PBS. The cells were counted using a haemocytometer and lysed with 1% Triton in the incubation buffer with 10 μM masking RNA (tRNA library from baker's yeast). Cell lysates were aliquoted and stored at –80°C. A 10× dilution of cell lysate was incubated with 5 nM of each of the 3 DNA probes, with or without 0.5 nM spiked-in miRNAs (mir21, 125b, 145), 0.5 nM fluorescein and 2.5 μM masking DNA. Incubation, injection and capillary conditions were performed as previously explained.

2.2.5. Spectrophotometric Determination of Target Concentration

MiRNA target concentration was determined by light absorption at 260 nm using the Nano-Drop ND-1000 Spectrophotometer (Thermo-Fisher Scientific). The stock concentration of the target was too high to measure directly, therefore, a small sample of the stock solution was serially diluted and absorbance of each sample at 260 nm was measured 3 times. The concentration of each sample was determined as $absorbance/\varepsilon l$ where ε is the molar extinction coefficient of the RNA target at 260 nm (provided by IDT) and l is the optical path-length. Using the concentrations of the serial dilutions, the original stock concentration was extrapolated.

2.3. Results and Discussion

2.3.1. Separation and Detection of Multiple Hybrid Peaks

Fig. 2.2B shows the result of electrophoretic separation in DQAMmiR which agrees with a hypothesis depicted in **Fig. 2.1**. SSB bound the excess probes and increased their mobility generating two adjoining peaks at approximately 3.4 and 3.6 min. The hybrids had no ssDNA

parts accessible for SSB to bind and, therefore, SSB did not affect their mobility. The negatively charged hairpin increased the electrophoretic mobility of the mir21 hybrid, while neutral biotin lowered the electrophoretic mobility of the mir145 hybrid with respect to the mir125b hybrid. All hybrid peaks were perfectly resolved and their areas could be accurately determined, which, in turn, allowed me to determine the quantities of the three miRNAs. The time window between the SSB-bound probes and the hybrids was 2 min. With the observed peak widths of the hybrids, the

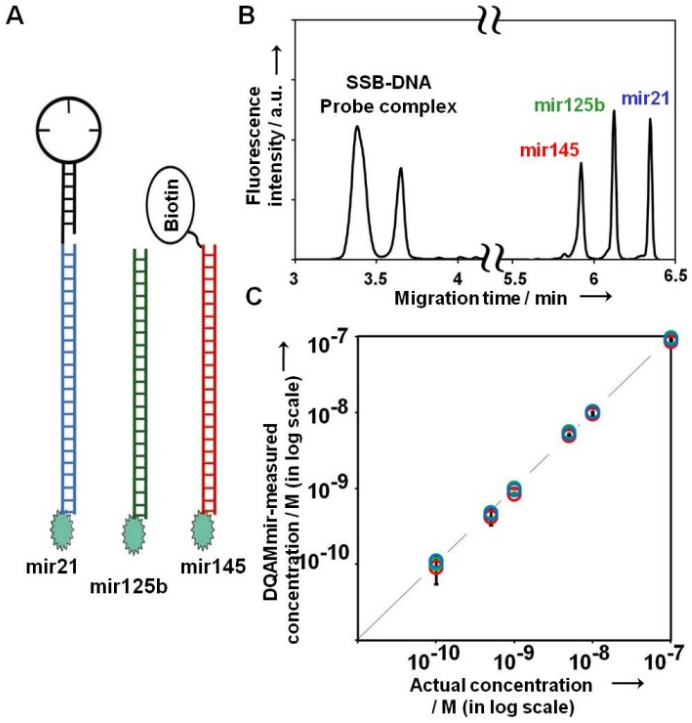

Figure 2.2. Panel A: Structures of 3 miRNA-DNA probe hybrids. **Panel B:** CE separation of the 3 hybrids from each other and from the excess probe facilitated by the drag tags on mir21 and mir145 and SSB in the run buffer. The concentrations of miRNAs were 5 nM each and the concentration of the probes were 50 nM each. **Panel C:** Quantitative properties of the analysis utilizing data of panel B at concentrations of miRNAs varying from 100 pM to 100 nM (three repetitions) processed with **eq. (2-8)**. Different concentrations of miRNAs were prepared by serial dilution of a stock solution. The concentration of the stock solution was determined by light absorbace at 260 nm. Standard deviation of DQAMmiR-measured miRNA concentrations was 6.6%.

2-min window is sufficient to resolve a maximum of approximately 20 peaks. While this maximum can be increased by optimizing the separation conditions, it is unlikely to exceed 30 – 40. This is the electrophoresis-associated limit for the maximum number of miRNAs that can be analyzed by DQAMmiR with fluorescence detection in a single spectral channel.

2.3.2. Quantitation of Multiple miRNAs

To determine the quantities of individual miRNAs from the experimental data similar to that in **Fig. 2.2B**, Victor Okhonin developed the mathematics of DQAMmiR that does not require resolving SSB-bound probes and takes into account a potential change of the quantum yield of fluorescence of the probe upon its binding to miRNAs or SSB. Here I show the derivation of the equation for the determination of concentrations of multiple miRNAs in DQAMmiR.

The unknown concentration of the *i*-th miRNA, $[\text{miRNA}]^i$, can be expressed through the area of its respective hybrid peak (A_H^i), using the unknown coefficient a and known quantum yield q_H^i:

$$[\text{miRNA}]^i = a\left(A_H{}^i / q_H{}^i\right) \tag{2–1}$$

The known concentration of the *j*-th probe, $[P]_{0,j}$ can be expressed through the areas of two peaks, the one of SSB-bound excess probe, $A_{P,j}$, and the one of the miRNA-bound probe, $A_{H,j}$, with the same coefficient a and known quantum yields $q_{H,j}$ and $q_{P,j}$:

$$[P]_{0,j} = aA_{P,j} / q_{P,j} + A_{H,j} / q_{H,j} \tag{2–2}$$

Accordingly, the known total concentration of N DNA probes can be expressed using the following equation:

$$\sum_{j=1}^{N}[\mathrm{P}]_{0,j} = a\left(\sum_{j=1}^{N} A_{\mathrm{P},j} / q_{\mathrm{P},j}\right) + a\left(\sum_{j=1}^{N} A_{\mathrm{H},j} / q_{\mathrm{H},j}\right) \tag{2–3}$$

Since the peaks of the hybrids are resolved, their corresponding areas $A_{\mathrm{H},j}$ can be experimentally determined; accordingly I treat them as known parameters. The peaks corresponding to the SSB-bound excess probes can, however, overlap. Therefore, I treat the areas corresponding to them, $A_{\mathrm{P},j}$, as unknowns along with the coefficient a. While the individual $A_{\mathrm{P},j}$ are unknown, their sum, A_{P}, can be experimentally measured and can thus be treated as a known parameter. To incorporate A_{P} in the equation, I need to isolate $A_{\mathrm{P},j}$ from $q_{\mathrm{P},j}$ by multiplying **eq. (2–3)** by $q_{\mathrm{P},j}$:

$$\sum_{j=1}^{N} q_{\mathrm{P},j}[\mathrm{P}]_{0,j} = a\left(\sum_{j=1}^{N} A_{\mathrm{P},j}\right) + a\left(\sum_{j=1}^{N}\left(q_{\mathrm{P},j} / q_{\mathrm{H},j}\right) A_{\mathrm{H},j}\right) \tag{2–4}$$

eq. (2–4) can be otherwise represented as:

$$\sum_{j=1}^{N} q_{\mathrm{P},j}[\mathrm{P}]_{0,j} = aA_{\mathrm{P}} + a\left(\sum_{j=1}^{N}\left(q_{\mathrm{P},j} / q_{\mathrm{H},j}\right) A_{\mathrm{H},j}\right) \tag{2–5}$$

Now I can solve **eq. (2–5)** for a:

$$a = \frac{\sum_{j=1}^{N} q_{\mathrm{P},j}[\mathrm{P}]_{0,j}}{A_{\mathrm{P}} + \sum_{j=1}^{N}\left(q_{\mathrm{P},j} / q_{\mathrm{H},j}\right) A_{\mathrm{H},j}} \tag{2–6}$$

By expressing a from **eq. (2–1)** and incorporating it into **eq. (2–6)** I get:

$$\frac{[\mathrm{miRNA}]^{i} q_{\mathrm{H}}{}^{i}}{A_{\mathrm{H}}{}^{i}} = \frac{\sum_{j=1}^{N} q_{\mathrm{P},j}[\mathrm{P}]_{0,j}}{A_{\mathrm{P}} + \sum_{j=1}^{N}\left(q_{\mathrm{P},j} / q_{\mathrm{H},j}\right) A_{\mathrm{H},j}} \tag{2–7}$$

I can finally express the unknown concentration of the *i*-th miRNA in the following way:

$$[\mathrm{miRNA}]_{i} = \frac{A_{\mathrm{H},i}}{A_{\mathrm{P}} + \sum_{j=1}^{N}\left(q_{\mathrm{P},j} / q_{\mathrm{H},j}\right) A_{\mathrm{H},j}} \left(\sum_{j=1}^{N}\left(q_{\mathrm{P},j} / q_{\mathrm{H},i}\right)[\mathrm{P}]_{0,j} \right) \tag{2–8}$$

where $[\mathrm{P}]_{0,j}$ is the total concentration of the *j*-th probe (composed of the hybrid and the miRNA-unbound probe), A_{H} is the area corresponding to the *i*-th or *j*-th hybrid, A_{P} is the cumulative area of the excess probe, q_{H} is the relative quantum yield of the *i*-th or *j*-th hybrid with respect to that of the free probe, $q_{\mathrm{P},j}$ is the relative quantum yield of the *j*-th probe in the presence of SSB with respect to that of the free probe and *N* is the total number of DNA probes. In this equation I assume that all target miRNAs are hybridized. Quantum yields can be found in **Table 2.1**.

Table 2.1. Quantum yields of DNA probes for the respective miRNAs. q_{P} is the quantum yield of SSB-bound probe and q_{H} is the quantum yield for the DNA probe-miRNA hybrids. These values were determined as explained in Chapter 1.3.

Quantum Yield	Mir145	mir125b	Mir21
q_{P}	0.29 ± 0.01	0.24 ± 0.02	0.14 ± 0.01
q_{H}	0.61 ± 0.05	0.63 ± 0.08	0.59 ± 0.06

eq. (2–8) was used to determine the amounts of miRNAs in the experiment shown in **Fig. 2.2B**. The results of the calculations shown in **Fig. 2.2C (**and **Table 2.2)** demonstrate the high accuracy (94%) and great signal linearity (R = 0.9999) of the DQAMmiR method in the range of at least 3 orders of magnitude. The LOD (defined as the miRNA concentration at which the respective peak signal is at a 3 to 1 ratio to the background noise) was determined to be 100 pM. It is important to emphasize that DQAMmiR does not require calibration curves.

2.3.3. Specificity of DQAMmiR

One of the major requirements of miRNAs analyses is specificity; any miRNAs detection method should be able to discriminate miRNAs from a similar sequence with a single nucleotide being different. Such specificity is typically based on the difference in melting temperatures between the full-match and 1-nt mismatch hybrids. The 1-nt mismatch of mir145 with the

Table 2.2. DQAMmiR-determined concentrations of the three miRNAs (mir21, 125b, 145) relative to their actual concentration as determined by light absorbance at 260 nm.

Actual miRNA Concentration (nM)	**DQAMmiR-Determined miRNA Concentration (nM)**		
	mir145	**mir125**	**mir21**
0.1	0.091 ± 0.036	0.101 ± 0.016	0.108 ± 0.001
0.5	0.42 ± 0.09	0.49 ± 0.06	0.46 ± 0.04
1	0.84 ± 0.02	1.01 ± 0.03	0.95 ± 0.01
5	4.9 ± 0.1	5.6 ± 0.3	5.3 ± 0.2
10	9.6 ± 0.6	10.3 ± 0.8	10.1 ± 0.4
100	85 ± 5	97 ± 3	92 ± 6

sequence 5'-GUCCAGUUUUC**A**CAGGAAUCCCU-3' was custom synthesized by IDT (Coralville, IA). 5 nM of mir145 or its respective 1-nt mismatch was incubated with 50 nM mir145 DNA probe and 1 nM fluorescein. Hybridization and injection conditions were performed as previously explained. I set the temperature of the capillary to 35°C, which was determined to be above the melting temperature of the 1-nt mismatch hybrid but below the melting temperature of the perfect-match hybrid. This allowed me to completely eliminate the mismatch peak while not affecting the miRNA peak (**Fig. 2.3**). Moreover, due to the thermal stability of SSB, this concept worked equally well at the elevated temperature. Thus, DQAMmiR has the potential for a single-nucleotide specificity required for miRNAs detection in biological samples.

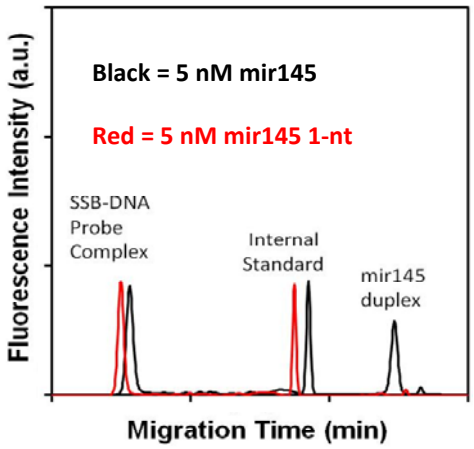

Figure 2.3. Electropherogram representing 1-nt differentiation of the mir145 DNA probe using DQAMmiR. Five nM mir145 (black) or 5 nM 1-nucleotide mismatch mir145 (red) were incubated with 50 nM mir145 DNA probe and 1 nM fluorescein. For each run the capillary temperature was increased to 35°C. At this temperature there was no 1-nucleotide mismatch duplex peak while the mir145 duplex peak remained intact.

2.3.4. Use of DQAMmiR for Biological Samples

After proving the concept of DQAMmiR, I tested the method for its tolerance to a complex biological matrix. The sample was made of 5 nM of the 3 miRNAs (mir21, mir125b, mir145) and 50 nM of the three respective DNA probes added to a 10× dilution of the *E. coli* cell lysate supplemented with 20nM fluorescein as an internal standard (to ensure controlled injection of the relatively viscous crude cell lysate) and 2.5 µM mask DNA and 1µM mask RNA. (to prevent degradation of miRNAs and DNA probes). The hybridization mixture was prepared, processed, and analyzed in the way described above for pure solutions of miRNAs. **Fig. 2.4** compares the results of DQAMmiR for the cell lysate and for a pure buffer as the sample matrices. Qualitative comparison of the data shows only insignificant differences. Moreover,

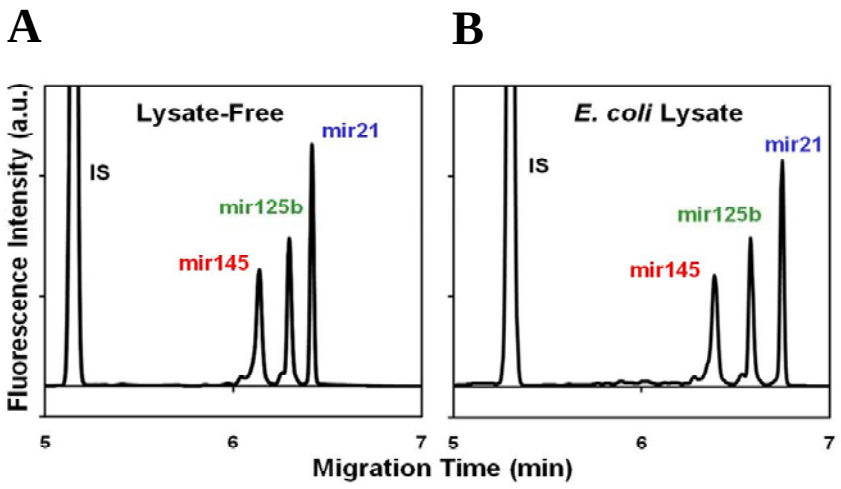

Figure 2.4. The influence of complex biological matrix on miRNAs analysis by DQAMmiR. **Panel A:** DQAMmiR of 3 miRNAs at 5 nM each in *E. coli* lysate and masking DNA/RNA in incubation buffer. **Panel B:** DQAMmiR of 3 miRNAs at 5 nM each in pure incubation buffer. IS labels the peak of the internal standard (fluorescein).

calculations of miRNA concentrations (**Table 2.3**) also produce similar results, thus confirming that neither the cell lysate nor masking DNA/RNA significantly affected the results and that DQAMmiR could be potentially directly used for complex biological samples without RNA extraction or other sample processing. To test this, I used DQAMmir on a MCF-7 cell lysate sample which is known to have up-regulated mir21 and down-regulated mir125b and mir145.**[18] Fig. 2.5** compares the DQAMmiR results for the pure MCF-7 cell lysate and the lysate with 3 miRNAs spiked into it. In the lysate-only sample a peak for the up-regulated mir21 was detected and the concentration of mir21 was determined to be 140 pM. The correctness of this value was confirmed by analyzing 140 pM mir21 in a pure buffer and observing an identical

Table 2.3. A comparison of miRNA concentrations determined by DQAMmiR with and without BL21 cell lysate. Five nM of each miRNAs (145, 125b, 21) were incubated with: a) 50 nM DNA probes (145, 125b, and 21), 20 nM fluorescein or b) 50 nM DNA probes (145, 125b, 21), 20 nM fluorescein, 10× diluted BL21 *E. coli* lysate, 2.5 μM masking DNA, and 1 μM masking RNA. Each miRNAs had comparable results with and without the cell lysate and masking DNA/RNA.

Sample	**DQAMmiR-determined miRNA concentration (nM)**		
	mir145	**mir125**	**mir21**
5 nM each miRNAs	5.15 ± 0.24	4.52 ± 0.22	5.33 ± 0.25
5 nM each miRNAs + Masking DNA/RNA + *E. coli* cell lysate	5.15 ± 0.20	4.52 ± 0.18	5.08 ± 0.16

peak. The peaks of the down-regulated mir125b and 145 were below the background noise. This result indicates that available commercial CE instrumentation may not be sensitive enough for DQAMmiR of low abundance miRNAs without their pre-concentration. The ultimate solution of

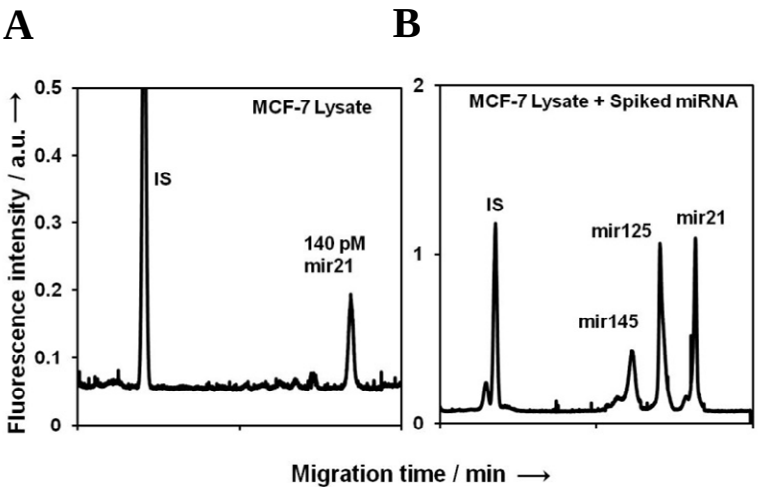

Figure 2.5. The influence of complex biological matrix on miRNAs analysis by DQAMmiR. **Panel A:** DQAMmiR of 3 DNA probes at 5 nM each incubated with MCF-7 cell lysate and masking DNA/RNA in incubation buffer. **Panel B:** DQAMmiR of 3 DNA probes at 5nM each plus 0.5 nM spiked in mir21, mir125b and mir145 incubated with MCF-7 cell lysate and masking DNA/RNA. IS labels the peak of the internal standard (fluorescein).

this limitation will be the commercialization of instrumentation with single-molecule fluorescence detection, which exists in experimental prototypes.

2.4. Conclusions

To conclude, DQAMmiR is the first approach that requires no miRNA modification in the sample while being quantitative and applicable to multiple miRNAs. With its characteristics, DQAMmiR has the potential of becoming a major tool for quantitative analysis of multiple miRNAs. Several limitations must, however, be overcome before its practical use in a clinical setting. I was able to separate and detect 3 miRNAs, which would not be a sufficient number of detectable miRNAs for most miRNA fingerprints. I need to find a practical way to further

increase the number of detectable miRNAs. Decreasing the overall assay time is also a priority for DQAMmiR's use in clinical setting. The LOD must be lowered to be able to analyze low abundance miRNAs as shown by the lack of detection of mir125b and mir145. An emphasis will be on lowering the LOD while maintaining the use of an automated, commercially available instrument. Finally, though I achieved 1-nt specificity of a single miRNA, I need to develop a technique that has 1-nt specificity of multiple miRNAs. Such improvements will be discussed in the following chapters.

CHAPTER 3: IMPROVING MULTIPLEXING CAPABILITIES OF DQAMMIR

3.1. Universal Drag Tag for Direct Quantitative Analysis of Multiple miRNAs (DQAMmiR)

3.1.1. Introduction to Universal Drag Tags

As previously mentioned, the deregulation of specific miRNAs can be characteristic of many human diseases. There are significant efforts directed towards combining sets of such deregulated miRNAs into fingerprints that can be used for disease diagnosis. Several papers have shown that these fingerprints only require 2 – 15 miRNA species to distinguish cancerous from non-cancerous tissues**[18, 20, 22, 73, 74]** and to even distinguish specific cancer cell subtypes.**[18]** Thus, fewer than 15 miRNA species would be required for a diagnostic miRNAs assay. There is a need for a method to detect such fingerprints, which requires direct, quantitative analysis of multiple miRNAs. DQAMmiR has the potential to be such a method, however in my proof of principle work I only detected 3 miRNAs simultaneously.**[75]** My goal was to find a

solution for increasing the number of miRNA species that could be analyzed by DQAMmiR simultaneously.

I previously used a biotin molecule and a hairpin loop-forming DNA extension as drag tags.**[75]** Though these two drag tags were able to achieve sufficient hybrid separation, they cannot be easily extended to increase the number of detectable hybrids. Practical applications of DQAMmiR require a more generic extendable drag tag that would allow for an increased number of detectable miRNAs. Jiang et al were able to detect multiple microRNA using drag tags in capillary gel electrophoresis. They attached adenosine tails of varying length to multiple miRNA-specific DNA probes.**[76]** Adjacent to the miRNA complementary sequence, each DNA probe also contained a DNA sequence complementary to a short, universal, fluorophore-labeled probe. Upon miRNAs binding, the universal probe is able to bind via a base-stacking effect. When both the miRNAs and universal probe were bound they were ligated together by T4 ligase. They were able to achieve great sensitivity (190 fM) and specificity, however the indirect nature of the ligation may cause sequence-specific biases as previously explained. Furthermore, in gel electrophoresis the polymerized gel has to be replaced after every run, making this technique quite tedious.

I thought that polymers were a logical choice for an extendable drag tag. Polymers would allow for easy extension, by simply increasing the number of monomers. I decided on using short peptides, which are commercially available, can have a precise number of amino acids (aa) and have been used previously as drag tags in DNA sequencing.**[77]** Our group recently published a rigorous theoretical analysis on the use of peptides as drag tags that determined the required

number of peptides that would allow sufficient separation of multiple hybrids.**[78]** It was determined that the peptide drag tag lengths must vary between 0 – 20 amino acids to detect 5 miRNAs and between 0 – 47 amino acids to detect 9 miRNAs.

Using this theoretical work I decided to detect 5 miRNAs using drag tags from 0 – 20 amino acids in length. One untagged probe and 4 tagged probes were developed by conjugating a neutral 5 amino acid repeat $(Gly\text{-}Ala\text{-}Gly\text{-}Thr\text{-}Gly)_n$, (where $n = 0, 1, 2, 3, 4$) to DNA sequences complementary to the 5 respective miRNAs. I measured travel times of tagged hybrids to the detector and found that the travel time decreased with the increased length of the peptide tag. Given the presence of electroosmotic flow (EOF), such behavior of the travel time means that the hybrid electrophoretic mobility decreased with the increased length of the tag as predicted. **[78]** This conclusion follows from the fact that both untagged and tagged hybrids migrate against EOF that is directed to the detector in the experiments. The 5 hybrids could be separated from each other and the tags did not interfere with SSB binding to the excess probes. As a result, I was able to quantitatively detect 5 miRNA species.

3.1.2. Materials and Methods

3.1.2.1. Oligonucleotides and Peptides

I developed DNA probes with drag tags of 0, 5, 10, 15, 20 amino acids in length for 5 miRNAs (mir125b, 155, 21, 10b, 145 respectively), which are known to be deregulated in breast cancer. Due to the similar length of all 5 miRNAs (mir125b, 21 have 22 nucleotides, mir155,10b,145 have 23 nucleotides) the peptide lengths were randomly chosen for the 5 probes,

regardless of probe length. All DNA and miRNAs for hybridization assays were custom synthesized by IDT (Coralville, IA, USA). The 5 miRNAs had the following sequences: mir10b: 5'-UACCCUGUAGAA-CCGAAUUUGUG-3' mir21: 5'-UAGCUUAUCAGACU-GAUGUUGA-3', mir125b: 5'-CCUGAGACCCUAACU-UGUGA-3', mir145: 5'-GUCCAGUUUUCCCAGGAAU-CCCU-3', mir155: 5'-UUAAUGCUAAUCGUGAUAGG-GGU-3'. The hybridization probes had the following sequences: probe for mir10b: 5'-ThiolC6S-S-CACAAATTCGGTTC-TACAGGGTA-Alexa488-3', probe for mir21: 5'-Thiol C6S-S-TCAACATCAGTCTGATAAGCTA-Alexa488-3', probe for mir125b: 5'-ThiolC6S-S-TCACA-AGTTAGGG-TCTCAGGGA-Alexa488-3', probe for mir145: 5'-Thiol C6S-S-AGGGATTCCTGGGAAAACTG-GAC-Alexa488-3', probe for mir155: 5'-ThiolC6S-S-ACCCCTATCACG-ATTAGCATTAA-Alexa488-3'.

3.1.2.2. Conjugation of DNA with Peptides

All of the peptides contained a maleimide modification on their N-terminus and were synthesized by Canpeptide (Pointe-Clare, QUE, Canada). The following amino acid sequences were used with respect to the DNA probe they were conjugated with: probe for mir155: C-term-Gly-Ala-Gly-Thr-Gly-N term, probe for mir21: C-term-Gly-Ala-Gly-Thr-Gly- Gly-Ala-Gly-Thr-Gly-N term, probe for mir10b: C-term-Gly-Ala-Gly-Thr-Gly-Gly-Ala-Gly-Thr-Gly-Gly-Ala-Gly-Thr-Gly-N term, probe for mir145: C-term-Gly-Ala-Gly-Thr-Gly-Gly-Ala-Gly-Thr-Gly-Gly-Ala-Gly-Thr-Gly-Gly-Ala-Gly-Thr-Gly-N term. All DNA probes contained a disulfide modification on their 5' end which needed to be reduced prior to conjugation. Tris(2-

carboxyethyl)phosphine (TCEP) was used as the reducing agent. 300 µl of TCEP reducing beads (Fisher Scientific, Ottawa, ON, Canada) were spun down at 10,000 rpm and the supernatant was removed. The beads were washed with a modified PBS containing 500 mM NaCl at pH 7.0 and spun again at 10,000 rpm. The PBS wash was removed and 2 µM of the DNA probe was incubated with the TCEP at 37°C with vigorous shaking for 2 h. The sample was spun down at 10,000 rpm for 5 min and the filtrate, containing the reduced DNA, was added to an equal volume of 200 µM maleimide-modified peptide. The final concentration of the DNA and peptide were 1 µM and 10 µM, respectively. The conjugation reaction was carried out for 1 h at 37°C with vigorous shaking. Purification was performed immediately after conjugation.

3.1.2.3. Purification of DNA-Peptide Conjugate

The DNA-peptide conjugate was purified from the excess of non-conjugated DNA by HPLC. HPLC was performed on a System Gold system (Beckman Coulter, Fullerton, CA, USA) equipped with a FP-2020 Plus fluorescence detector (Jasco, Easton, MD, USA) and Gen-Pak FAX anionic exchange column (Waters, Milford, MA, USA). The eluted conjugate was collected and the HPLC buffer was exchanged with deionized H_2O by centrifuging with an Amicon Ultracel 3K filter (Millipore, Billerica, MA). The sample was frozen at −80°C and lypholized for storage.

3.1.2.4. Hybridization Conditions

Hybridization was carried out in Mastercycler 5332 thermocycler (Eppendorf, Hamburg, Germany). Working-stock solutions of DNA and miRNA were kept at 37°C to reduce sticking to the test tube walls. Various concentrations of the miRNA species (mir10b, 21, 125b, 145, 155) were incubated with 50 nM of their respective hybridization probes along with 50 nM bodipy (internal standard) in the incubation buffer (50 mM Tris-Ac, 50 mM NaCl, 10 mM EDTA, pH 8.2). Temperature was increased to a denaturing 80°C and then lowered to 37°C at a rate of 20°C/min and was held at 37°C for 1 h to allow annealing.

3.1.2.5. CE-LIF

All experiments were performed using a P/ACE MDQ CE instrument (Beckman-Coulter, Fullerton, CA, USA) equipped with an LIF detector. We used bare fused-silica capillaries with an outer diameter of 365 μm, an inner diameter of 75 μm, and a total length of 50 cm. The distance from the injection end of the capillary to the detector was 39 cm. The running buffer was 25 mM sodium tetraborate, pH 9.2, with 50 nM SSB. The capillary was flushed prior to every CE run with 0.1 M HCl, 0.1 M NaOH, deionized H_2O and running buffer for 1 min each. Samples were injected at the positive end by a pressure pulse of 0.5 psi (3.45 kPa) for 5 s, the volume of the injected sample was ~14 nL. Electrophoresis was driven by an electric field of 500 V/cm for 15 min with normal polarity and coolant controlled temperature maintained at 20°C. Electropherograms were analyzed using 32 Karat Software. Peak areas were divided by the corresponding migration times to compensate for the dependence of the residence time in the

detector on the electrophoretic velocity of species. All areas were normalized by dividing them by the area of internal standard, bodipy. Concentrations of miRNAs were determined using **eq. (2–8)**.

3.1.2.6. DQAMmiR in Cell Lysate

MCF-7 cells were purchased from ATCC and grown in an incubator at 37°C in the atmosphere of 5% CO_2. Cells were grown in DMEM media (Invitrogen) with FBS and 10,000 μg/mL penicillin, streptomycin in a 100 mm Petri dish. When cells covered roughly 90% of the plate they were washed with PBS, trypsinized to detach them from bottom of dish and centrifuged at 300 × g for 5 min. Pellet was washed twice with PBS. The cells were counted using a haemocytometer and lysed with 1% Triton in the incubation buffer with 10 μM masking RNA (tRNA library from baker's yeast). Cell lysates were aliquoted and stored at –80°C. A 10× diluted cell lysate was incubated with 50 nM of each of the 5 DNA probes, 10 nM of each miRNAs (mir10b, 21, 125b, 145, 155), 50 nM bodipy and 1 μM masking DNA. Masking DNA was a 20-nt DNA strand, with the sequence of 5'-CAAAAAATGAGTCATCCGGA-3'.

3.1.2.7. Spectrophotometric Determination of Target Concentration

MiRNA target concentration was determined by light absorption at 260 nm using the Nano-Drop ND-1000 Spectrophotometer (Thermo-Fisher Scientific). The stock concentration of the target was too high to measure directly, therefore, a small sample of the stock solution was serially diluted and absorbance of each sample at 260 nm was measured 3 times. The

concentration of each sample was determined as *absorbance*/εl where ε is the molar extinction coefficient of the RNA target at 260 nm (provided by IDT) and l is the optical path-length. Using the concentrations of the serial dilutions, the original stock concentration was extrapolated.

3.1.3. Results and Discussion

3.1.3.1. Effects of Peptide Drag Tags on SSB, miRNAs Binding to Probe

Prior to testing the separative abilities of these drag tags, I had to ensure that the peptides had no hindering effects on the analysis. The peptides could potentially interfere with miRNAs binding to their respective probe, causing either a reduction in quantitative accuracy or slowing binding, thereby increasing hybridization time. I also had to determine whether the drag tags could hinder SSB-binding to the DNA, which is required for all DNA probes in DQAMmiR. Due to the short lengths of peptides used, I did not expect any negative effects.

SSB binds non-specifically to all DNA probes and due to its large size causes all probes (regardless of drag tag size) to migrate with the same mobility, forming a single peak. Shifting all probes to a single peak allows me to have a large separation window, which I utilized for detecting multiple hybrid peaks. If peptide drag tags interfered with SSB-binding, the separation window would be significantly reduced, preventing the detection of multiple miRNAs. To observe the impact of the drag tags on SSB-binding I injected all 5 DNA-peptide probes into the capillary with SSB in the run buffer (**Fig. 3.1.1**). All 5 probes bound to the SSB and formed a single peak, showing that the drag tags did not interfere with SSB binding.

To ensure that the peptide drag tags did not interfere with the probes ability to bind to miRNAs, I incubated each of the 5 miRNA species with their respective DNA probe, both with and without the drag tag. In agreement with my previous work,**[75]** the drag tags did not interfere with miRNAs binding (data not shown). Thus, the new peptide drag tags did not interfere with either SSB or miRNAs binding, allowing for their use in DQAMmiR.

3.1.3.2. Effects of Peptides on Peak Separation

I next studied the mobility of the 5 DNA-peptide probes. Though the theoretical work was based on the separation of hybrids, I assumed that a similar shift would be observed when the 5 probes were injected into the capillary without either miRNAs or SSB present. Though all of the drag tags caused a mobility shift relative to the untagged probe (**Fig. 3.1.1**), there was an

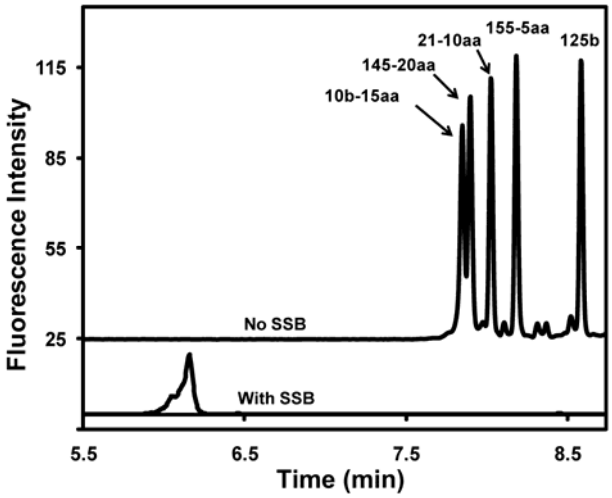

Figure 3.1.1. Separation of the 5 DNA probes. Upper) Peptides drag tags with lengths of 0, 5, 10, 15, 20 amino acids were conjugated to DNA probes for mir125b, 155, 21, 10b, 145 respectively. The peptides caused a mobility shift from the untagged probe (125b). The DNA probes 10b-15aa and 145-20aa have a similar mobility. Lower) Presence of SSB in running buffer caused all 5 probes to shift into a single peak.

unexpected lack of separation between the 15, and 20 amino acid drag tag probes. Interestingly, the DNA probe with 15aa had a more significant mobility shift than the 20aa probe. The mobility of single-stranded DNA was not the focus of this paper, so I did not explore why this occurred, however I can speculate that it was most likely due to the DNA probes having dissimilar conformations when not in double-stranded form.

Regardless of the lack of separation between the 15aa and 20aa probes I went on to test the separation between the 5 hybrids. I incubated all 5 DNA probes with their respective miRNAs and injected a small plug into the capillary (**Fig. 3.1.2**). I observed 5 distinct peaks representing each of the respective hybrids. The lack of separation that occurred with the ssDNA probes was resolved, most likely due to the conformational rigidness of a double-stranded hybrid.

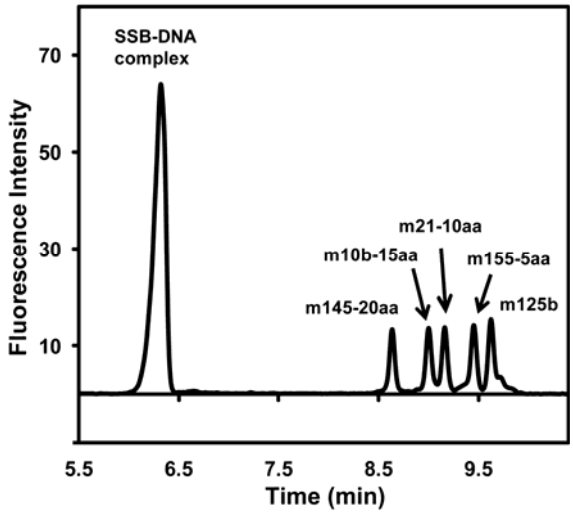

Figure 3.1.2. Separation of 5 miRNA-probe hybrids. 50 nM of the 5 DNA probes (125b, 155-5aa, 21-10aa, 10b-15aa, 145-20aa) and 10nM of their respective miRNAs were injected into the capillary with 50nM SSB in the running buffer. 5 distinct hybrid peaks are present, with sufficient separation between hybrids to allow quantitation. Peak areas are normalized by quantum yields.

The separation between each of the hybrids was not uniform with the mir125b and mir155, as well as the mir21 and mir10b peaks being relatively close. This was due to the slight difference in miRNAs length as previously mentioned. The 22-nucleotide long hybrids (mir125b, mir21) have a lower electrophoretic mobility than the longer 23-nucleotide hybrids (mir145, mir10b, mir155) regardless of drag tag, which is in agreement with the theoretical work.**[78]** If required, greater separation could easily be achieved by changing the drag tag, probe combinations, however I wanted to show that regardless of miRNAs length, separation could be achieved. Though the 5 miRNAs detected here are of similar length, miRNAs of varying length can also be simultaneously detected. As long as the shorter DNA probes are conjugated to the longer peptides, sufficient separation between hybrid peaks will be achieved.**[78]**

Given that the experimental and theoretical peak migration times reasonably agree (data not shown), I proved that, in agreement with our group's initial theory, drag tags ranging from 0 – 20 amino acids were sufficient for the detection of 5 miRNAs. This allows me to confidently design DNA probes with sufficient drag tag lengths to detect an even greater number of miRNAs. The quality of separation of the hybrids from each other and the hybrids from the SSB-bound excess probes suggests that up to 25 miRNAs can be analyzed simultaneously by further increasing drag tag lengths.

3.1.3.3. Quantitation of 5 miRNAs

Though the peptide drag tags did not interfere with miRNAs binding, they did have a quenching effect on the probe signal. I was able to take this quenching effect into account to

maintain quantitative accuracy (**Tables 3.1 – 3.3**). As explained in chapter 1.3 I also determined the quantum yields of each of the DNA probes with respect to when they are SSB bound and miRNAs-bound.

Table 3.1. Quantum yields of the DNA probes for the respective miRNAs. q_P is the quantum yield of SSB-bound probe and q_H is the quantum yield for the DNA probe-miRNA hybrid. These values were determined as explained in Chapter 1.3.

Quantum Yield	**Mir145 DNA probe**	**Mir10b DNA probe**	**Mir21 DNA probe**	**Mir155 DNA probe**	**Mir125b DNA probe**
$\boldsymbol{q_P}$	0.13 ± 0.01	0.14 ± 0.01	0.22 ± 0.01	0.17 ± 0.03	0.24 ± 0.02
$\boldsymbol{q_H}$	0.36 ± 0.09	0.58 ± 0.07	0.68 ± 0.09	0.63 ± 0.16	0.63 ± 0.08

Table 3.2. After the conjugation of peptides to the miRNA-specific DNA probes, the variation of fluorescence intensity was taken into account. The fluorescence intensity of all DNA probes was normalized by determining their quantum yields ($\boldsymbol{q_D}$) with respect to an untagged DNA probe (the untagged probe for miR125b was used as a reference).

Quantum Yield	**Mir145-20aa DNA probe**	**Mir10b-15aa DNA probe**	**Mir21-10aa DNA probe**	**Mir155-5aa DNA probe**	**Mir125b DNA probe**
$\boldsymbol{q_D}$	0.38 ± 0.01	0.58 ± 0.01	0.46 ± 0.003	0.47 ± 0.003	1

Table 3.3. Quantum yields of DNA probes conjugated to peptides upon binding to SSB ($\boldsymbol{q_P}$') and upon hybridization with miRNA ($\boldsymbol{q_H}$'). They were obtained by multiplying $\boldsymbol{q_P}$ and $\boldsymbol{q_H}$ by $\boldsymbol{q_D}$.

Quantum Yield	**Mir145-20aa DNA probe**	**Mir10b-15aa DNA probe**	**Mir21-10aa DNA probe**	**Mir-155-5aa DNA probe**	**Mir125b DNA probe**
$\boldsymbol{q_P}$**'**	0.05 ± 0.004	0.08 ± 0.006	0.11 ± 0.006	0.08 ± 0.014	0.24 ± 0.02
$\boldsymbol{q_H}$**'**	0.14 ± 0.035	0.34 ± 0.042	0.31 ± 0.043	0.30 ± 0.076	0.63 ± 0.08

Using **eq. (2–8)** I was able to accurately determine the concentrations of all 5 miRNAs, ranging from 100 pM to 100 nM. (**Fig. 3.1.3**).

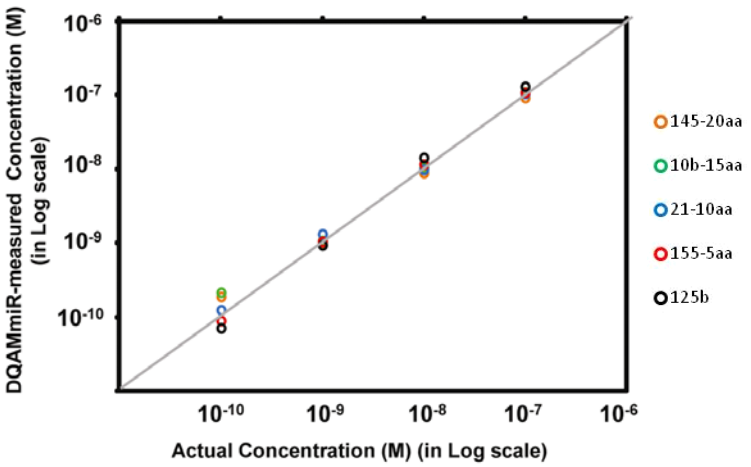

Figure 3.1.3. Quantitative analysis of 5 miRNAs was processed simultaneously using **eq. (2–8)**. Excess of the 5 DNA probes was incubated with all 5 respective miRNAs, ranging in concentration from 100 pM to 100 nM. The different concentrations of miRNAs were prepared by serial dilution of a stock solution. The concentration of the stock solution was determined by light absorbance at 260 nm.

3.1.3.4. Effects of Biological Samples on Separation and Quantitation

For proof of principle, the new probes were introduced into a complex biological matrix to show their potential in biological samples. The 5 DNA probes were incubated with MCF-7 cell lysate spiked with miRNAs (**Fig. 3.1.4**). Masking DNA and RNA were included in the sample to prevent probe and miRNAs degradation respectively. Though the peak height of the mir125b hybrid appears to be greater than the other peak heights, the peak areas remain similar showing that the lysate had negligible effect on the quantitative analysis of all 5 hybrid peaks (**Fig. 3.1.4** and **Table 3.4)**. As mentioned previously, I plan to improve the limit of detection in future work, since I cannot detect all 5 endogenous miRNA targets directly from the cell lysate. Thus, I was required to spike in miRNAs at a concentration greater than biologically-relevant (pM or lower) concentrations.

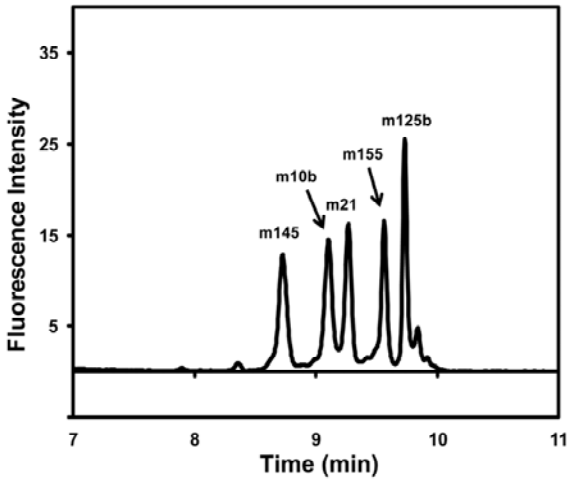

Figure 3.1.4. Detection of miRNAs from a biological matrix. 50nM of the 5 DNA probes (145-20aa, 10b-15aa, 21-10aa, 155-5aa, 125b) and 10nM of their respective miRNAs were spiked into MCF-7 cell lysate. All 5 hybrid peaks were observed. Small peaks to the left of the miRNA peaks indicate impurities from the lysate.

Table 3.4. A quantitative comparison of the hybrid peak areas shown in Figure 3.1.4. The peak areas were divided by migration time to account for time in the detection window and are relative to the internal standard (bodipy) peak. Each hybrid peak consisted of 10 nM of their respective miRNAs.

	mir145	**mir10b**	**mir21**	**mir155**	**mir125b**
Hybrid Peak Area	5.23	5.23	4.86	4.97	4.92

3.1.4. Conclusions

Here I have demonstrated the design of DNA probes with a universal drag tag and in a proof-of-principle DQAMmiR experiment achieved separation of 5 hybrids. The use of a universal drag tag allows for an increasing number of miRNAs to be detected by simply increasing the number of amino acids. The agreement between experimental and theoretical analysis allows for future DNA probes to be designed with confidence that the respective hybrids

will achieve baseline separation allowing for quantitation. My experimental results suggest that I can separate up to 25 hybrids. Universal drag tags simplify DNA probe design, increasing the number of detectable miRNAs.

3.2. Improvements to Direct Quantitative Analysis of Multiple miRNAs Facilitating Faster Analysis

The presented material was published previously and reprinted with permission from "Ghasemi, F.; Wegman, D.W.; Kanoatov, M.; Yang, B.B.; Liu, S.K.; Yousef, G.M.; Krylov, S.N. Improvements to direct quantitative analysis of multiple microRNAs facilitating faster analysis. *Anal Chem*, **2013**, *85*, 10062 – 10066". Copyright 2013 American Chemical Society. My contribution to the article was: (i) planning all experiments, (ii) assisted in performing experiments, (iii) interpreting results, (iv) preparing all figures, (v) writing first draft of manuscript, excluding materials and methods.

3.2.1. Introduction to a Post-Storage Purification Procedure to Facilitate Faster Analysis

DQAMmiR has been shown to be capable of detecting 5 miRNAs simultaneously, however, a few technical limitations were discovered during the analysis of 5 miRNAs in **section 3.1**. Presence of fluorescent impurities, such as DNA degradation products or by-products of the drag-tag conjugation reaction, interferes with detection of miRNA-DNA hybrids. Detecting an increasing number of miRNAs results in an increase in such impurities due to the higher number of DNA probes involved. Moreover, the interfering fluorescent impurities tend to reappear over time due to sample degradation. Diligent storage procedures mitigate this issue, but are often not sufficient, prompting for additional post-storage purification steps. Failure to eliminate the interfering fluorescent impurities imposes a limitation on the maximum concentration of DNA

probes that can be used in the assay, often restricted to be no more than 50 nM. As a consequence, the incubation time of the DNA probes with miRNAs increases, usually requiring a 60 min hybridization time (defined as the time required to hybridize over 90% of miRNA targets).**[79]** With the CE part of the analysis requiring less than 10 min, such a prolonged period of hybridization presents a major shortcoming of the method. Furthermore, the long incubation time of the DNA probes, especially within complex biological samples, necessitates the use of anti-nuclease masking DNA. Addition of masking DNA requires careful sequence and concentration optimization to prevent non-specific hybridization, further reducing the robustness of DQAMmiR. Thus, the long incubation is a major obstacle in adaptation of DQAMmiR to the clinical setting.

In this work, I introduce a set of improvements to DQAMmiR that address the described technical limitations. First, I have devised a quick and simple post-storage purification procedure that efficiently eliminates the interfering fluorescent impurities from DNA probe preparations. This filtration-based approach decreased the concentrations of interfering impurities by a factor of ~ 25 to the levels of < 0.005% of the probe concentrations. This significantly alleviates the limitation on maximum probe concentrations used in the assay. Second, I have optimized the assay concentrations of the DNA probe to decrease the hybridization time to 10 min. This improvement allows completion of a single DQAMmiR measurement in approximately 20 min – the shortest analysis time for any available method for multiple-miRNAs quantitation. Lastly, I demonstrate that the increased probe concentrations and decreased incubation time removes the need for masking DNA, further simplifying the method and increasing its robustness. The

presented modifications bring DQAMmiR closer to use in a clinical setting, making it, arguably, the most suitable method for miRNA-based diagnostics.

3.2.2. Materials and Methods

3.2.2.1. Oligonucleotides

All DNA and miRNAs for hybridization assays were custom synthesized by IDT (Coralville, IA, USA). The miRNA species used for all of the runs was miR-21, 5'-UAGCUUAUCAGACUGAUGUUGA-3', and its respective DNA hybridization probe had the following sequence: 5'-Alexa488-TCAACATCAGTCTGATAAG CTA-3'.

3.2.2.2. Hybridization Conditions

Hybridization was carried out in Mastercycler 5332 thermocycler (Eppendorf, Hamburg, Germany). Working-stock solutions of DNA and miRNAs were kept at 37°C to reduce sticking to the test tube walls. Various concentrations of the miR-21 DNA probe were incubated either with or without 100 pM miR-21 for various time periods in incubation buffer (50 mM Tris-Ac, 50 mM NaCl, 10 mM EDTA, pH 8.2). 20 nM of fluorscein was included in each run as an internal standard. Temperature was increased to a denaturing 80°C and then lowered to 37°C at a rate of 20°C/min and was held at 37°C to allow annealing. To minimize miRNAs degradation, a nuclease-free environment was used while handling miRNAs samples.

3.2.2.3. CE-LIF

All experiments were performed using a P/ACE MDQ CE instrument (Beckman-Coulter, Fullerton, CA, USA) equipped with an LIF detector. I used bare fused-silica capillaries with an outer diameter of 365 μm, an inner diameter of 75 μm, and a total length of 50 cm. The distance from the injection end of the capillary to the detector was 39 cm. The running buffer was 25 mM sodium tetraborate, pH 9.2, with or without 50 nM SSB. The capillary was flushed prior to every CE run with 0.1 M HCl, 0.1 M NaOH, deionized H_2O and running buffer for 1 min each. Samples were injected at the positive end by a pressure pulse of 0.5 psi (3.45 kPa) for 5 s, the volume of the injected sample was ~14 nL. Electrophoresis was driven by an electric field of 500 V/cm with normal polarity and coolant controlled temperature maintained at 15°C. Electropherograms were analyzed using 32 Karat software. Peak areas were divided by the corresponding migration times to compensate for the dependence of the residence time in the detector on the electrophoretic velocity of species. All areas were normalized by dividing them by the area of the internal standard, fluorescein. Concentrations of miRNAs were determined using **eq. (2–8)**.

3.2.2.4. Detection of Multiple miRNAs

For the analysis of 5 miRNAs, 4 other miRNAs were included in addition to miR-21. The other miRNAs had the following sequences: miR-10b, 5'-UACCCUGUAGAACCGAAUUUGUG-3'; miR-125b, 5'-CCUGAGACCCUAACUUGUGA-3'; miR-145, 5'-GUCCAGUUUUCCCAGGAAUCCCU-3'; miR-155, 5'-

UUAAUGCUAAUCGUGAUAGGGGU-3'. To allow separation of the 5 hybrid peaks, peptide drag tags of varying size were conjugated to the DNA probes via a thioether bond. The conjugation reaction, (described in **section 3.1.2.2**) occurs between a thiol group on the 5' end of the DNA probes and a maleimide group on the N terminus of each peptide. All maleimide modified peptides were synthesized by Canpeptide (Pointe-Clare, QUE, Canada). The hybridization probes had the following sequences: probe for miR-10b, 5'-ThiolC6S-S-CACAAATTCGGTTCTACAGGGTA-Alexa488-3'; probe for miR-21, 5'-ThiolC6S-S-TCAACATCAGTCTGATA-AGCTA-Alexa488-3'; probe for miR-125b, 5'-ThiolC6S-S-TCACAAGTTAGGG-TCTCAGGGA-Alexa488-3'; probe for miR-145, 5'-Thiol C6S-S-AGGGATTCCTGGG-AAAACTGGAC-Alexa488-3'; probe for miR-155, 5'-ThiolC6S-S-ACCCCTATCACGATTAGCATTAA-Alexa488-3'. The following amino acid sequences were used with respect to the DNA probe they were conjugated with: probe for miR-155, C-term-Gly-Ala-Gly-Thr-Gly-N term; probe for miR-21, C-term-Gly-Ala-Gly-Thr-Gly-Gly-Ala-Gly-Thr-Gly-N term; probe for miR-10b, C-term-Gly-Ala-Gly-Thr-Gly-Gly-Ala-Gly-Thr-Gly-Gly-Ala-Gly-Thr-Gly-N term; probe for miR-145, C-term-Gly-Ala-Gly-Thr-Gly-Gly-Ala-Gly-Thr-Gly-Gly-Ala-Gly-Thr-Gly-Gly-Ala-Gly-Thr-Gly-N term.

3.2.2.5. Removal of Impurities from DNA-Peptide Probes

After conjugation and purification, each DNA-peptide probe was centrifuged with an Amicon Ultracel 10K filter (Millipore, Billerica, MA) for 20 min at 5,500 rpm to remove impurities. The retentate, which contained the probe, was collected and further centrifuged with

an Amicon Ultracel 3K filter (Millipore, Billerica, MA) for 30 min at 5,500 rpm to reduce the volume to make a stock solution.

3.2.2.6. DQAMmiR in Cell Lysate

An *E.coli* BL21 cell culture was grown to an OD600 of 1.6, harvested by centrifugation at 5,000 × g for 10 min at 4 °C and resuspended in sonication buffer: 50 mM Tris-HCl, 2.5 mM $MgCl_2$, 5 mM KCl at pH 8.3. They were lysed by sonication on ice with 5 s ‘‘on’’/15 s ‘‘off’’ intervals for a total of 10 min. Cell lysates were aliquoted and stored at –80 °C. A 50× dilution of the lysed cells was incubated with various ratios of DNA probe to masking DNA concentrations. For detection of miRNAs in lysate, 100 pM of miR-21 was spiked into the lysate, along with a large excess (10 μM) of masking RNA. The masking RNA was a tRNA library from baker’s yeast from Sigma-Aldrich (Oakville, ON, Canada). The mammalian cell line used for comparison of degradation was MCF-7. MCF-7 cells were purchased from ATCC and grown in an incubator at 37°C in the atmosphere of 5% CO_2. Cells were grown in DMEM media (Invitrogen) with FBS and 10,000 μg/mL penicillin, streptomycin in a 100 mm Petri dish. When cells covered roughly 90% of the plate they were washed with PBS, trypsinized to detach them from bottom of dish and centrifuged at 300 × g for 5 min. Pellet was washed twice with PBS. The cells were counted using a haemocytometer and lysed with 1% Triton-X100 in the incubation buffer with 10 μM masking RNA. Cell lysates were aliquoted and stored at –80°C. Incubation, injection and capillary conditions were performed as described in **section 3.2.2.3**.

3.2.2.7. Spectrophotometric Determination of Target Concentration

MiRNA target concentration was determined by light absorption at 260 nm using the Nano-Drop ND-1000 Spectrophotometer (Thermo-Fisher Scientific). The stock concentration of the target was too high to measure directly, therefore, a small sample of the stock solution was serially diluted and absorbance of each sample at 260 nm was measured 3 times. The concentration of each sample was determined as $absorbance/\varepsilon l$ where ε is the molar extinction coefficient of the RNA target at 260 nm (provided by IDT) and l is the optical path-length. Using the concentrations of the serial dilutions, the original stock concentration was extrapolated.

3.2.3. Results and Discussion

3.2.3.1. Filter Purification of DNA Probes

The presence of fluorescent impurities in the DNA probe preparations significantly undermines DQAMmiR's LOD. As evident from **Fig. 3.2.1,** top trace, even after dual reverse-phase HPLC purification the sample contained a significant amount of impurities. At the total probe concentration of 500 nM, the peaks associated with fluorescent impurities completely obscured the presence of a hybrid peak corresponding to 100 pM of miRNA. Conjugation of the DNA probes to a peptide drag tag, through a recently reported procedure, further increased the level of interfering impurities in the preparation (**Fig. 3.2.1**, middle trace).**[79]** Elimination of the observed impurities was required in order to ensure sufficient limits of miRNAs quantitation. At the same time, to be viable in a clinical setting, the method of post-storage purification must be fast, inexpensive and accessible. According to the observed CE migration patterns, the interfering

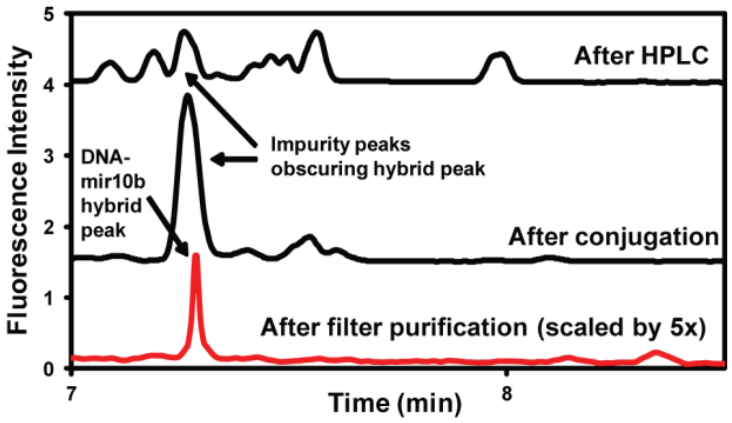

Figure 3.2.1. Impurity peaks in a 500 nM miR-10b DNA probe sample at different steps of purification. Each sample also contained 100 pM miR-10b. **Top trace:** miR-10b DNA probe purified with dual reverse-phase HPLC. The DNA probe-miR-10b hybrid peak cannot be observed due to its overlapping impurity peaks. **Middle trace:** miR-10b DNA probe conjugated to a 15aa peptide. Impurity peaks once again obscure the hybrid peak. **Bottom trace**: miR-10b-15aa probe that has been purified with the molecular weight filter; the trace scaled up by a factor of 5. The absence of impurity peaks allows for the detection of the hybrid peak (red trace), which is the only observable peak. The running buffer contained 50 nM SSB for each run.

impurities are most likely comprised of truncated DNA probe fragments. As a result I have attempted to remove these impurities through molecular weight filtration. After testing a number of strategies and products, I have determined that the Amicon Ultracel filter from Millipore with a 10K Dalton pore size achieves sufficient level of purification within a single filtration step. Briefly, after conjugation and purification, each DNA-peptide probe was centrifuged with the Amicon Ultracel 10K filter (Millipore, Billerica, MA) for 20 min at 5,500 rpm to remove the impurities. This filter was able to retain full-sized conjugated DNA probes, while allowing the impurities to pass through. The retentate, which contained the probe, was collected and further

centrifuged with an Amicon Ultracel 3K filter (Millipore, Billerica, MA) for 30 min at 5,500 rpm to reduce the volume to make a stock solution. Incorporating this post-storage purification step decreased the overall yield of DNA probe purification by 15%, a loss which, I believe, is well worth the improved quantitation limit. The inexpensive filters can be easily adapted for use by clinical technicians, and only require the use of a common centrifuge. As shown in **Fig. 3.2.1,** bottom trace, the 100 pM miRNA peak can be easily distinguished when a purified DNA probe preparation is used for its detection.

3.2.3.2. Optimization of Probe Concentration

With elimination of fluorescent impurities, the limit on maximum assay concentration of the DNA probe is significantly alleviated. As a result, the probe concentration can be increased to facilitate faster hybridization with its miRNA target. In previous implementations of DQAMmiR, hybridization time required a minimum length of 1 h. My goal was to decrease the hybridization time to be comparable with time of capillary pre-conditioning steps, which take approximately 10 min. This way, sample hybridization can be performed concurrently with capillary pre-conditioning, followed by a 10-min CE analysis step, reducing the overall time of a single DQAMmiR measurement to approximately 20 min. Reduction of the hybridization time below 10 min would not significantly shorten DQAMmiR analysis time, but would raise the analysis cost by increasing consumption of the fluorescent DNA probes. To find the optimum DNA probe concentration, at which the intended 10-min hybridization time was achieved, I incubated a 100 pM miRNAs sample with increasing concentrations of its probe, starting from 1 nM. As

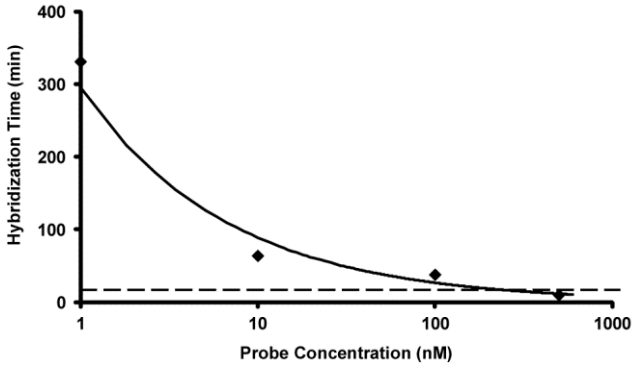

Figure 3.2.2. Optimization of DNA probe concentration to achieve target hybridization time. 100 pM of miR-21 was incubated with increasing concentrations of its respective DNA probe until a 10-min hybridization time (indicated by the dashed line) was achieved. Hybridization time steadily decreased from 5 h with 1 nM down to the goal of 10 min, which was achieved with 500 nM DNA probe.

shown in **Fig. 3.2.2**, the hybridization time steadily decreased with increasing probe concentrations, starting from 5 h for 1 nM probe, and reaching the goal hybridization time of 10 min at a concentration of 500 nM. Molecular-size filtered preparations of the probes used at this concentration did not show significant presence of interfering fluorescent impurities.

3.2.3.3. Effects of Biological Samples on Probe Degradation

One of the great advantages of DQAMmiR is its ability to be applied directly to complex biological samples. Previous applications of DQAMmiR to cell lysate-containing mixtures, with the prolonged incubation times, required the use of masking DNA to suppress nuclease-facilitated degradation of the DNA probes. In order to prevent the formation of non-specific probe/masking DNA duplexes, and to avoid interference of masking DNA with formation of probe/target duplexes, both the sequence and the concentration of the masking DNA required

careful consideration. Furthermore, the use of high concentrations of masking DNA significantly raised DQAMmiR analysis cost.

With the achieved reduction in hybridization time, however, the need for masking DNA was re-examined. I studied the kinetics of DNA probe degradation within the context of a bacterial cell lysate. The choice of a bacterial cell lysate was intentional, as it displayed a higher extent of probe degradation when compared to mammalian cell lysate (**Fig. 3.2.3)**. The extent of DNA probe degradation, taken at 500 nM concentration, was assessed based on the decrease of the DNA peak area from CE analysis. No masking DNA was used. As seen in **Fig. 3.2.4,** 5-h incubation, without masking DNA, resulted in an unacceptable 60% level of probe degradation. Ten-minute incubation, however, resulted only in 4% degradation, which was lower than the

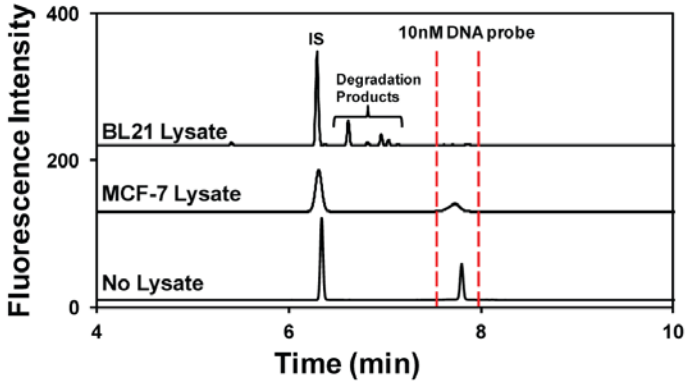

Figure 3.2.3. Comparison of DNA probe degradation by BL21 and MCF-7 cell lines. 10 nM DNA probe and 20 nM fluorescein were incubated with a bacterial cell lysate (BL21), a mammalian cell lysate (MCF-7), and no lysate for 60 min. The DNA probe was degraded with both cell lines as seen by the reduced DNA peak area between the two red dashed lines. The MCF-7 lysate caused a loss in DNA and the BL21 completely degraded the DNA probe. Degradation peaks are observed to the left of the DNA probe peak in the BL21 sample.

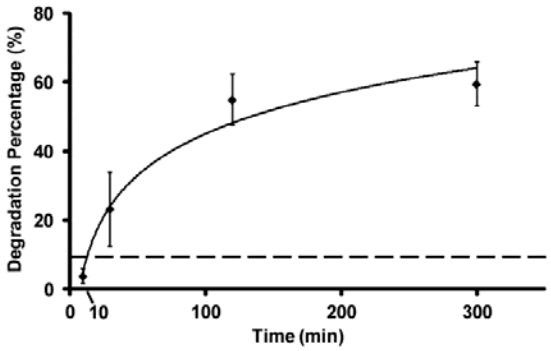

Figure 3.2.4. Degradation of DNA probe by cell lysate over time. 500 nM of miR-21 DNA probe was incubated with a bacterial cell lysate over various time periods. Using CE, degradation of the probe was determined based on the decrease in DNA peak area. Minimal degradation was observed after 10-min incubation. The dashed line represents the degradation level for 5-h incubation with the presence of masking DNA.

amount of degradation at 5-h incubation with added masking DNA (**Fig. 3.2.4,** dashed line). Furthermore, since SSB binds DNA non-specifically, the removal of masking DNA allowed a lower SSB concentration to be used. These results suggests that not only do our modifications to DQAMmiR remove the need for the masking DNA, but it also improves the robustness of the method.

3.2.3.4. Quantitation of miRNAs with Optimum Probe Concentration

To test the modified DQAMmiR method, I incubated 5 different miRNA-specific DNA probes, each at 500 nM, with their respective miRNAs for 10 min in the presence of bacterial cell

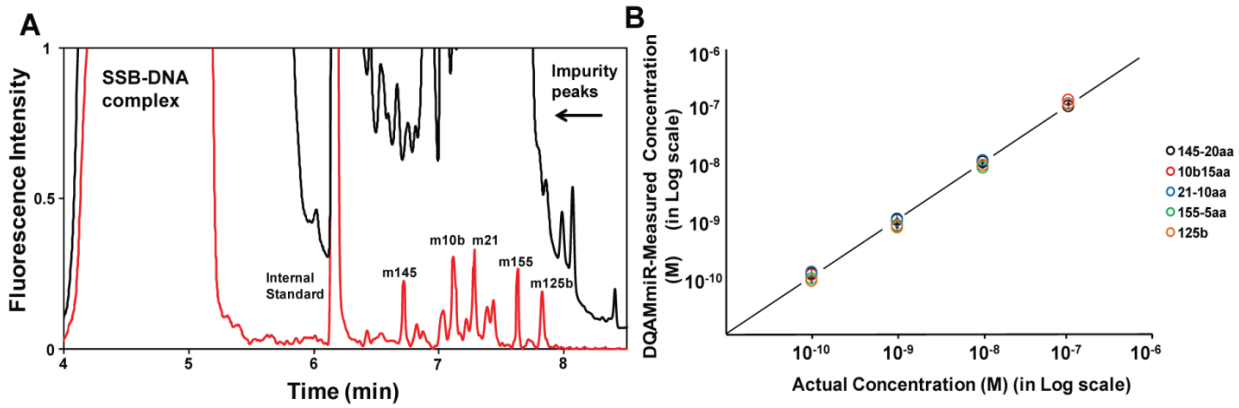

Figure 3.2.5. Separation, detection and quantitation of 5 miRNA species. 100 pM to 100 nM of miR-125b, 155, 21, 10b, 145 were incubated with 500 nM of their respective DNA-peptide probes (m125b, m155-5aa, m21-10aa, m10b-15aa, m145-20aa) in the presence of cell lysate for 10 min. **Panel A:** The detection of 100 pM of 5 DNA-miRNA hybrid peaks, along with the internal standard, fluorscein, and the SSB-DNA complex peak using the optimized protocol (red trace). For comparison (black trace), the previous DQAMmiR protocol (60 min incubation, with masking DNA, no filtering) was also used to detect 100 pM of 5 miRNA species. The large impurity peaks overlapping the hybrid peaks (black trace) prevented the detection and quantitation of the miRNAs. All hybrid peak areas were normalized by their respective quantum yields. **Panel B:** Quantitative analysis of 100 pM to 100 nM of all 5 miRNAs (miR-125b, 155, 21, 10b, and 145), with error bars included. Actual concentrations of miRNAs were determined by light absorbance at 260 nm.

lysate, without addition of masking DNA. The DNA probe preparation was subjected to molecular weight filtration prior to experiments which significantly reduced the impurity peaks in comparison to the previous DQAMmiR protocol (**Fig. 3.2.5A**). The increased concentrations of the DNA probe did not reveal significant interfering impurities, and did not affect the ability to separate and detect all 5 hybrid peaks. This allowed me to accurately quantify the miRNAs (**Fig. 3.2.5A)** in a short time**,** while maintaining the sensitivity and multiplexing ability of the method. The measurements were successfully repeated with varying concentrations of the 5 miRNA

targets, between 100 pM and 100 nM, showing that the dynamic range of the method spans over 3 orders of magnitude (**Fig. 3.2.5B)**. This shows that I was able to significantly improve on the deficiencies of the DQAMmiR method, while retaining all of its advantages.

3.2.4. Conclusions

I have presented a set of modifications to DQAMmiR method that make it more compatible with applications in a clinical setting. I have developed a quick and simple DNA probe purification procedure that significantly reduces the negative effect of interfering fluorescent impurities in the sample. I have optimized the hybridization probe concentration to reduce the overall assay time to approximately 20 min. The reduction in assay time also removed the need for masking DNA. The introduced modifications make DQAMmiR a much faster and more robust method for quantitation of multiple miRNAs. Furthermore I am now able to improve the LOD of DQAMmiR as I can pre-concentrate the sample to increase the hybrid peak heights. This would not have been achievable with the impurities present as any pre-concentration technique would cause the impurity peaks to increase in size as well. With the impurities no longer an issue I will now focus on improving the LOD of DQAMmiR by introducing a pre-concentration technique.

CHAPTER 4: HIGHLY-SENSITIVE AMPLIFICATION-FREE ANALYSIS OF MULTIPLE MIRNAS BY CAPILLARY ELECTROPHORESIS.

The presented material was published previously and reprinted with permission from "Wegman, D.W.; Ghasemi, F.; Khorshidi, A.; Yang, B.B.; Liu, S.K.; Yousef, G.M.; Krylov, S.N. Highly-sensitive amplification-free analysis of multiple miRNAs by capillary electrophoresis. *Anal Chem*, **2015**, *87*, 1404 – 1410". Copyright 2015 American Chemical Society. My contribution to the article was: (i) planning all experiments, (ii) performing all experiments, (iii) interpreting results, (iv) preparing all figures, (v) writing first draft of manuscript.

4.1. Introduction to Isotachophoresis

The concentration LOD of DQAMmiR using the most sensitive commercial CE instrument available is 100 pM of miRNAs, which is insufficient to detect low-abundance miRNAs.**[75]** Efforts from our group showed that decreasing concentration LOD through improving a fluorescence detector requires considerable development.**[79]** Therefore, to bring DQAMmiR closer to a practical approach for validation of miRNA signatures, I explored sample pre-concentration as a potential solution.

The requirement of keeping DQAMmiR's suitability for automation limits me to pre-concentration inside the capillary. Isotachophoresis (ITP) is an electrophoretic separation technique which can be used for analyte concentration.**[80-83]** Like other electrophoretic techniques, ITP separates molecules based on their electrophoretic mobility, μ, with the

migration velocity, U, of the molecules defined as $U = \mu E$ where E is the electric field strength. Unlike most other electrophoretic techniques, the electric field strength is not uniform throughout the capillary (defined as a discontinuous electrolyte system) as two buffers with different mobilities are used. A leading electrolyte (LE) is chosen with anions of greater mobility than the target analyte (miRNA-probe hybrids in our case) and a trailing electrolyte (TE) is chosen with anions of lesser mobility than the target analyte. When an electric field is applied the ions are separated based on mobility, with the LE anion speeding ahead, the TE anion falling behind and the target analyte being sandwiched in the middle. This initial separation process is quite fast and the zones of LE, sample, TE resolve quickly. Once the zones are separated the buffers and analytes migrate through the capillary at the same velocity, hence the name" iso" meaning "same" and "tacho" meaning "speed".

As mentioned, this is a discontinuous electrolyte system, which causes a non-uniform electric field throughout the capillary. According to a variation of Ohm's law $J = kE$, (where J is the current density, k is conductivity and E is electric field strength) when the current (and thus current density) is constant, the electric field strength will always be inversely proportional to the conductivity of the buffer (**Fig. 4.1**). Similar to mobility, LE has a greater conductivity and TE has a lower conductivity with respect to the target analyte. Thus, in the presence of LE there would be a lower electric field strength and in the presence of TE there would be a higher electric field strength. This discontinuous system, with varying electric field strengths causes the pre-concentration of the sample between the TE and LE. If a target analyte migrates into the LE zone it comes into contact with a lesser electric field and drops back into its respective zone

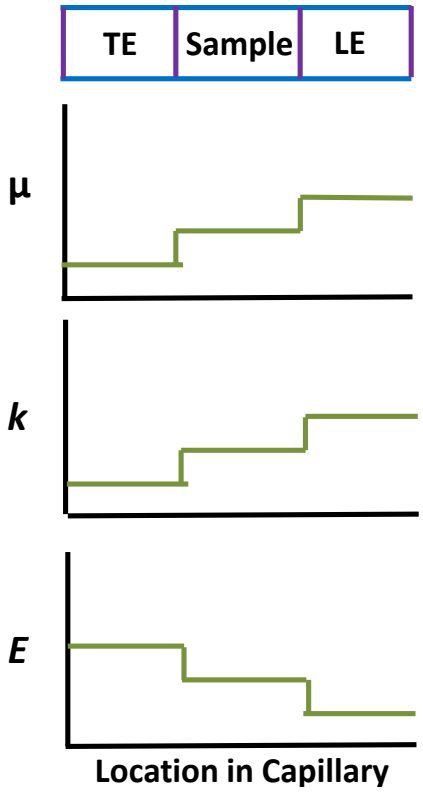

Figure 4.1 A comparison of mobility (μ), conductivity (*k*) and local electric field (*E*) throughout the capillary using a discontinuous electrolyte system containing a leading electrolyte (LE) and a trailing electrolyte (TE).

(**Fig. 4.2A**). Conversely, if the target analyte happens to fall back into the TE zone it comes into contact with a higher electric field strength and is pushed back into the narrow sample window.

To pre-concentrate a target analyte by ITP, a large fraction of the capillary is filled with the target sample sandwiched between the high-conductivity leading electrolyte (LE) and the low-conductivity trailing electrolyte (TE) (**Fig. 4.2B**). When an electric field is applied, over time the analytes focus on the interface between LE and TE causing a significant increase in local concentration.

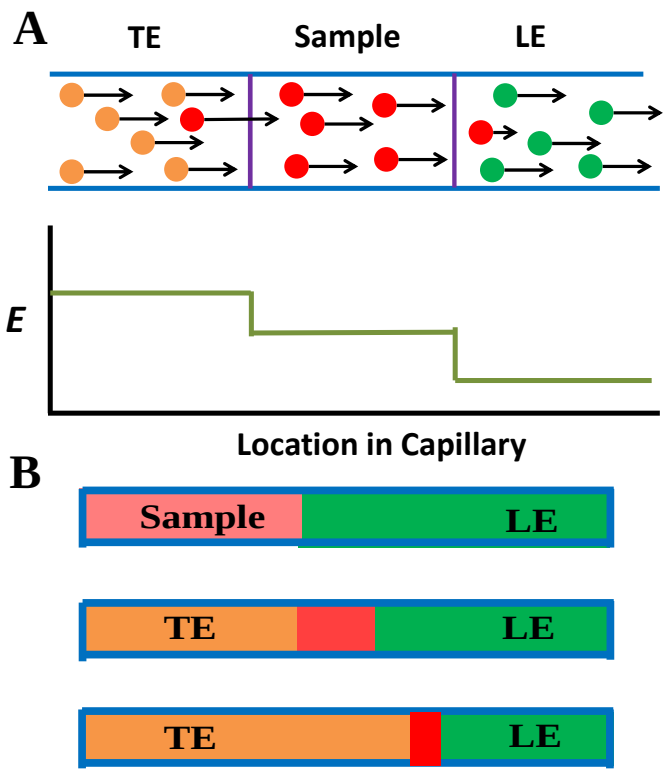

Figure 4.2. **Panel A:** In a discontinuous electrolyte system, when a voltage is applied the TE has a greater local electric field while the LE as a lower local electric field with respect to the target analyte. If the target analyte (red circles) falls back into the TE zone, it comes into contact with a higher electric field and is pushed back towards its narrow window. Similarly if a target analyte enters the LE zone, it falls back into the narrow window. **Panel B:** If a large sample is injected into the capillary sandwiched between LE and TE buffer, it will focus into a narrow window, increasing local concentration.

Santiago's group suggested the use of ITP for miRNAs analysis in a chip format with an impressive concentration LOD of 5 pM.**[80]** Even though their approach was only applicable to the analysis of a single miRNA,**[80, 81]** it motivated my attempt to combine ITP pre-concentration with DQAMmiR. My goal was to develop streamlined ITP-DQAMmiR which first pre-concentrates multiple hybrids and unreacted probes by ITP and then separates the probes

from the hybrids and hybrids from each other using DQAMmiR. **Fig. 4.3** depicts all essential steps of ITP-DQAMmiR with details described in the figure legend for convenience. I was able to successfully pre-concentrate, separate, and detect multiple miRNAs in a single capillary, using a commercial instrument with no manual steps required.

4.2. Materials and Methods

4.2.1. Oligonucleotides

All miRNAs and hybridization probes were custom-synthesized by IDT (Coralville, IA, USA). To allow separation of the 5 hybrid peaks, peptide drag tags of varying size were conjugated to the DNA probes via a thioether bond. The conjugation reaction, (described in **section 3.1.2.2**) occurs between a thiol group on the 5' end of the DNA probes and a maleimide group on the N terminus of each peptide. All maleimide modified peptides were synthesized by Canpeptide (Pointe-Clare, QUE, Canada). All miRNAs, DNA probe and peptide sequences can be found in **Table 4.1**.

4.2.2. Hybridization conditions.

Hybridization was carried out in Mastercycler 5332 thermocycler (Eppendorf, Hamburg, Germany). Working-stock solutions of DNA and miRNAs were kept at 37°C to reduce sticking to the test tube walls. Various concentrations of the five miRNA species (miR10b, miR21 miR125b, miR145, miR155) were incubated with 5 nM of their respective DNA probes along with 1 nM fluorescein (internal standard) and 10 nM Masking RNA in TE-hybridization buffer

(20 mM Tris, 10 mM HEPES, 10 mM NaCl, pH 8.3). The masking RNA was a tRNA library from baker's yeast from Sigma-Aldrich (Oakville, ON, Canada). Temperature was increased to a denaturing 80°C and then lowered to 37°C at a rate of 20°C/min and was held at 37°C for 1 h to allow annealing. To minimize miRNAs degradation, a nuclease-free environment was used while handling miRNAs samples.

Table 4.1. List of target miRNAs, their nucleotide sequences, sequences of corresponding DNA hybridization probes and their respective peptide drag tags.

Name of sequence	**miRNA Nucleotide sequence**	**Hybridization probe sequence with modifications**	**Peptide drag tag sequence**
mir-125b	5'-CCU GAG ACC CUA ACU UGU GA-3'	5'-ThiolC6S-S-TCA CAA GTT AGG GTC TCA GGG A-Alexa488-3'	none
mir-155	5'-UUA AUG CUA AUC GUG AUA GGG GU-3'	5'-ThiolC6S-S-ACC CCT ATC ACG ATT AGC ATT AA-Alexa488-3'	C-term-Gly-Ala-Gly-Thr-Gly-N term
mir-21	5'-UAG CUU AUC AGA CUG AUG UUG A-3'	5'-ThiolC6S-S-TCA ACA TCA GTC TGA TAA GCT A-Alexa488-3'	C-term-Gly-Ala-Gly-Thr-Gly-Gly-Ala-Gly-Thr-Gly-N term
mir-10b	5'-UAC CCU GUA GAA CCG AAU UUG UG-3'	5'-ThiolC6S-S CAC AAA TTC GGT TCT ACA GGG TA-Alexa488-3'	C-term-Gly-Ala-Gly-Thr-Gly-Gly-Ala-Gly-Thr-Gly-Gly-Ala-Gly-Thr-Gly-N term
mir-145	5'-GUC CAG UUU UCC CAG GAA UCC CU-3'	5'-Thiol C6S-S-AGG GAT TCC TGG GAA AAC TGG AC-Alexa488-3'	C-term-Gly-Ala-Gly-Thr-Gly-Gly-Ala-Gly-Thr-Gly-Gly-Ala-Gly-Thr-Gly-Gly-Ala-Gly-Thr-Gly-N term

4.2.3. ITP-DQAMmiR

I used a P/ACE MDQ capillary electrophoresis system (Beckman-Coulter, Fullerton, CA) with laser-induced fluorescence detection. I used bare fused-silica capillaries with an outer diameter of 365 μm, an inner diameter of 75 μm, and a total length of 79.4 cm. The distance from

the end of the capillary in Reservoir #1 (**Fig. 4.3**) to the detector was 69.0 cm. The capillary was flushed prior to every CE run with 0.1 M HCl, 0.1 M NaOH, deionized H_2O and TE buffer (20 mM Tris, 10 mM HEPES, pH 8.3) for one minute each. Samples were injected from Reservoir #2 by a pressure pulse of 3.0 psi (20.7 kPa) for 99 s. The volume of the injected sample was 1.9 μL. The buffer in Reservoir #2 was switched to LE buffer (50 mM Tris-Cl, 10 mM NaCl, pH 8.0) and electric field was applied in the reverse direction. Electrophoresis was driven by an electric field of 312.5 V/cm. The voltage was turned off at t_{cr} − 10 s, where t_{cr} is the predetermined "critical time-point" explained in **section 4.3.3**. The buffer in Reservoir #1 was switched to LE + 50 nM SSB and an electric field of 312.5 V/cm was applied in the forward direction. When the samples passed the detector, the fluorescence was excited with a 488 nm continuous wave solid-state laser (JDSU, Santa Rosa, CA, USA). Electropherograms were analyzed using 32 Karat Software. Peak areas were divided by the corresponding migration times to compensate for the dependence of the residence time in the detector on the electrophoretic velocity of species. Concentrations of miRNAs were determined using **eq. (2–8)**.

4.2.5. Spectrophotometric Determination of Target Concentration

MiRNA target concentration was determined by light absorption at 260 nm using the Nano-Drop ND-1000 Spectrophotometer (Thermo-Fisher Scientific). The stock concentration of the target was too high to measure directly, therefore, a small sample of the stock solution was serially diluted and absorbance of each sample at 260 nm was measured 3 times. The concentration of each sample was determined as $absorbance/\varepsilon l$ where ε is the molar extinction

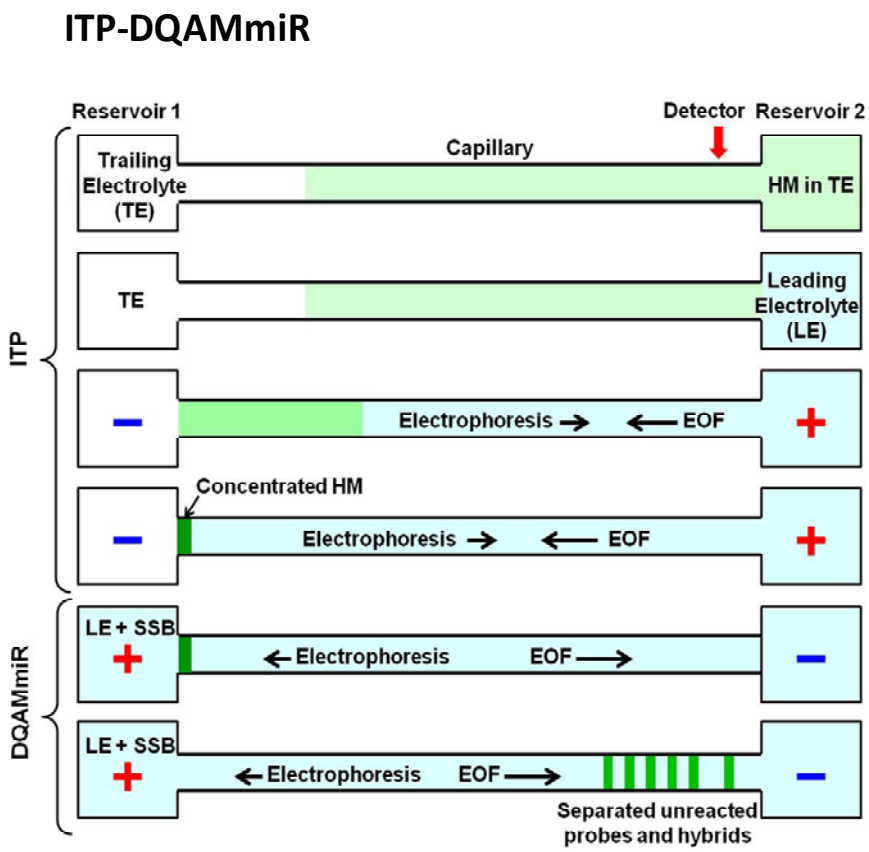

Figure 4.3. Conceptual depiction of streamlined combination of isotachophoresis (ITP) and DQAMmiR. The major stages of the ITP-DQAMmiR tandem analysis are shown. In the ITP stage, the capillary is pre-filled with a trailing electrolyte (TE) of low conductivity by a pressure-driven flow from Reservoir 1. The hybridization mixture (HM) is prepared in TE and a large predetermined part of the capillary is filled with HM by a pressure-driven flow from Reservoir 2 (detection end of the capillary). HM in Reservoir 2 is replaced with a leading electrolyte (LE) with high conductivity and a voltage is applied with positive electrode being in Reservoir 2. The electroosmotic flow (EOF) from positive to negative electrode is faster than the electrophoretic migration of the hybrids and probes in the opposite direction. This leads to the concentration of probes and hybrids inside the capillary near Reservoir 1. In the DQAMmiR stage, TE in Reservoir 1 is replaced with SSB-containing LE. The voltage is now applied with the positive electrode being in Reservoir 1. Continuously supplied SSB migrates faster than the probes and hybrids and overruns them. The latter facilitates SSB-driven separation of the unreacted probes from the hybrids.

coefficient of the RNA target at 260 nm (provided by IDT) and *l* is the optical path-length. Using the concentrations of the serial dilutions, the original stock concentration was extrapolated.

4.3. Results and Discussion

For ITP-DQAMmiR to work, its multiple steps shown in **Fig. 4.3** must be smoothly interfaced by choosing proper compositions, concentrations, and pH of LE and TE. Five requirements should be satisfied: (i) there should be no buffer mismatch between the final step in ITP and initial step in DQAMmiR, (ii) ITP should pre-concentrate all components of the hybridization mixture into a single narrow zone, (iii) electro-osmotic flow (EOF)-mediated analyte dispersion must be limited, (iv) SSB-mediated hybrid dissociation must be limited, and (v) the ITP step must be stopped when the concentrated hybridization mixture reaches the end of the capillary.

4.3.1. Selection of LE and TE Buffers

First, to avoid buffer mismatch, I required an LE for ITP that could also be used as the electrolyte in DQAMmiR. Matching the LE with the DQAMmiR run buffer turned out to be an easy task. Tris-Cl, which is a very common LE in ITP is also often used for CE separation. My attempt to use Tris-Cl as the run buffer in DQAMmiR was successful, as shown by the separation of 5 DNA probes with a resolution comparable to my previous work (**Fig. 4.4**).

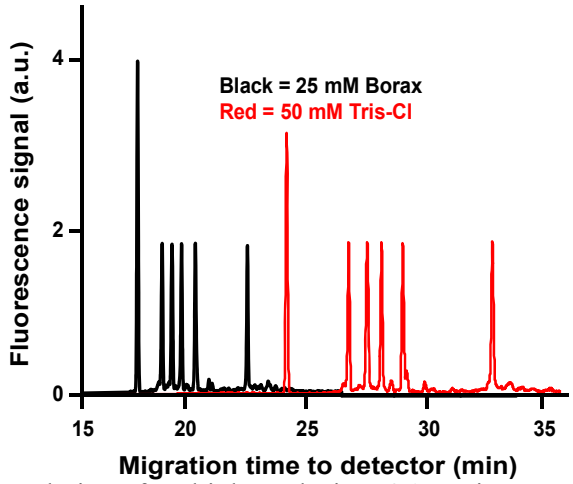

Figure 4.4. Compares the resolution of multiple peaks in DQAMmiR runs (without ITP) with either original DQAMmiR electrolyte (25 mM Borax) or LE (50 mM Tris-Cl). The sample for each run contained 10 nM fluorescein (left peak) and 5 nM of 5 DNA probes with peptide drag tags of 20, 15, 10, 5, and 0 amino acids in length, respectively, from left to right. The resolution of peaks was similar with both buffers

Second, pre-concentration of multiple analytes into a single narrow band requires that (i) the concentration of LE (and TE) be much greater than the cumulative concentration of all the analytes and (ii) the mobility difference between LE and TE is maximized.**[84]** Considering that the DNA probe and miRNAs concentrations are in the pM to nM range, the first requirement can be easily satisfied by using LE and TE concentrations in the mM range. Since I had already chosen Tris-Cl as an LE, satisfying the second requirement depended solely on the choice of TE - the mobility of TE should be as low as possible. Tris-HEPES is known to have a lower mobility than most other TE buffers used with ITP of nucleic acids.**[81]** With the use of mM amounts of Tris-Cl and Tris-HEPES as LE and TE, respectively, I successfully pre-concentrated all target analytes, observed by the single, narrow peak in an ITP-only run (**Fig. 4.5**).

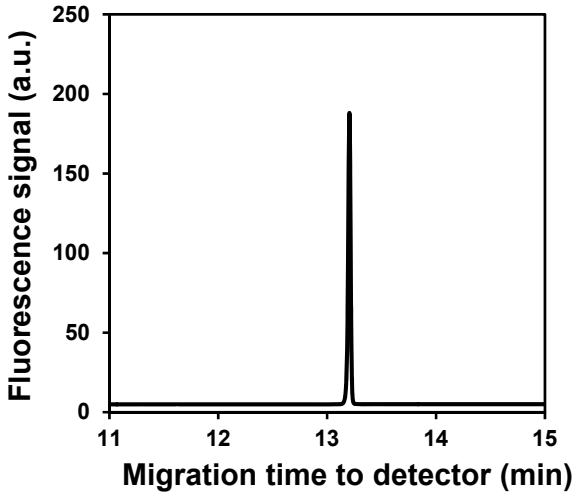

Figure 4.5. ITP concentration of all target analytes. A sample containing 1 nM mir125b, 155, 21, 10b and 145, 1 nM fluorescein and 10 nM of all 5 respective DNA-peptide probes was injected into a capillary. A voltage was applied and ITP was performed using 50 mM Tris-Cl, pH 8.0 as LE and 20-10 mM Tris-HEPES, pH 8.3 as TE. All target analytes were concentrated into a narrow zone between the two buffers, as depicted by the sharp single peak.

4.3.2. Optimization of Buffer Composition, pH and Concentration

Third, with my chosen buffers I required optimum pH and ionic strengths that would limit any ITP disruption and dispersion by EOF. Slight changes in pH and ionic strength of the buffers not only affect ITP focusing but can also affect the EOF velocity, changing the effective length of ITP separation and potentially causing analyte dispersion.**[84]** Thus, by varying concentration within the predetermined mM range and pH within the Tris buffering range (pK_a = 8.2) I was able to find the optimum conditions for pre-concentration of multiple analytes by ITP (**Fig. 4.6**).

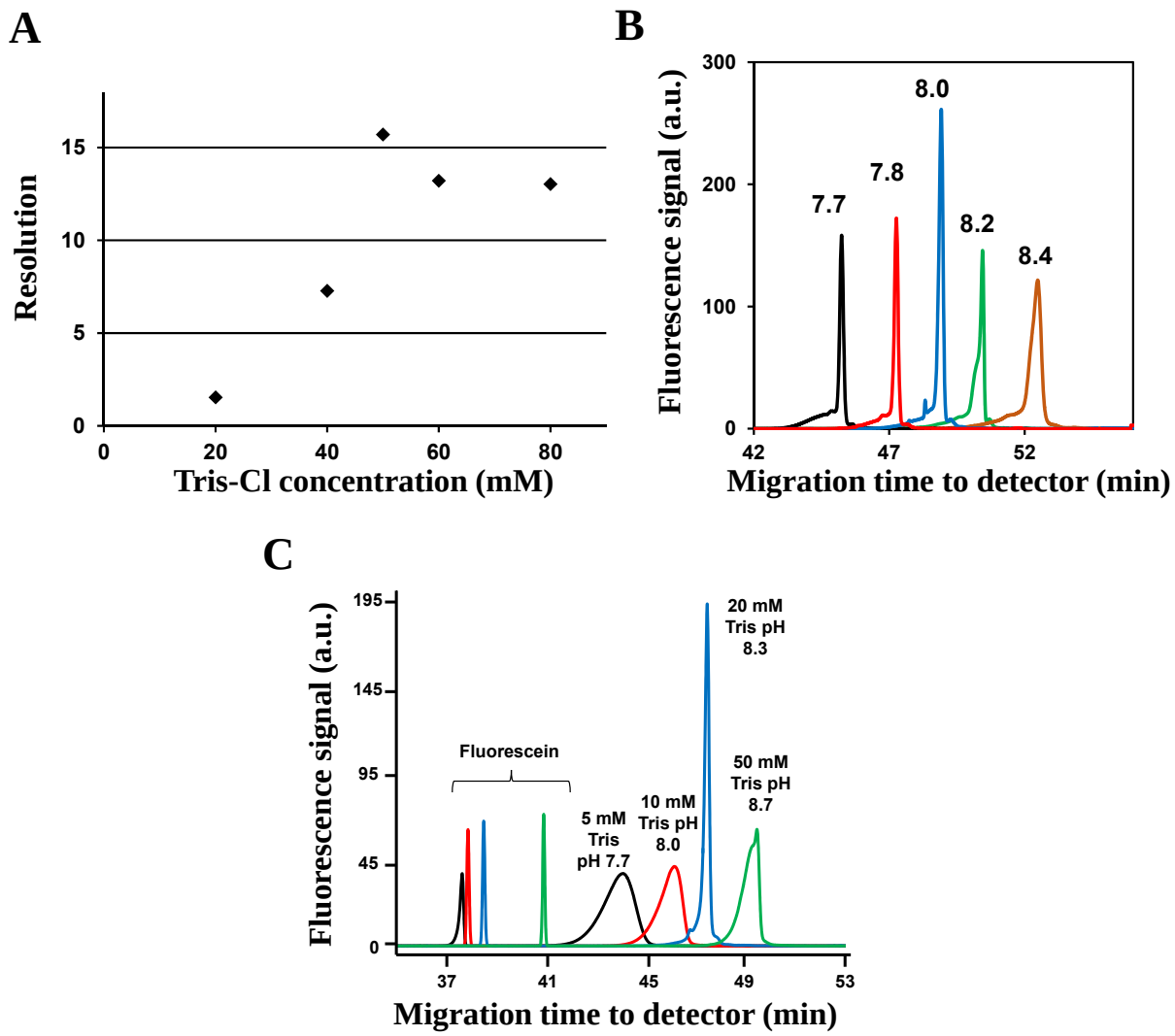

Figure 4.6. Optimization of LE (**A,B**) and TE **(C**) concentration and pH. **Panel A:** ITP-DQAMmiR was performed on a 1 nM 125 DNA, 1 nM fluorescein sample using an LE buffer with varying Tris-Cl concentration. Resolution between the fluorescein and DNA probe peak was measured. The greatest resolution occurred when using 50 mM Tris-Cl. **Panel B:** ITP-DQAMmiR was performed on a 1 nM 125 DNA, 1 nM fluorescein sample using 50 mM Tris-Cl LE buffer with pH ranging from 7.7 – 8.4. The highest, sharpest peak (as well as greatest resolution, not shown) occurred with pH 8.0. It should be noted that TE was not optimized at this point, which explains the significant peak fronting. **Panel C** ITP-DQAMmiR was performed on 1 nM fluorescein and 1 nM miR125b DNA sample using TE buffer with varying concentration and pH. The greatest resolution and narrowest peaks were observed with 20 mM Tris and 10 mM HEPES, pH 8.3.

Fourth, SSB has the ability to dissociate weakly-bound hybrids especially in low-ionic-strength buffers.**[85]** Thus, in DQAMmiR, the incubation buffer (20 mM Tris, 10 mM HEPES, pH 8.3) must include a sufficient concentration of salt to stabilize the hybrid. The inclusion of extra salt (NaCl in this case), on the other hand, alters the conductivity of the buffers and my challenge was to introduce NaCl without affecting ITP pre-concentration. To maintain optimum pre-concentration by ITP I needed to find the minimum required concentration of NaCl that would prevent SSB-mediated hybrid dissociation. I included a range of NaCl concentrations (0-100 mM) to the incubation buffer (IB) and ran SSB-mediated CE to test if the hybrid peak was present (**Fig. 4.7**). The minimum concentration of NaCl in IB that maintained hybrid integrity was 10 mM. NaCl was only added to IB and LE as adding chloride ion (leading electrolyte) in TE buffer disrupts the ITP process.

4.3.3. Determination of "Critical" Point

Fifth and final, in ITP-DQAMmiR, the pre-concentrated hybridization mixture should be stopped before leaving the capillary so that the following separation of its components in the opposite direction could be accomplished. My task was to find a way to stop ITP in a robust fashion before the concentrated sample leaves the capillary with as little residual TE remaining as possible as it could deteriorate the quality of CE separation. After exploring a number of options I focused on the value of electrical current as an indicator of ITP stop time, t_{st} similar to Reinhoud's work in the early 90's.**[86]** The displacement of TE with LE during ITP is accompanied by gradually increasing electrical current. There is a "critical" point, t_{cr}, on the

current versus time dependence where the slope abruptly changes from finite to zero (**Fig. 4.8A**).This time likely corresponds to the moment of the completion of electrolyte displacement. Importantly, t_{cr} was very stable; its deviation was only 0.4% or 4 s. I thus decided to relate t_{st} to

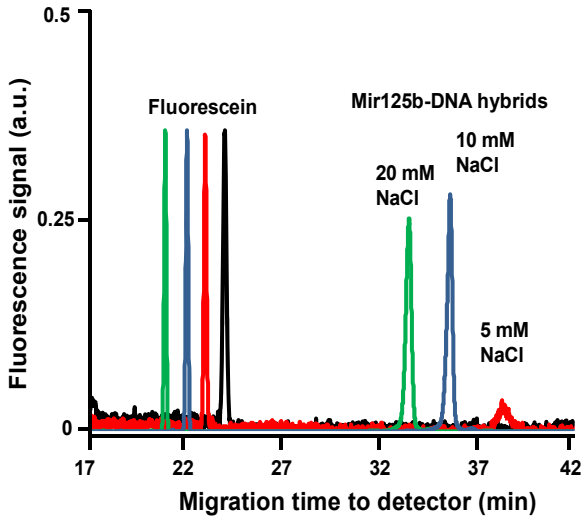

Figure 4.7. The determination of the minimum NaCl concentration required in incubation buffer to prevent SSB-mediated hybrid dissociation. A range of NaCl concentrations (0-100 nM) were added to TE and used as incubation buffer for hybridization mixture. SSB-mediated DQAMmiR was performed with a sample containing 10 nM miR125b DNA probe, 1 nM miR125b, and 1 nM fluorescein, and hybrid peak areas were assessed. The minimum NaCl concentration that prevented hybrid dissociation (manifested by decreasing hybrid peak area) was 10 mM. To note, the black trace contains 0 mM NaCl and did not produce a hybrid peak. Hybrid peaks for NaCl concentrations higher than 20 mM were not observed due to the disruption of the ITP process (the hybrid could not reach the detection end of the capillary).

this critical point. I studied how stopping ITP at different times $t_{st} = t_{cr} \pm x$, where x varied between –60 and +60 s with an increment of 5 s, would influence resolution between the fluorescein peak and miR125b DNA probe peak. I wanted to find the optimum ITP time, defined

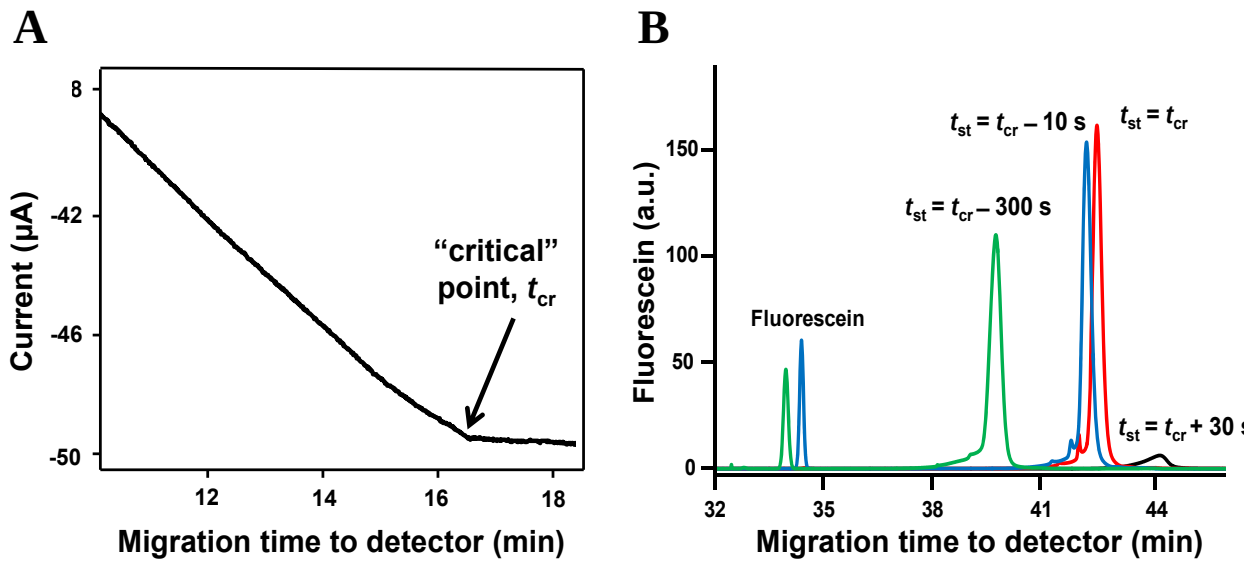

Figure 4.8. Determining the "critical" point, t_{cr}, of ITP-DQAMmiR. **Panel A:** A current versus time plot is shown for a typical ITP-DQAMmiR run, focusing on the "critical" time-point. During ITP, the displacement of TE with LE is observed with a gradually increasing electrical current. ITP is run in the reverse direction, as such, the current is negative. The t_{cr}, is observed with an arrow, indicating the time where the slope abruptly changes from finite to zero. **Panel B** illustrates the determination of optimum ITP stop time (t_{st}), the time point at which the concentrated sample nears the end of the capillary and maximum resolution is achieved without any loss of sample. I varied t_{st} with respect to the "critical" point (t_{cr}), the time-point at which the current versus time slope abruptly changes to zero. Using a sample containing 1 nM fluorescein and 10 nM miR125b DNA probe we found that $t_{st} = t_{cr} - 10$ s had the greatest resolution without the loss of DNA or fluorescein (as observed in the $t_{st} = t_{cr}$ run).

as the time at which maximum peak resolution occurs without the loss of any sample. ITP times considerably (300 s) shorter than t_{cr} led to lowered resolution while longer ITP times led to hybridization mixture elution from the capillary and loss of target analytes. I found that stopping ITP at $t_{st} = t_{cr} - 10$ s achieved maximum resolution without the loss of any target analytes (**Fig. 4.8B**). I used $t_{st} = t_{cr} - 10$ s to automatically stop ITP and start CE separation by changing the

polarity. The observed consistency of the optimum ITP time using different capillaries (of the same length) on different days allowed for the automation of this process.

4.3.4. LOD Improvement with ITP

After resolving the challenges of combining ITP with DQAMmiR I could study the performance of ITP-DQAMmiR. The first aspect to assess was the concentration LOD. I compared peaks of a hybrid for DQAMmiR and ITP-DQAMmiR. The minimum concentration of miRNAs that could be detected by DQAMmiR was 100 pM while ITP-DQAMmiR could detect as low as 1 pM miRNA (**Fig. 4.9**). Slight differences in DNA probe fluorescent intensity prevented all miRNAs from achieving 1 pM LOD, however they all achieved an LOD of 5 pM or lower. Thus, with ITP-DQAMmiR, I was able to improve the LOD 100 times in comparison to the LOD of DQAMmiR alone with only a 35 minute increase in overall assay time. The 100 times improvement was consistent with the increase in hybridization mixture volume injected; in DQAMmiR it was 14 nL while in ITP-DQAMmiR it was 1.9 μL. This suggests that increasing the capillary length can lead to even lower LODs, though this would inherently be linked with an increase in total assay time.

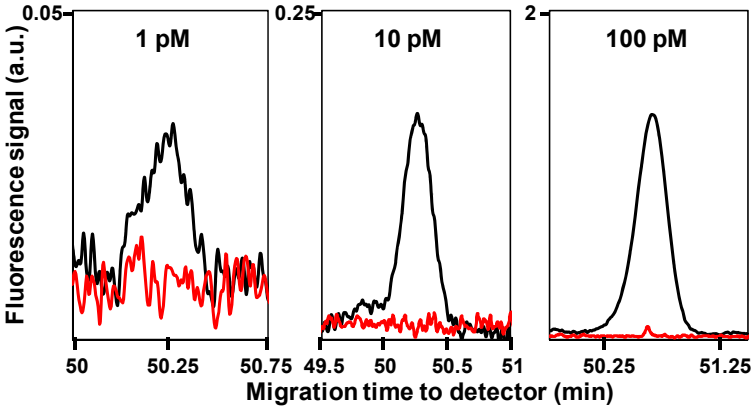

Figure 4.9. Comparison of limit of detection between DQAMmiR (red trace) and ITP-DQAMmiR (black trace). Each peak represents the hybrid of varying miR125b concentrations (1, 10, and 100 pM) with 5 nM of its respective DNA probe. DQAMmiR could only detect 100 pM miR125b while ITP-DQAMmiR detected 1 pM miR125b, a 100 times improvement.

4.3.5. Quantitation of miRNAs in Low pM Concentrations

The second aspect investigated was the accurate quantitation of multiple miRNAs in ITP-DQAMmiR. Interestingly, the resolution between hybrid peaks achieved with ITP-DQAMmiR was greater than the resolution achieved with DQAMmiR. Such excellent resolution potentially allows ITP-DQAMmiR to simultaneously detect up to 25 miRNAs. As a proof of principle, the separation of 5 distinct hybrid peaks (**Fig. 4.10A**) allowed me to accurately quantitate 5 miRNA species over a dynamic range of 1 to 1000 pM (**Fig. 4.10B**). Thus, I was able to accurately quantitate multiple miRNAs in the low pM range without affecting dynamic range.

4.3.6. Detection of Low Abundance MiRNAs

Finally, I applied ITP-DQAMmiR to the analysis of multiple miRNAs from a biological sample. In my previous work,**[75]** I was only able to detect the highly abundant miR21, whose peak was close to the limit of detection. With ITP-DQAMmiR the goal was to shift the dynamic

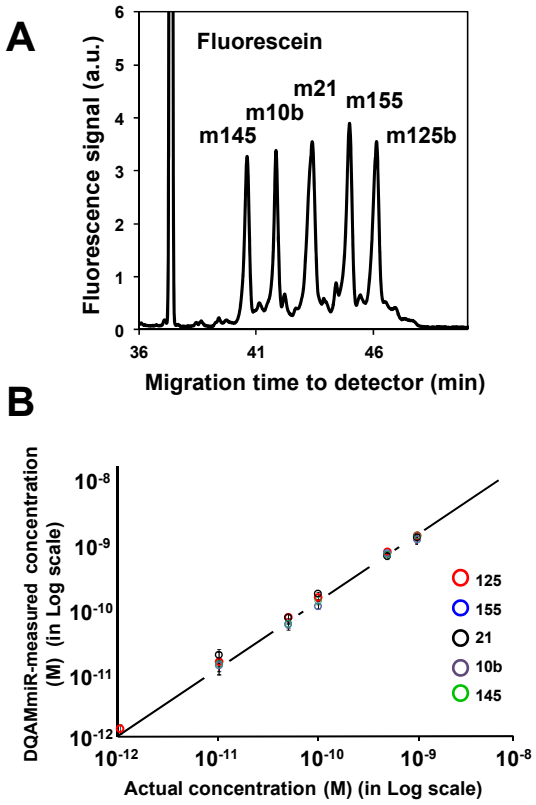

Figure 4.10. Separation, detection, and quantitation of 5 miRNA species. **Panel A** shows the detection of 5 DNA−miRNA hybrid peaks, along with the internal standard, fluorescein using ITP-DQAMmiR. All hybrid peak areas were normalized by their respective quantum yields. **Panel B** Quantitative analysis of 1 pM to 1 nM of all 5 miRNAs (miR-125b, 155, 21, 10b, and 145), with error bars included. Concentrations of miRNAs were validated by light absorbance of the miRNAs stock solution at 260 nm. Each data point is based on 3 measurements. Error bars represent a standard deviation.

range to allow the detection of low abundant miRNAs while still being able to detect the highly abundant miRNAs without oversaturation of the detectors. I achieved this which is demonstrated by simultaneously detecting highly abundant (miR21) and low abundant (miR155 and miR125b) miRNAs**[18, 87, 88]** from a MCF-7 RNA extract sample (**Fig. 4.11**). With the low-abundance miRNAs close to the limit of detection and the miR21 peak not oversaturated, it shows that I can now detect low, mid and high abundance miRNAs simultaneously. Known concentrations of the three miRNAs were spiked into the RNA extract samples to account for any effects the RNA extract matrix had on quantification, which was found to be negligible (data not shown). The ability to detect the majority of miRNA species shows that ITP-DQAMmiR is one step closer to its use in the validation of miRNA signatures. Such signatures (tentative) are selected from large

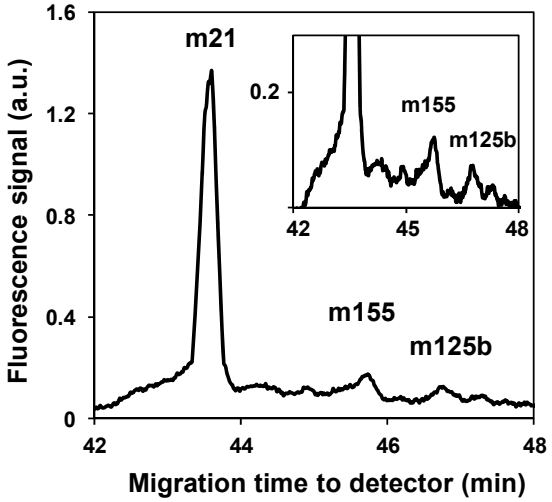

Figure 4.11. Detection of multiple miRNAs from a biological sample using ITP-DQAMmiR. An MCF-7 RNA extract was incubated with 5 nM of the respective probes for miR125b, miR155 and miR21. ITP-DQAMmiR was performed as previously explained. Both the highly abundant miR21 and low abundant miR155 and miR125b were detected in the same run.

sets of miRNAs. Essentially, the choice of miRNAs for a tentative signature would depend on whether or not it can be reliably detected. Since I can now detect a large range of biologically-relevant concentrations, it makes it much easier to choose the miRNAs for the tentative fingerprint.

4.4. Conclusion

I have demonstrated the successful combination of ITP and DQAMmiR in a single capillary using a commercial instrument for simultaneous analysis of multiple miRNAs. This allows for the fully automated pre-concentration, separation, and quantitation of multiple miRNAs in a single experiment. I was able to detect miRNAs amounts in the low pM range with an LOD of 1 pM, which is a 100-time improvement over the best previous result with DQAMmiR. I have optimized a compatible set of buffers which allowed for both ITP and DQAMmiR to be performed without hindrance. The ability to pre-concentrate and separate multiple miRNAs makes ITP-DQAMmiR a viable method for use in the validation of miRNA signatures. This improvement to the LOD takes DQAMmiR another step towards use in a clinical setting, with the final hurdle left being the ability to achieve 1-nt specificity of multiple miRNAs.

CHAPTER 5: ACHIEVING SINGLE-NUCLEOTIDE SPECIFICITY IN DIRECT QUANTITATIVE ANALYSIS OF MULTIPLE MIRNAS (DQAMMIR)

The presented material was published previously and reprinted with permission from "Wegman, D.W.; Ghasemi, F.; Stasheuski, A.; Khorshidi, A.; Yang, B.B.; Liu, S.K.; Yousef, G.M.; Krylov, S.N. Achieving single-nucleotide specificity in direct quantitative analysis of multiple microRNAs (DQAMmiR). *Anal Chem*, **2016**, *88*, 2472 – 2477". Copyright 2016 American Chemical Society. My contribution to the article was: (i) planning all experiments, (ii) performing all experiments, (iii) interpreting results, (iv) preparing all figures, (v) writing first draft of manuscript.

5.1. Introduction to LNA Bases

The remaining limitation of DQAMmiR is the inability to achieve 1-nt specificity for multiple miRNAs. An inherent problem with any miRNAs hybridization assay is that there is a wide variance in melting temperatures for the different miRNA-DNA hybrids. Each DNA probe has a specific temperature at which target miRNA binding occurs while non-specific binding does not. Thus, for the detection of multiple miRNAs with 1-nt specificity, a single hybridization temperature should be used. To solve this problem, I incorporated locked nucleic acid (LNA) bases into our DNA probes. LNA bases are modified RNA nucleotides, that are "locked" into a conformation that enhances base stacking, thus improving strength of hybridization. The addition of a single LNA base can increase the melting temperature of a hybrid by 2–4°C.**[89]** By varying

the number of LNA bases in each of the DNA probes I can equalize the melting temperatures of all the respective hybrids, allowing for 1-nt sensitivity of multiple miRNAs.**[89]** LNA bases have been previously used to achieve 1-nt sensitivity in analyses of multiple miRNAs showing that specificity can be achieve by equalizing the melting temperatures of all target hybrids.**[90, 91]**

Achieving such specificity with DQAMmiR, however, is not a trivial matter, requiring both the ability to dissociate all respective mismatches from their respective probes at a single temperature and the maintenance of this temperature at the locations of the capillary where mismatches and DNA probes are both present and able to interact. Here I resolve these issues by (i) introducing (LNA) bases to the DNA probes as explained and (ii) introducing a novel dual-temperature technique designed to support proper hybridization at the injection end of the capillary while using a lower temperature during the main part of CE separation.

The introduction of both LNA-DNA probes and the dual-temperature technique, explained in detail later, allowed me to achieve 1-nt specificity while maintaining the ability to separate and accurately quantitate multiple miRNAs.

5.2. Materials and Methods

5.2.1. Oligonucleotides

All miRNAs and mismatch RNAs were custom-synthesized by IDT (Coralville, IA, USA). All LNA-DNA probes were custom-synthesized by Exiqon (Woburn, MA, USA), with a 3’ FAM (6-fluorescein amidite) for detection and a 5’ thiol group for conjugation with peptide drag tags. Each probe had an RNA-specific melting temperature of 83°C. To allow separation of

the 5 hybrids, 4 peptide drag tags of varying lengths were conjugated to the LNA-DNA probes *via* a thioether bond. The conjugation reaction, (described in **section 3.1.2.2**) occurred between the thiol group on the 5' end of the LNA-DNA probes and a maleimide group on the N-terminus of the peptide drag tags. All maleimide modified peptides were synthesized by Canpeptide (Pointe-Clare, QC, Canada). The sequences of all miRNAs, mismatch RNAs, LNA-DNA probes, and peptides can be found in **Table 5.1**.

Table 5.1. List of target miRNAs, their nucleotide sequences, their respective single nucleotide mismatch sequence with mismatch highlighted in red, sequences of corresponding LNA-DNA hybridization probes and their respective peptide drag tags. As it is proprietary information to Exiqon, I do not know the locations or the number of LNA bases in each probe. I did ensure that there were multiple LNA-free stretches of at least 3 DNA bases in each probe to allow proper SSB binding.

Name of sequence	**miRNA Nucleotide sequence**	**Single nucleotide mismatch sequence**	**Hybridization probe sequence with modifications**	**Peptide drag tag sequence**
mir-21	5'-UAG CUU AUC AGA CUG AUG UUG A-3'	5'-UAG CUU AUC A**U**A CUG AUG UUG A-3'	5'-ThiolC6S-S-TCA ACA TCA GTC TGA TAA GCT A-FAM-3'	none
mir-125b	5'-UCC CUG AGA CCC UAA CUU GUG A-3'	5'-UCC CUG AGA **A**CC UAA CUU GUG A-3'	5'-ThiolC6S-S-TCA CAA GTT AGG GTC TCA GGG A-FAM-3'	C-term-Gly-Ala-Gly-Thr-Gly-N term
mir-145	5'-GUC CAG UUU UCC CAG GAA UCC CU-3'	5'-GUC CAG UUU UC**A** CAG GAA UCC CU-3'	5'-Thiol C6S-S-AGG GAT TCC TGG GAA AAC TGG AC-FAM-3'	C-term-Gly-Ala-Gly-Thr-Gly-Gly-Ala-Gly-Thr-Gly-N term
mir-155	5'-UUA AUG CUA AUC GUG AUA GGG GU-3'	5'-UUA AUG CUA AUC **C**UG AUA GGG GU-3'	5'-ThiolC6S-S-ACC CCT ATC ACG ATT AGC ATT AA-FAM-3'	C-term-Gly-Ala-Gly-Thr-Gly-Gly-Ala-Gly-Thr-Gly-Gly-Ala-Gly-Thr-Gly-N term
mir-10b	5'-UAC CCU GUA GAA CCG AAU UUG UG-3'	5'-UAC CCU GUA GA**A** CCG AAU UUG UG-3'	5'-ThiolC6S-S CAC AAA TTC GGT TCT ACA GGG TA-FAM-3'	C-term-Gly-Ala-Gly-Thr-Gly-Gly-Ala-Gly-Thr-Gly-Gly-Ala-Gly-Thr-Gly-Gly-Ala-Gly-Thr-Gly-N term

5.2.2. Hybridization conditions

Hybridization was carried out in Mastercycler 5332 thermocycler (Eppendorf, Hamburg, Germany). Working-stock solutions of LNA-DNA probes and miRNAs were kept at 37°C to reduce sticking to the test tube walls. Various concentrations of the five miRNA species (miR10b, miR21, miR125b, miR145, and miR155) were incubated with 500 nM of their respective DNA or LNA-DNA probes along with 10 nM fluorescein (internal standard) in incubation buffer (50 mM Tris-acetate, 50 mM NaCl, 10 mM EDTA, pH 8.2). Temperature was increased to a denaturing 80°C and then lowered to 57°C at a rate of 20°C/min and was held at 57°C for 10 min to allow hybridization. To minimize miRNAs degradation, a nuclease-free environment was used while handling miRNAs samples.

5.2.3. CE-LIF

I used a P/ACE MDQ capillary electrophoresis system (Beckman-Coulter, Fullerton, CA) with laser-induced fluorescence detection. I used bare fused-silica capillaries with an outer diameter of 365 μm, an inner diameter of 75 μm, and a total length of 79.4 cm. The distance from the injection end of the capillary to the fluorescence detector was 69.0 cm. The temperature was set at 37°C when using DNA probes and 57°C when using LNA-DNA probes. The capillary was flushed prior to every CE run with 0.1 M HCl, 0.1 M NaOH, deionized H_2O and run buffer (25 mM Borax, pH 9.2 containing 100 nM SSB) for 1 min each. Samples were injected by a pressure pulse of 0.5 psi (3.45 kPa) for 5 s. The volume of the injected sample was ~14 nL. Electrophoresis was driven by an electric field of 378 V/cm (positive electrode at the injection

end). Laser-induced fluorescence of the FAM label was used for detection; a continuous wave solid-state laser emitting at 488 nm (JDSU, Santa Rosa, CA, USA) was used as an excitation source. Electropherograms were analyzed using 32 Karat Software. For dual-temperature DQAMmiR the capillary was set at 57°C for the first 2 min after injection of the sample. The voltage was then shut off, and the capillary was allowed to cool down to 20°C (which took 7 min). Once the capillary temperature reached 20°C the voltage was reapplied and the run continued until the samples passed the detector.

5.2.4. ITP-DQAMmiR

The ITP-DQAMmiR experiments were performed using the same length capillary as previously mentioned with an initial temperature of 20°C. The capillary was flushed prior to every CE run with 0.1 M HCl, 0.1 M NaOH, deionized H_2O and TE buffer (20 mM Tris, 10 mM HEPES, pH 8.3) for 1 min each. Varying concentrations of target miRNAs or the 1-nt mismatches were incubated with 10 nM of their respective LNA-DNA probes and were injected from the outlet end by a pressure pulse of 3.0 psi (20.7 kPa) for 99 s. The volume of the injected sample was 1.9 µL. The buffer in the outlet end was switched to LE buffer (50 mM Tris-Cl, 10 mM NaCl, pH 8.0), and an electric field was applied in the reverse direction (negative electrode at the injection end). Electrophoresis was driven by an electric field of 378 V/cm. The voltage was turned off at t_{cr} − 10 s, where t_{cr} is the predetermined "critical time-point" explained in chapter 4.**[92]** The capillary was allowed to heat up to 57°C (which took 8 min) and kept at 57°C for 10 min to allow annealing. The buffer in the inlet end was switched to LE supplemented

with 100 nM SSB. An electric field of 378 V/cm was applied in the forward direction (positive electrode at the injection end) for 2 min at 57°C. The voltage was then shut off, and the capillary was allowed to cool down to 20°C (which took 7 min). Once the capillary temperature reached 20°C the voltage was reapplied and the run continued until the electrophoretic zones of all miRNA-probe hybrids passed the detector. Peak areas were divided by the corresponding migration times to compensate for the dependence of the residence time in the detector on the electrophoretic velocity of species. Concentrations of miRNAs were determined using **eq.** (**2**–**8)**.

5.2.5. Spectrophotometric Determination of Target Concentration

MiRNA target concentration was determined by light absorption at 260 nm using the Nano-Drop ND-1000 Spectrophotometer (Thermo-Fisher Scientific). The stock concentration of the target was too high to measure directly, therefore, a small sample of the stock solution was serially diluted and absorbance of each sample at 260 nm was measured 3 times. The concentration of each sample was determined as $absorbance/\varepsilon l$ where ε is the molar extinction coefficient of the RNA target at 260 nm (provided by IDT) and l is the optical path-length. Using the concentrations of the serial dilutions, the original stock concentration was extrapolated.

5.3. Results and Discussion

Prior to the 1-nt experiments I first had to show that I could use these LNA-DNA probes with the DQAMmiR method as it is known that SSB cannot bind to LNA oligonucleotides.**[93]** I determined that the LNA bases had no detrimental effects on the LNA-DNA probe's ability to

bind to SSB as there were a sufficient number of DNA bases in each probe to allow SSB binding (data not shown).

5.3.1. Determination of Hybridization Temperature

I next had to find the hybridization temperature that allowed for differentiation between the target miRNAs and their respective 1-nt mismatch for each LNA-DNA probe. Commonly

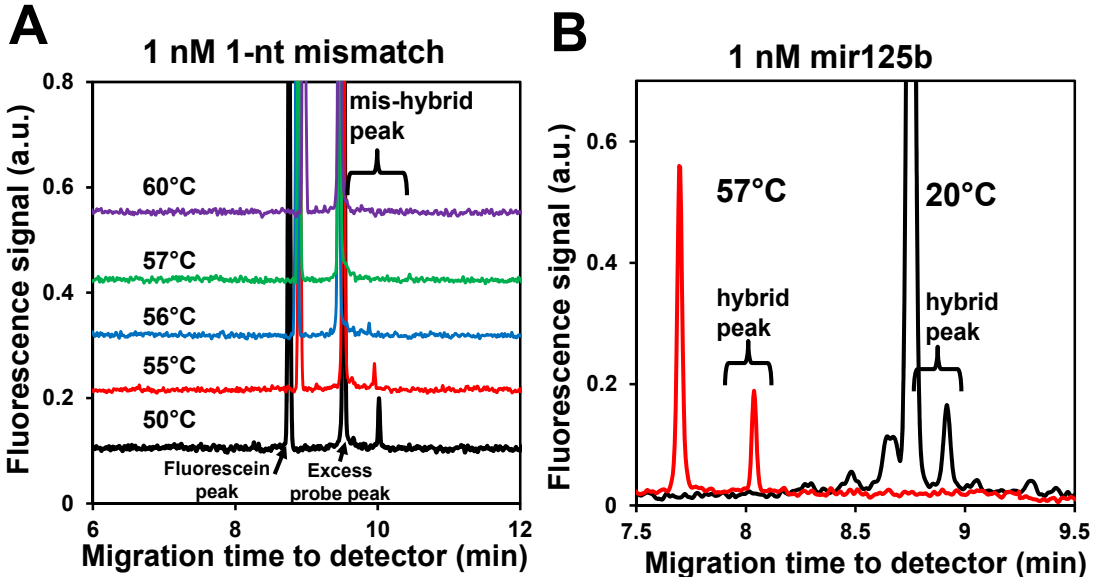

Figure 5.1. Optimization of capillary temperature to allow for 1-nt specificity. **Panel A:** 1 nM of a 1-nt mismatch of mir125b was incubated with 10 nM mir125b-specific LNA-DNA probe and injected into the capillary at varying temperatures. The mismatch hybrid peak was present at temperatures below 57°C, indicating that no mismatch binding occurs at 57°C or higher. **Panel B:** 1 nM of mir125b was incubated with 10 nM mir125b-specific LNA–DNA probe and injected into the capillary at 57°C (red trace) and 1 nM of mir125b was incubated with 100 nM mir125b-specific LNA–DNA probe and injected into the capillary at 20°C (black trace) to determine if complete hybridization still occurred at 57°C. The 57°C hybrid peak was comparable to the 20°C hybrid peak indicating that complete hybridization occurs at 57°C. This showed that a capillary temperature of 57°C can achieve 1-nt specificity.

this is estimated to be 30°C below the melting temperature.**[94]** When determining the optimum temperature I also had to consider the loss of peak resolution in CE due to peak broadening, caused by increasing capillary temperatures.**[95]** With this taken into account the optimum temperature was defined as the lowest temperature at which differentiation between the miRNAs and a 1-nt mismatch occurs. To determine the optimum temperature I gradually increased the capillary temperature until it reached the point (which was found to be 57°C) at which the 1-nt mismatch could no longer bind to the LNA probe causing an absence of the respective "mis-hybrid" peak. I then confirmed that the miRNAs could still fully bind to the LNA probe at 57°C by comparing peak areas with the miRNA-probe hybrid at our typical ambient temperature of 20°C (**Fig. 5.1**). It should be noted that I could not just incubate the sample at 57°C prior to its injection into a capillary at 20°C. I found that the hybridization of LNA-DNA probes to miRNAs was so fast that the probes began binding to the mismatches inside the capillary even when a voltage was applied immediately after sample injection (with a 15-s instrument-induced delay). Thus, I required the capillary to be set at 57°C, which would maintain the dissociation between the probes and their respective 1-nt mismatches.

5.3.2. 1-nt Specificity Using LNA-DNA Probes

With the optimum hybridization temperature determined I compared the specificity of multiple miRNAs both with LNA-DNA probes and with DNA probes. When using DNA probes (and pre-determined optimum temperature for one of the miRNA hybrids) the differentiation of even as few as two miRNAs *vs* their respective 1-nt mismatches could not be achieved

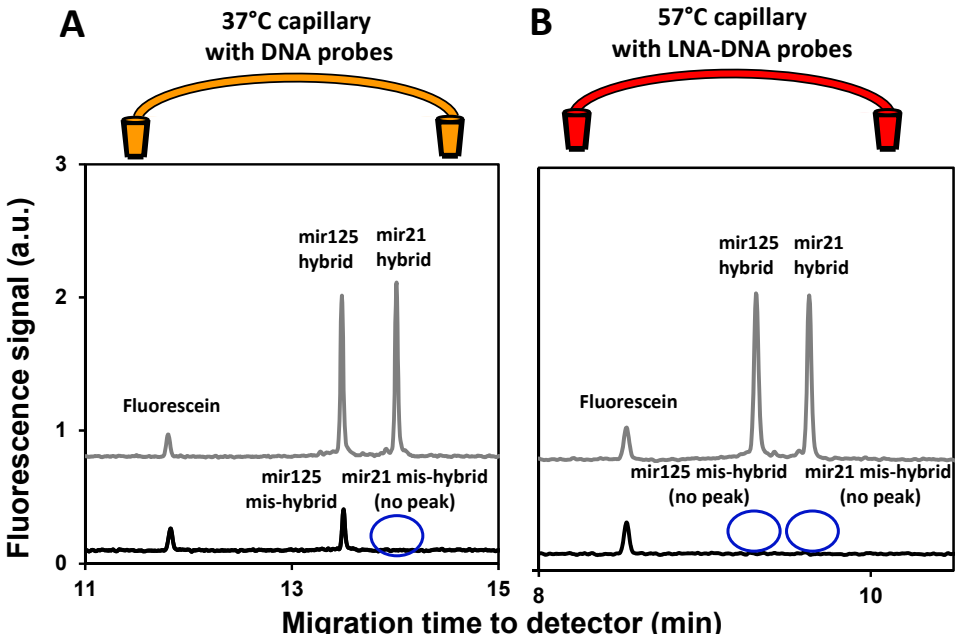

Figure 5.2. 1-nt specificity of two miRNA-specific probes consisting of DNA **(A)** or DNA-LNA **(B)**. **Panel A**: Two DNA-only probes were incubated with 5 nM of the two respective miRNAs, mir21 and mir125b (grey trace) or 50 nM of the 1-nt mismatches (1-nt) of the two miRNAs (black trace) at 37°C. 1-nt specificity of multiple miRNAs was not achieved as seen by presence of the mir125b mis-hybrid peak. 37°C was the optimum temperature for mir21 specificity. **Panel B**: Two DNA-LNA probes were incubated with 5 nM of the two respective miRNAs, mir21 and mir125b (grey trace) or 50 nM of the 1-nt mismatches of the two miRNAs (black trace) at 57°C. Inclusion of LNA bases allowed for 1-nt specificity as seen by the absence of the mis-hybrid for both mir125 and mir21 probes. 57°C was the optimum temperature for both mir21 and mir125b with their respective LNA-DNA probes. Blue circles indicate where peaks would appear if present.

(**Fig. 5.2A**). With the LNA-DNA probes, when the capillary was set at 57°C, I was able to differentiate both miRNAs from their respective mismatches, even with the mismatches at a concentration 10 times higher than that of the miRNAs (**Fig. 5.2B)**. This confirmed that equalizing the melting temperature is vital for specificity of analysis of multiple miRNAs. Though the use of a melting temperature of 83°C and a hybridization temperature of 57°C gave successful results, I do not imply that these specific temperatures are universal or optimal. Lowering the melting temperature (by incorporating fewer LNA bases in the DNA probe) may potentially be beneficial as this can improve SSB binding and reduce peak broadening. Lowering the melting temperature should not raise any major issues, as all mismatch hybrids should theoretically have lower melting temperatures than the target miRNA hybrids. The one caveat (regardless of the set melting temperature) is that 1-nt mismatch binding can vary, depending on its sequence and location of the mismatch, making it difficult to determine accurately how close the melting temperature of its hybrid is to that of the target miRNAs. As such, 1-nt specificity must be tested for each new set of target miRNAs.

Placing LNA bases at the location of known mismatches (such as close family members) can help increase the difference in melting temperature between the target miRNAs and its respective mismatch.**[96]** This makes it possible to achieve 1-nt specificity regardless of mismatch location.**[90, 97]** Thus, for future work we suggest specifically locating LNA bases to the location of known 1-nt mismatches.

5.3.3. Specificity of Multiple miRNAs Using Dual-Temperature Technique

The next step was to determine whether I could differentiate 5 different miRNA hybrids from their respective 1-nt mis-hybrids, using the LNA-DNA probes and the capillary temperature of 57°C. To allow sufficient separation of the 5 hybrid peaks I required the use of peptide drag tags with lengths of 0, 5, 10, 15, and 20 amino acids, described in **chapter 3.1**.**[98]** Similar to our experiments with 2 miRNAs (**Fig. 5.2B**), I successfully differentiated all 5 miRNAs from their mismatches. All 5 miRNA peaks were present, while no mismatch peaks were observed (**Fig. 5.3A**). This showed that the 57°C hybridization temperature was optimal for all 5 probe-miRNA hybrids. This achievement was accompanied, however, by a significant loss in resolution, with very little separation between the hybrid peaks and the excess LNA-DNA probes. The loss of resolution was expected as increased capillary temperatures caused peak broadening.**[95]** Also, a worsening of SSB binding was apparent, with the shift of the LNA-DNA probes back towards the hybrid peaks. I needed to resolve this issue as the lack of separation limits the number of detectable miRNAs and makes it difficult to accurately quantitate the peak areas of each of the hybrids. I hypothesized that the 57°C dissociation temperature is required only in the beginning of separation to minimally separate the hybrids from the excess probes to prevent re-association of the probes with mismatches. This initial separation is possible due to residual binding of SSB to the probes even at this high temperature. Based on the velocities of the hybrids and the SSB-bound probes, I calculated that there is sufficient separation between the RNA and SSB-bound LNA-DNA probes to prevent re-association after 2 min under the separation conditions. Thus, if I maintained the capillary temperature at 57°C for the first 2 min, the capillary temperature could

be reduced to 20°C for the rest of separation to facilitate full-strength SSB binding and hybrid separation. Thus, for dual-temperature DQAMmiR the capillary was set at 57°C for the first 2 min after injection of the sample. The voltage was then shut off, and the capillary was allowed to

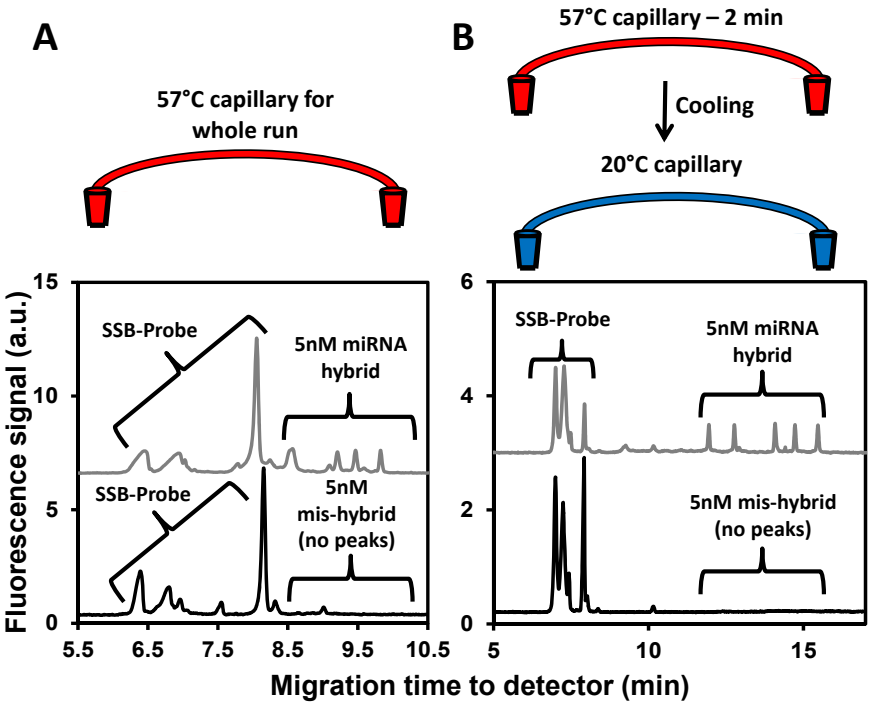

Figure 5.3: Separation and detection of 5 miRNA-probe hybrid peaks with a 57°C capillary **(A)** and by using the dual temperature technique **(B)**. **Panel A:** With a capillary at 57°C, 5 LNA-DNA probes were incubated with their respective miRNAs (grey trace) or with 1-nt mismatches of the 5 miRNAs (black trace). 1-nt specificity was achieved for all 5 miRNAs as observed by the absence of 1-nt mis-hybrid peaks. Though specificity was achieved, 57°C caused a loss of resolution and a lack of SSB-probe binding, preventing the separation and detection of all 5 miRNA hybrids. **Panel B:** Using a dual temperature technique, 5 LNA-DNA probes were incubated with their respective miRNAs (grey trace) or with 1-nt mismatches of the 5 miRNAs (black trace). The capillary was set at 57°C for the first 2 min of the run to allow 1-nt specificity. The capillary is then cooled down to 20°C to allow proper SSB-binding and separation of the 5 hybrid peaks. Using the dual-temperature technique the separation of all 5 hybrid peaks is observed while 1-nt specificity is maintained.

cool down to 20°C (which takes 7 min). Once the capillary temperature reached 20°C the voltage was reapplied and the run continued until the samples passed the detector. With this dual-temperature technique I was able to achieve a resolution sufficient for the detection of 5 miRNA hybrids, while still maintaining 1-nt specificity (**Fig. 5.3B**).

5.3.4. 1-nt Specificity of Multiple miRNAs with Inclusion of ITP

The final step was to ensure that I could still achieve 1-nt specificity and sufficient hybrid separation with in-capillary pre-concentration of the sample with ITP. A very long plug of the hybridization mixture was injected into a 20°C capillary from the outlet end. As described in **chapter 4**, the components of the hybridization mixture were focused at the interface between a high conductivity LE and a low conductivity TE, increasing the local sample concentration by two orders of magnitude.**[92]** A voltage was applied in the reverse direction (negative electrode at the injection end). The voltage was turned off at t_{cr} – 10 s, where t_{cr} is the predetermined "critical time-point" explained in chapter 4 and the capillary was allowed to heat up to 57°C (which takes 8 min). The inlet and outlet ends of the capillary were placed in vials with LE supplemented with 100 nM SSB and an electric field was applied in the forward direction (positive electrode at the injection end) for 2 min at 57°C. The voltage was then shut off, and the capillary was allowed to cool down to 20°C within 7 min. Once the capillary temperature reached 20°C the voltage was reapplied and the run continued until the electrophoretic zones of all miRNA-probe hybrids passed the detector.

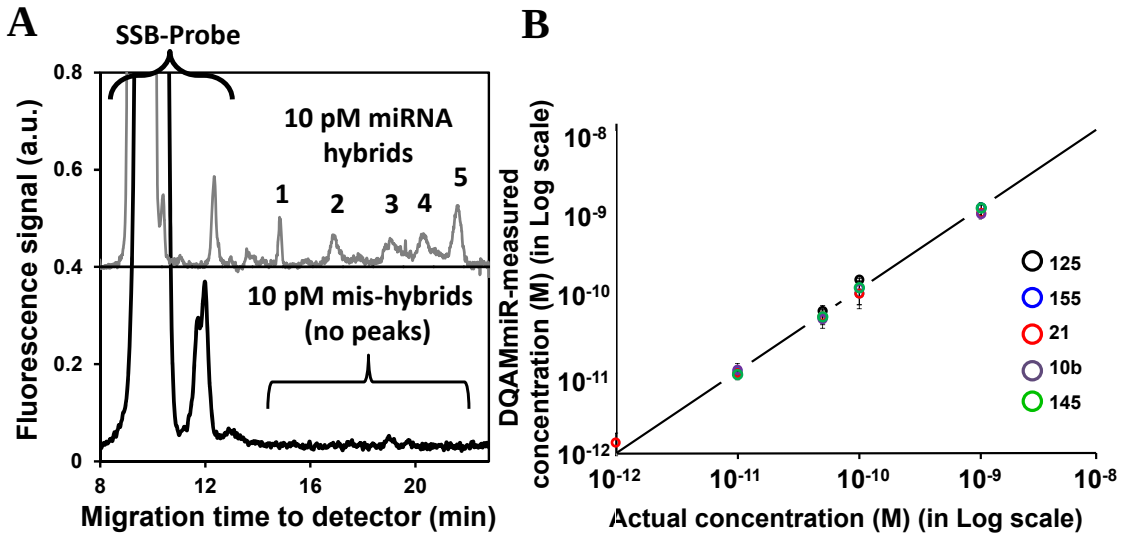

Figure 5.4: Applying dual-temperature technique to DQAMmiR with ITP pre-concentration. **Panel A**: Detection of either 10 pM of 5 miRNAs (grey trace) or 10 pM of their respective 1-nt mismatches using the ITP-DQAMmiR tandem. Labels 1 – 5 indicate the 5 hybrid peaks from left to right corresponding to mir10b, mir155, mir145, mir125b, and mir21. **Panel B:** Quantitation of the 5 respective miRNAs over a range of concentrations from 1 pM to 1 nM.

The introduction of the dual-temperature technique did not interfere with ITP's ability to pre-concentrate our samples. Furthermore, having the capillary temperature at the required hybridization temperature allowed me to incubate the sample inside the capillary after ITP. This reduced the overall assay time as the increase in concentration of the sample significantly reduced the required incubation time.**[99]** I performed ITP-DQAMmiR with the dual temperature technique, allowing for the separation and detection of 5 hybrids at the low pM concentrations (**Fig. 5.4A**). Thus, I achieved 1-nt specificity of multiple miRNAs while maintaining high quality separation and low LOD. It should be noted that ITP in its nature is very sensitive to its buffer composition. Even slight changes in buffer concentration, pH or temperature can significantly affect the result. Optimization of all buffers is required with any parameter changes including

temperature, voltage, and sample concentration. With this in mind, I was still able to use this technique over multiple days with multiple users and achieved reproducible results over a range of concentrations (**Fig. 5.4B**).

5.4. Conclusions

In conclusion, I successfully achieved 1-nt specificity while detecting multiple miRNAs simultaneously with the DQAMmiR method. LNA bases were introduced into the DNA probes to equalize the respective hybrid's melting temperatures. At a temperature of 57°C all 5 miRNAs were able to bind to their respective probes while the 1-nt mismatches could not. The use of the dual-temperature technique allowed me to achieve proper resolution of hybrid peaks while maintaining 1-nt specificity. This technique works with the recently introduced ITP-DQAMmiR combination, allowing me to have both great specificity and a great LOD in a single run. 1-nt specificity of multiple miRNAs was the final hurdle for the use of DQAMmiR in a clinical setting. DQAMmiR is now ready to be used for the analysis of miRNA fingerprints from real clinical samples.

LIMITATIONS

The most significant limitation for DQAMmiR still remains to be its LOD. Though I was able to lower the LOD down to 1 pM using ITP, DQAMmiR cannot detect low abundance miRNAs when working with biological samples. Fortunately, the detection of hundreds of miRNAs (in relative abundances) with microarrays has given me a wide selection of target miRNAs to choose from. Thus, when selecting miRNA fingerprints, I can choose higher abundance miRNAs. The selection of high abundance miRNAs may not, however, always be an option and this still does not solve the problem of LOD. It will especially be a challenge working with blood samples as the majority of circulating miRNAs are quite low in abundance.

One of my goals for DQAMmiR is to detect miRNAs directly from cell lysate, which I cannot currently do when using ITP. ITP requires the sample to be as "pure" as possible so the detection of miRNAs from biological samples requires RNA extraction prior to analysis. Even with the use of an RNA extract, it took a significant amount of time to optimize the conditions to achieve reproducible results. ITP is very sensitive to changes in the experimental parameters with even minor changes to pH, buffer concentration and capillary length significantly affecting the results, reducing the quantitative accuracy of the method. In the long term future of DQAMmiR, it would simplify the protocol if ITP was not required. The Krylov lab is currently working on the development of an in-house CE detection set-up designed to reduce the limit of detection down to hundreds of miRNA copies. The incorporation of such an instrument would allow DQAMmiR to analyse low abundance miRNAs without the need for ITP.

Another limitation for DQAMmiR is related to the design and conjugation of drag tags longer than 20 aa in length. Canpeptide had a difficult time creating the 20 aa peptide drag tag because it was difficult to solubilize in water. This was due to the lack of charge in any of the amino acids (repeats of Gly, Ser, Thr), creating a lengthy, neutral, hydrophobic molecule. This hinders the development of peptides greater than 20 aa in length when using this sequence. Thus, if I want to detect greater than 5 miRNAs I need to design new peptides that do not just contain neutral amino acids. The addition of negatively and positively charged amino acids can resolve the solubility issue, however their inclusion may create some other problems. Having too many negatively-charged amino acids may prevent proper separation between hybrids as there will be a lack of difference in size to charge ratio between the probes. The bigger issue may be with the addition of positively-charged amino acids as they could potentially stick to the capillary walls, preventing proper migration through the capillary. Careful consideration would need to be taken when choosing the next set of repeating amino acids to prevent such issues from occurring.

CONCLUDING REMARKS

The following major parameters are used to characterize the use of a miRNAs detection method in a clinical setting: analysis time, number of miRNAs analyzed simultaneously, specificity, LOD, accuracy, and tolerance to biological matrices. With no sample processing involved, the analysis time for DQAMmiR is limited by hybridization and separation times only. In the proof of principle work I used a hybridization time of 60 min. I reduced the hybridization time down to 10 min by optimizing the concentration of the probes. Including separation time the total assay time is now approximately 60 min (30 min without ITP). The resolution between the SSB-bound probes and the hybrids in DQAMmiR roughly suggests that a maximum of approximately 25 miRNAs can be reliably analyzed in a single spectral channel without further optimization of the analysis. The design of suitable drag tags and methods of their conjugation to the probes were crucial for DQAMmiR to reach its maximum number of miRNAs that can be simultaneously analyzed. I developed such drag tags, conjugating repeating peptides of various lengths to the DNA probes, which increased the number of detectable miRNAs to 5. I believe this universal drag tag can be further increased in length (with an optimized peptide sequence) to increase the number of detectable miRNAs to 25. DQAMmiR is now capable of 1-nt differentiation for multiple miRNAs. I introduced LNA bases to normalize the melting temperature of all probe-miRNA hybrids and by increasing the capillary temperature above the melting temperatures of all the mismatched hybrids I achieved 1-nt specificity. A novel dual-temperature technique was developed to maintain the excellent separation to detect and quantitate 5 miRNA hybrids while achieving 1-nt specificity. The LOD of DQAMmiR is

restricted by that of CE with fluorescence detection. Commercially available CE instruments have an LOD of approximately 100 pM. By introducing the pre-concentration technique, ITP, to DQAMmiR, I was able to lower the LOD down to 1 pM while still using a commercially available CE instrument. This LOD should be sufficient for the analysis of the majority of relevant miRNAs.**[100]** I've developed a simple mathematical approach to accurately quantitate multiple miRNAs that takes into account the quantum yields of SSB-bound and target-bound probes. With no modifications to the miRNAs there are no sequence related biases involved with DQAMmiR. The experiments with cell lysate suggest that DQAMmiR is also highly tolerant to impurities in the sample, which makes the method applicable to crude biological samples.

In conclusion, I have developed a miRNAs detection technique that I believe to be a strong candidate for use in a clinical setting. DQAMmiR is now quantitative, specific, fast, capable of detecting multiple miRNAs, has a low LOD and can be used with crude biological samples all within an automated, commercially available instrument. The proof of principle stages are over and the next step is to validate DQAMmiR, allowing its use with real biological samples.

FUTURE PLANS

DQAMmiR continues to be developed in the Krylov lab, with the future focus on comparing and validating DQAMmiR with qRT-PCR. The proper validation will lead to the application of DQAMmiR to real samples with our collaborators here at York University and at Sunnybrook hospital.

In order to validate the capability of DQAMmiR for practical analysis, we are planning a comparative study with qRT-PCR, the "gold standard" of miRNAs detection for biological samples. This study will be done for two purposes, the first being to validate our method, comparing the analysis of miRNAs between DQAMmiR and qRT-PCR under optimum conditions for qRT-PCR. We would like to show that our numbers are comparable to qRT-PCR when we are analyzing a synthetic miRNAs in a pure buffer solution or a total RNA extract (as RNA extraction is a common step required for qRT-PCR analysis of real samples). The second purpose of this study is to compare the two methods when analyzing miRNAs in more "crude" biological samples, meaning detecting miRNAs directly from sample tissue and blood samples without the use of any RNA extraction kits. Experimentally, we will spike a known concentration of a synthetic miRNA target into five different matrices, including buffer solution, tRNA library, total RNA extraction, cell lysate and blood samples. We are expecting the results to show that both DQAMmiR and qRT-PCR exhibit excellent ability for miRNAs quantification under simple matrices, such as buffer solution, tRNA library, and total RNA extraction. We also expect to see that qRT-PCR will be significantly affected by the cell lysate and blood samples while DQAMmiR will retain its excellent performance. The conclusion should be that both DQAMmiR

and qRT-PCR are effective methods for miRNAs analysis using relatively pure miRNAs samples, however DQAMmiR is much more reliable when working with more complex samples. This will show that with DQAMmiR we can skip the extraction step, reducing assay time and removing any potential biases and sample loss involved. We are currently in discussion with the Chun Peng lab here at York University to use DQAMmiR to analyze specific miRNA targets in placental tissues. We are also planning on analyzing miRNAs from patient-derived tissue samples from the Yousef lab at Sunnybrook Hospital. We will compare normal Renal Cells to both clear cell Renal Cell Carcinoma and papillary Renal Cell Carcinoma showing that DQAMmiR can be used for the analysis of cancer subtype-specific fingerprints from real tissue samples.

LIST OF PUBLICATIONS

1) **Wegman, D.W**.; Ghasemi, F.; Stasheuski, A.S.; Khorshidi, A.; Yang, B.B.; Liu, S.K.; Yousef, G.M.; Krylov, S.N. Achieving single-nucleotide specificity in direct quantitative analysis of multiple microRNAs (DQAMmiR). *Analytical Chemistry* **2016**, *88*, 2472 – 2477.

2) **Wegman, D.W**.; Ghasemi, F.; Khorshidi, A.; Yang, B.B.; Liu, S.K.; Yousef, G.M.; Krylov, S.N. Highly-sensitive amplification-free analysis of multiple miRNAs by combining capillary isotachophoresis and electrophoresis. *Analytical Chemistry* **2015**, 87, 1404 – 1410.

3) Ghasemi, F.; **Wegman, D.W**.; Kanoatov, M.; Yang, B.B.; Liu, S.K.; Yousef, G.M.; Krylov, S.N. Improvements to direct quantitative analysis of multiple microRNAs facilitating faster analysis. *Analytical Chemistry* **2013**, 85, 10062 – 10066.

4) **Wegman, D.W**.; Cherney, L.T; Yousef, G.; Krylov, S.N. Universal drag tag for direct quantitative analysis of multiple microRNAs. *Analytical Chemistry* **2013**, 85, 6518 – 6523.

5) **Wegman, D.W**.; Krylov, S.N. Direct miRNA-hybridization assays and their potential in diagnostics. *Trends in Analytical Chemistry* **2013**, 44, 121 – 130.

6) Mazouchi, A.; Dodgson, B.J.; **Wegman, D.W**.; Krylov, S.N.; Gradinaru, C.C. Ultrasensitive on-column laser-induced fluorescence in capillary electrophoresis using multiparameter confocal detection. *Analyst* **2012**, 137, 5538 – 5545.

7) Dodgson, B.J.; Mazouchi, A.; **Wegman, D.W**.; Gradinaru, C.C.; Krylov, S.N. Detection of a thousand copies of miRNA without enrichment or modification. *Analytical Chemistry* **2012**, 84, 5470 – 5474.

8) Woon, E.C.Y.; Demetriades, M.; Bagg, E.A.L.; Aik, W.S.; Krylova, S.M.; Ma, J.H.Y.; Chan, M.C.; Walport, L.J.; **Wegman, D.W**.; Dack, K.N.; McDonough, M.A.; Krylov, S.N.; Schofield, C.J. Dynamic combinatorial mass spectrometry leads to inhibitors of a 2-oxoglutarate dependent nucleic acid demethylase. *Journal of Medicinal Chemistry* **2012**, 55, 2173 – 2184.

9) **Wegman, D.W**.; Krylov, S.N. Direct quantitative analysis of multiple miRNAs (DQAMmiR). *Angewandte Chemie International Edition* **2011**, 50, 10335 – 10339.

10) Krylova, S.M.; **Wegman, D.W**.; Krylov, S.N. Making DNA hybridization assays in capillary electrophoresis quantitative. *Analytical Chemistry* **2010**, 82, 4428 – 4433.

REFERENCES

1. Lee, R. C.; Feinbaum, R. L.; Ambros, V., The C. elegans heterochronic gene lin-4 encodes small RNAs with antisense complementarity to lin-14. *Cell* **1993,** 75, (5), 843-854.
2. Friedman, R. C.; Farh, K. K.-H.; Burge, C. B.; Bartel, D. P., Most mammalian mRNAs are conserved targets of microRNAs. *Genome Research* **2009,** 19, (1), 92-105.
3. Hsu, P. W. C.; Huang, H.-D.; Hsu, S.-D.; Lin, L.-Z.; Tsou, A.-P.; Tseng, C.-P.; Stadler, P. F.; Washietl, S.; Hofacker, I. L., miRNAMap: genomic maps of microRNA genes and their target genes in mammalian genomes. *Nucleic Acids Research* **2006,** 34, (suppl 1), D135-D139.
4. Yates, Luke A.; Norbury, Chris J.; Gilbert, Robert J. C., The Long and Short of MicroRNA. *Cell* **2013,** 153, (3), 516-519.
5. Helwak, A.; Kudla, G.; Dudnakova, T.; Tollervey, D., Mapping the Human miRNA Interactome by CLASH Reveals Frequent Noncanonical Binding. *Cell* **2013,** 153, (3), 654-665.
6. Buscaglia, L. E. B.; Li, Y., Apoptosis and the target genes of microRNA-21. *Chinese Journal of Cancer* **2011,** 30, (6), 371-380.
7. Papagiannakopoulos, T.; Shapiro, A.; Kosik, K. S., MicroRNA-21 Targets a Network of Key Tumor-Suppressive Pathways in Glioblastoma Cells. *Cancer Research* **2008,** 68, (19), 8164-8172.
8. Lee, I.; Ajay, S. S.; Yook, J. I.; Kim, H. S.; Hong, S. H.; Kim, N. H.; Dhanasekaran, S. M.; Chinnaiyan, A. M.; Athey, B. D., New class of microRNA targets containing simultaneous 5′-UTR and 3′-UTR interaction sites. *Genome Research* **2009,** 19, (7), 1175-1183.
9. Place, R. F.; Li, L.-C.; Pookot, D.; Noonan, E. J.; Dahiya, R., MicroRNA-373 induces expression of genes with complementary promoter sequences. *Proceedings of the National Academy of Sciences* **2008,** 105, (5), 1608-1613.
10. Qin, W.; Shi, Y.; Zhao, B.; Yao, C.; Jin, L.; Ma, J.; Jin, Y., miR-24 Regulates Apoptosis by Targeting the Open Reading Frame (ORF) Region of FAF1 in Cancer Cells. *PLoS ONE* **2010,** 5, (2), e9429.
11. Aguda, B. D.; Kim, Y.; Piper-Hunter, M. G.; Friedman, A.; Marsh, C. B., MicroRNA regulation of a cancer network: Consequences of the feedback loops involving miR-17-92, E2F, and Myc. *Proceedings of the National Academy of Sciences* **2008,** 105, (50), 19678-19683.
12. Suh, M.-R.; Lee, Y.; Kim, J. Y.; Kim, S.-K.; Moon, S.-H.; Lee, J. Y.; Cha, K.-Y.; Chung, H. M.; Yoon, H. S.; Moon, S. Y.; Kim, V. N.; Kim, K.-S., Human embryonic stem cells express a unique set of microRNAs. *Developmental Biology* **2004,** 270, (2), 488-498.
13. Liang, Y.; Ridzon, D.; Wong, L.; Chen, C., Characterization of microRNA expression profiles in normal human tissues. *BMC Genomics* **2007,** 8, (1), 166.

14. Xu, P.; Vernooy, S. Y.; Guo, M.; Hay, B. A., The Drosophila MicroRNA Mir-14 Suppresses Cell Death and Is Required for Normal Fat Metabolism. *Current Biology* **2003,** 13, (9), 790-795.
15. Hatfield, S. D.; Shcherbata, H. R.; Fischer, K. A.; Nakahara, K.; Carthew, R. W.; Ruohola-Baker, H., Stem cell division is regulated by the microRNA pathway. *Nature* **2005,** 435, (7044), 974-978.
16. Visone, R.; Rassenti, L. Z.; Veronese, A.; Taccioli, C.; Costinean, S.; Aguda, B. D.; Volinia, S.; Ferracin, M.; Palatini, J.; Balatti, V.; Alder, H.; Negrini, M.; Kipps, T. J.; Croce, C. M., Karyotype-specific microRNA signature in chronic lymphocytic leukemia. *Blood* **2009,** 114, (18), 3872-3879.
17. Calin, G. A.; Dumitru, C. D.; Shimizu, M.; Bichi, R.; Zupo, S.; Noch, E.; Aldler, H.; Rattan, S.; Keating, M.; Rai, K.; Rassenti, L.; Kipps, T.; Negrini, M.; Bullrich, F.; Croce, C. M., Frequent deletions and down-regulation of micro- RNA genes miR15 and miR16 at 13q14 in chronic lymphocytic leukemia. *Proceedings of the National Academy of Sciences of the United States of America* **2002,** 99, (24), 15524-15529.
18. Iorio, M. V.; Ferracin, M.; Liu, C.-G.; Veronese, A.; Spizzo, R.; Sabbioni, S.; Magri, E.; Pedriali, M.; Fabbri, M.; Campiglio, M.; Menard, S.; Palazzo, J. P.; Rosenberg, A.; Musiani, P.; Volinia, S.; Nenci, I.; Calin, G. A.; Querzoli, P.; Negrini, M.; Croce, C. M., MicroRNA Gene Expression Deregulation in Human Breast Cancer. *Cancer Res* **2005,** 65, (16), 7065-7070.
19. Lu, J.; Getz, G.; Miska, E. A.; Alvarez-Saavedra, E.; Lamb, J.; Peck, D.; Sweet-Cordero, A.; Ebert, B. L.; Mak, R. H.; Ferrando, A. A.; Downing, J. R.; Jacks, T.; Horvitz, H. R.; Golub, T. R., MicroRNA expression profiles classify human cancers. *Nature* **2005,** 435, (7043), 834-838.
20. Yanaihara, N.; Caplen, N.; Bowman, E.; Seike, M.; Kumamoto, K.; Yi, M.; Stephens, R. M.; Okamoto, A.; Yokota, J.; Tanaka, T.; Calin, G. A.; Liu, C.-G.; Croce, C. M.; Harris, C. C., Unique microRNA molecular profiles in lung cancer diagnosis and prognosis. *Cancer Cell* **2006,** 9, (3), 189-198.
21. McDermott, A. M.; Miller, N.; Wall, D.; Martyn, L. M.; Ball, G.; Sweeney, K. J.; Kerin, M. J., Identification and Validation of Oncologic miRNA Biomarkers for Luminal A-like Breast Cancer. *PLoS ONE* **2014,** 9, (1), e87032.
22. Mar-Aguilar, F.; Luna-Aguirre, C. M.; Moreno-Rocha, J. C.; Araiza-ChÁVez, J.; Trevino, V.; RodrÍGuez-Padilla, C.; ResÉNdez-PÉRez, D., Differential expression of miR-21, miR-125b and miR-191 in breast cancer tissue. *Asia-Pacific Journal of Clinical Oncology* **2013,** 9, (1), 53-59.
23. Srinivasan, M.; Sedmak, D.; Jewell, S., Effect of Fixatives and Tissue Processing on the Content and Integrity of Nucleic Acids. *The American Journal of Pathology* **2002,** 161, (6), 1961-1971.
24. Wester, K.; Wahlund, E.; Sundström, C.; Ranefall, P.; Bengtsson, E.; Russell, P. J.; Ow, K. T.; Malmström, P.-U.; Busch, C., Paraffin Section Storage and Immunohistochemistry: Effects of Time, Temperature, Fixation, and Retrieval Protocol

with Emphasis on p53 Protein and MIB1 Antigen. *Applied Immunohistochemistry & Molecular Morphology* **2000,** 8, (1), 61-70.
25. Chung, J.-Y.; Braunschweig, T.; Williams, R.; Guerrero, N.; Hoffmann, K. M.; Kwon, M.; Song, Y. K.; Libutti, S. K.; Hewitt, S. M., Factors in Tissue Handling and Processing That Impact RNA Obtained From Formalin-fixed, Paraffin-embedded Tissue. *Journal of Histochemistry and Cytochemistry* **2008,** 56, (11), 1033-1042.
26. Xi, Y.; Nakajima, G.; Gavin, E.; Morris, C. G.; Kudo, K.; Hayashi, K.; Ju, J., Systematic analysis of microRNA expression of RNA extracted from fresh frozen and formalin-fixed paraffin-embedded samples. *RNA* **2007,** 13, (10), 1668-1674.
27. Varnholt, H.; Drebber, U.; Schulze, F.; Wedemeyer, I.; Schirmacher, P.; Dienes, H.-P.; Odenthal, M., MicroRNA gene expression profile of hepatitis C virus–associated hepatocellular carcinoma. *Hepatology* **2008,** 47, (4), 1223-1232.
28. Mitchell, P. S.; Parkin, R. K.; Kroh, E. M.; Fritz, B. R.; Wyman, S. K.; Pogosova-Agadjanyan, E. L.; Peterson, A.; Noteboom, J.; O'Briant, K. C.; Allen, A.; Lin, D. W.; Urban, N.; Drescher, C. W.; Knudsen, B. S.; Stirewalt, D. L.; Gentleman, R.; Vessella, R. L.; Nelson, P. S.; Martin, D. B.; Tewari, M., Circulating microRNAs as stable blood-based markers for cancer detection. *Proceedings of the National Academy of Sciences* **2008,** 105, (30), 10513-10518.
29. Chen, X.; Ba, Y.; Ma, L.; Cai, X.; Yin, Y.; Wang, K.; Guo, J.; Zhang, Y.; Chen, J.; Guo, X.; Li, Q.; Li, X.; Wang, W.; Zhang, Y.; Wang, J.; Jiang, X.; Xiang, Y.; Xu, C.; Zheng, P.; Zhang, J.; Li, R.; Zhang, H.; Shang, X.; Gong, T.; Ning, G.; Wang, J.; Zen, K.; Zhang, J.; Zhang, C.-Y., Characterization of microRNAs in serum: a novel class of biomarkers for diagnosis of cancer and other diseases. *Cell Res* 18, (10), 997-1006.
30. Liu, J.; Gao, J.; Du, Y.; Li, Z.; Ren, Y.; Gu, J.; Wang, X.; Gong, Y.; Wang, W.; Kong, X., Combination of plasma microRNAs with serum CA19-9 for early detection of pancreatic cancer. *International Journal of Cancer* **2012,** 131, (3), 683-691.
31. Ohtsuka, E.; Nishikawa, S.; Fukumoto, R.; Tanaka, S.; Markham, A. F.; Ikehara, M.; Sugiura, M., Joining of Synthetic Ribotrinucleotides with Defined Sequences Catalyzed by T4 RNA Ligase. *European Journal of Biochemistry* **1977,** 81, (2), 285-291.
32. McLaughlin, L. W.; Romaniuk, E.; Romaniuk, P. J.; Neilson, T., The Effect of Acceptor Oligoribonucleotide Sequence on the T4 RNA Ligase Reaction. *European Journal of Biochemistry* **1982,** 125, (3), 639-643.
33. Weiss, E. A.; Gilmartin, G. M.; Nevins, J. R., Poly(A) site efficiency reflects the stability of complex formation involving the downstream element. *EMBO J.* **1991,** 10, (1), 215-219.
34. Liu, C.-G.; Calin, G. A.; Meloon, B.; Gamliel, N.; Sevignani, C.; Ferracin, M.; Dumitru, C. D.; Shimizu, M.; Zupo, S.; Dono, M.; Alder, H.; Bullrich, F.; Negrini, M.; Croce, C. M., An oligonucleotide microchip for genome-wide microRNA profiling in human and mouse tissues. *Proceedings of the National Academy of Sciences of the United States of America* **2004,** 101, (26), 9740-9744.

35. Lao, K.; Xu, N. L.; Yeung, V.; Chen, C.; Livak, K. J.; Straus, N. A., Multiplexing RT-PCR for the detection of multiple miRNA species in small samples. *Biochemical and Biophysical Research Communications* **2006,** 343, (1), 85-89.
36. Morin, R. D.; O'Connor, M. D.; Griffith, M.; Kuchenbauer, F.; Delaney, A.; Prabhu, A.-L.; Zhao, Y.; McDonald, H.; Zeng, T.; Hirst, M.; Eaves, C. J.; Marra, M. A., Application of massively parallel sequencing to microRNA profiling and discovery in human embryonic stem cells. *Genome Research* **2008,** 18, (4), 610-621.
37. Wu, Q.; Wang, C.; Lu, Z.; Guo, L.; Ge, Q., Analysis of serum genome-wide microRNAs for breast cancer detection. *Clinica Chimica Acta* 413, (13â€“14), 1058-1065.
38. Wyman, S. K.; Parkin, R. K.; Mitchell, P. S.; Fritz, B. R.; O'Briant, K.; Godwin, A. K.; Urban, N.; Drescher, C. W.; Knudsen, B. S.; Tewari, M., Repertoire of microRNAs in Epithelial Ovarian Cancer as Determined by Next Generation Sequencing of Small RNA cDNA Libraries. *PLoS ONE* **2009,** 4, (4), e5311.
39. Stoddart, D.; Heron, A. J.; Mikhailova, E.; Maglia, G.; Bayley, H., Single-nucleotide discrimination in immobilized DNA oligonucleotides with a biological nanopore. *Proceedings of the National Academy of Sciences* **2009,** 106, (19), 7702-7707.
40. Manrao, E. A.; Derrington, I. M.; Laszlo, A. H.; Langford, K. W.; Hopper, M. K.; Gillgren, N.; Pavlenok, M.; Niederweis, M.; Gundlach, J. H., Reading DNA at single-nucleotide resolution with a mutant MspA nanopore and phi29 DNA polymerase. *Nat Biotech* 30, (4), 349-353.
41. Driskell, J. D.; Seto, A. G.; Jones, L. P.; Jokela, S.; Dluhy, R. A.; Zhao, Y. P.; Tripp, R. A., Rapid microRNA (miRNA) detection and classification via surface-enhanced Raman spectroscopy (SERS). *Biosensors and Bioelectronics* **2008,** 24, (4), 917-922.
42. Izumi, Y.; Takimura, S.; Yamaguchi, S.; Iida, J.; Bamba, T.; Fukusaki, E., Application of electrospray ionization ion trap/time-of-flight mass spectrometry for chemically-synthesized small RNAs. *Journal of Bioscience and Bioengineering* 113, (3), 412-419.
43. Sforza, S.; Scaravelli, E.; Corradini, R.; Marchelli, R., Unconventional method based on circular dichroism to detect peanut DNA in food by means of a PNA probe and a cyanine dye. *Chirality* **2005,** 17, (9), 515-521.
44. Gao, Z.; Yang, Z., Detection of MicroRNAs Using Electrocatalytic Nanoparticle Tags. *Analytical Chemistry* **2006,** 78, (5), 1470-1477.
45. Yang, H.; Hui, A.; Pampalakis, G.; Soleymani, L.; Liu, F.-F.; Sargent, E. H.; Kelley, S. O., Direct, Electronic MicroRNA Detection for the Rapid Determination of Differential Expression Profiles. *Angewandte Chemie International Edition* **2009,** 48, (45), 8461-8464.
46. Fan, Y.; Chen, X.; Trigg, A. D.; Tung, C.-h.; Kong, J.; Gao, Z., Detection of MicroRNAs Using Target-Guided Formation of Conducting Polymer Nanowires in Nanogaps. *Journal of the American Chemical Society* **2007,** 129, (17), 5437-5443.
47. Zhang, G.-J.; Chua, J. H.; Chee, R.-E.; Agarwal, A.; Wong, S. M., Label-free direct detection of MiRNAs with silicon nanowire biosensors. *Biosensors and Bioelectronics* **2009,** 24, (8), 2504-2508.

48. Baker, M. B.; Bao, G.; Searles, C. D., In vitro quantification of specific microRNA using molecular beacons. *Nucleic Acids Research* 40, (2), e13-e13.
49. Kang, W. J.; Cho, Y. L.; Chae, J. R.; Lee, J. D.; Choi, K.-J.; Kim, S., Molecular beacon-based bioimaging of multiple microRNAs during myogenesis. *Biomaterials* 32, (7), 1915-1922.
50. Paiboonskuwong, K.; Kato, Y., Detection of the mature, but not precursor, RNA using a fluorescent DNA probe. *Nucleic Acids Symposium Series* **2006,** 50, (1), 327-328.
51. Persat, A.; Santiago, J. G., MicroRNA Profiling by Simultaneous Selective Isotachophoresis and Hybridization with Molecular Beacons. *Analytical Chemistry* 83, (6), 2310-2316.
52. Hartig, J. S.; Grune, I.; Najafi-Shoushtari, S. H.; Famulok, M., Sequence-Specific Detection of MicroRNAs by Signal-Amplifying Ribozymes. *Journal of the American Chemical Society* **2004,** 126, (3), 722-723.
53. Neely, L. A.; Patel, S.; Garver, J.; Gallo, M.; Hackett, M.; McLaughlin, S.; Nadel, M.; Harris, J.; Gullans, S.; Rooke, J., A single-molecule method for the quantitation of microRNA gene expression. *Nat Meth* **2006,** 3, (1), 41-46.
54. Yin, B.-C.; Liu, Y.-Q.; Ye, B.-C., One-Step, Multiplexed Fluorescence Detection of microRNAs Based on Duplex-Specific Nuclease Signal Amplification. *Journal of the American Chemical Society* 134, (11), 5064-5067.
55. Varallyay, E.; Burgyan, J.; Havelda, Z., MicroRNA detection by northern blotting using locked nucleic acid probes. *Nat. Protocols* **2008,** 3, (2), 190-196.
56. Kim, S. W.; Li, Z.; Moore, P. S.; Monaghan, A. P.; Chang, Y.; Nichols, M.; John, B., A sensitive non-radioactive northern blot method to detect small RNAs. *Nucleic Acids Research* 38, (7), e98-e98.
57. Yang, W.-J.; Li, X.-B.; Li, Y.-Y.; Zhao, L.-F.; He, W.-L.; Gao, Y.-Q.; Wan, Y.-J.; Xia, W.; Chen, T.; Zheng, H.; Li, M.; Xu, S.-q., Quantification of microRNA by gold nanoparticle probes. *Analytical Biochemistry* **2008,** 376, (2), 183-188.
58. Roy, S.; Soh, J. H.; Gao, Z., A microfluidic-assisted microarray for ultrasensitive detection of miRNA under an optical microscope. *Lab on a Chip* 11, (11), 1886-1894.
59. Wang, Y.; MacLachlan, E.; Nguyen, B. K.; Fu, G.; Peng, C.; Chen, J. I. L., Direct detection of microRNA based on plasmon hybridization of nanoparticle dimers. *Analyst* **2015,** 140, (4), 1140-1148.
60. Wang, Q.; Li, Q.; Yang, X.; Wang, K.; Du, S.; Zhang, H.; Nie, Y., Graphene oxide–gold nanoparticles hybrids-based surface plasmon resonance for sensitive detection of microRNA. *Biosensors and Bioelectronics* **2016,** 77, 1001-1007.
61. Joshi, G. K.; Deitz-McElyea, S.; Liyanage, T.; Lawrence, K.; Mali, S.; Sardar, R.; Korc, M., Label-Free Nanoplasmonic-Based Short Noncoding RNA Sensing at Attomolar Concentrations Allows for Quantitative and Highly Specific Assay of MicroRNA-10b in Biological Fluids and Circulating Exosomes. *ACS Nano* **2015,** 9, (11), 11075-11089.
62. Chang, P.-L.; Chang, Y.-S.; Chen, J.-H.; Chen, S.-J.; Chen, H.-C., Analysis of BART7 MicroRNA from Epstein−Barr Virus-Infected Nasopharyngeal Carcinoma Cells by Capillary Electrophoresis. *Analytical Chemistry* **2008,** 80, (22), 8554-8560.

63. Khan, N.; Cheng, J.; Pezacki, J. P.; Berezovski, M. V., Quantitative Analysis of MicroRNA in Blood Serum with Protein-Facilitated Affinity Capillary Electrophoresis. *Analytical Chemistry* 83, (16), 6196-6201.
64. Gazzani, S.; Lawrenson, T.; Woodward, C.; Headon, D.; Sablowski, R., A Link Between mRNA Turnover and RNA Interference in Arabidopsis. *Science* **2004,** 306, (5698), 1046-1048.
65. Schramke, V.; Sheedy, D. M.; Denli, A. M.; Bonila, C.; Ekwall, K.; Hannon, G. J.; Allshire, R. C., RNA-interference-directed chromatin modification coupled to RNA polymerase II transcription. *Nature* **2005,** 435, (7046), 1275-1279.
66. Garcia, V.; García, J. M.; Peña, C.; Silva, J.; Domínguez, G.; Rodríguez, R.; Maximiano, C.; Espinosa, R.; España, P.; Bonilla, F., The GADD45, ZBRK1 and BRCA1 pathway: quantitative analysis of mRNA expression in colon carcinomas. *The Journal of Pathology* **2005,** 206, (1), 92-99.
67. Berezovski, M.; Krylov, S. N., Using DNA-Binding Proteins as an Analytical Tool. *Journal of the American Chemical Society* **2003,** 125, (44), 13451-13454.
68. Al-Mahrouki, A. A.; Krylov, S. N., Calibration-Free Quantitative Analysis of mRNA. *Analytical Chemistry* **2005,** 77, (24), 8027-8030.
69. Li, T.; Zhang, D.; Luo, W.; Lu, M.; Wang, Z.; Song, Y.; Wang, H., Metal Cation Mediated-Capillary Electrophoresis of Nucleic Acids. *Analytical Chemistry* **2010,** 82, (2), 487-490.
70. Dedionisio, L.; Raible, A. M.; Gryaznov, S. M., The detection of oligonucleotide N3′ → P5′ phosphoramidate/RNA duplexes with capillary gel electrophoresis. *Electrophoresis* **1998,** 19, (8-9), 1265-1269.
71. Berezovski, M.; Krylov, S. N., Nonequilibrium Capillary Electrophoresis of Equilibrium Mixtures − A Single Experiment Reveals Equilibrium and Kinetic Parameters of Protein−DNA Interactions. *Journal of the American Chemical Society* **2002,** 124, (46), 13674-13675.
72. Zhang, H.; Li, X.-F.; Le, X. C., Tunable Aptamer Capillary Electrophoresis and Its Application to Protein Analysis. *Journal of the American Chemical Society* **2007,** 130, (1), 34-35.
73. Chow, T.-f. F.; Youssef, Y. M.; Lianidou, E.; Romaschin, A. D.; Honey, R. J.; Stewart, R.; Pace, K. T.; Yousef, G. M., Differential expression profiling of microRNAs and their potential involvement in renal cell carcinoma pathogenesis. *Clinical Biochemistry* **2010,** 43, (1–2), 150-158.
74. Schetter, A. J.; Leung, S. Y.; Sohn, J. J.; Zanetti, K. A.; Bowman, E. D.; Yanaihara, N.; Yuen, S. T.; Chan, T. L.; Kwong, D. L. W.; Au, G. K. H.; Liu, C.-G.; Calin, G. A.; Croce, C. M.; Harris, C. C., MicroRNA Expression Profiles Associated With Prognosis and Therapeutic Outcome in Colon Adenocarcinoma. *JAMA* **2008,** 299, (4), 425-436.
75. Wegman, D. W.; Krylov, S. N., Direct Quantitative Analysis of Multiple miRNAs (DQAMmiR). *Angewandte Chemie International Edition* 50, (44), 10335-10339.

76. Jiang, R.-M.; Chang, Y.-S.; Chen, S.-J.; Chen, J.-H.; Chen, H.-C.; Chang, P.-L., Multiplexed microRNA detection by capillary electrophoresis with laser-induced fluorescence. *Journal of Chromatography A* **2011,** 1218, (18), 2604-2610.
77. Meagher, R. J.; McCormick, L. C.; Haynes, R. D.; Won, J.-I.; Lin, J. S.; Slater, G. W.; Barron, A. E., Free-solution electrophoresis of DNA modified with drag-tags at both ends. *Electrophoresis* **2006,** 27, (9), 1702-1712.
78. Cherney, L. T.; Krylov, S. N., Theoretical estimation of drag tag lengths for direct quantitative analysis of multiple miRNAs (DQAMmiR). *Analyst* 138, (2), 553-558.
79. Dodgson, B. J.; Mazouchi, A.; Wegman, D. W.; Gradinaru, C. C.; Krylov, S. N., Detection of a Thousand Copies of miRNA without Enrichment or Modification. *Analytical Chemistry* 84, (13), 5470-5474.
80. Bahga, S. S.; Han, C. M.; Santiago, J. G., Integration of rapid DNA hybridization and capillary zone electrophoresis using bidirectional isotachophoresis. *Analyst* 138, (1), 87-90.
81. Garcia-Schwarz, G.; Rogacs, A.; Bahga, S. S.; Santiago, J. G., On-chip Isotachophoresis for Separation of Ions and Purification of Nucleic Acids. **2012**, (61), e3890.
82. Bočker, P.; Gebauer, P.; Deml, M., Migration behaviour of the hydrogen ion and its role in isotachophoresis of cations. *Journal of Chromatography A* **1981,** 217, (0), 209-224.
83. Kaniansky, D.; Masár, M.; Marák, J.; Bodor, R., Capillary electrophoresis of inorganic anions1. *Journal of Chromatography A* **1999,** 834, (1–2), 133-178.
84. Rogacs, A.; Marshall, L. A.; Santiago, J. G., Purification of nucleic acids using isotachophoresis. *Journal of Chromatography A* **2014,** 1335, (0), 105-120.
85. Soengas, M. a. S.; Gutiérrez, C.; Salas, M., Helix-destabilizing Activity of φ29 Single-stranded DNA Binding Protein: Effect on the Elongation Rate During Strand Displacement DNA Replication. *Journal of Molecular Biology* **1995,** 253, (4), 517-529.
86. Reinhoud, N. J.; Tjaden, U. R.; van der Greef, J., Automated isotachophoretic analyte focusing for capillary zone electrophoresis in a single capillary using hydrodynamic back-pressure programming. *Journal of Chromatography A* **1993,** 641, (1), 155-162.
87. Tu, J.; Ge, Q.; Wang, S.; Wang, L.; Sun, B.; Yang, Q.; Bai, Y.; Lu, Z., Pair-barcode high-throughput sequencing for large-scale multiplexed sample analysis. *BMC Genomics* **2012,** 13, (1), 43.
88. Wu, Q.; Wang, C.; Lu, Z.; Guo, L.; Ge, Q., Analysis of serum genome-wide microRNAs for breast cancer detection. *Clinica Chimica Acta* **2012,** 413, (13–14), 1058-1065.
89. Kloosterman, W. P.; Wienholds, E.; de Bruijn, E.; Kauppinen, S.; Plasterk, R. H. A., In situ detection of miRNAs in animal embryos using LNA-modified oligonucleotide probes. *Nat Meth* **2006,** 3, (1), 27-29.
90. Castoldi, M.; Schmidt, S.; Benes, V.; Noerholm, M.; Kulozik, A. E.; Hentze, M. W.; Muckenthaler, M. U., A sensitive array for microRNA expression profiling (miChip) based on locked nucleic acids (LNA). *RNA* **2006,** 12, (5), 913-920.
91. Lee, J. M.; Jung, Y., Two-Temperature Hybridization for Microarray Detection of Label-Free MicroRNAs with Attomole Detection and Superior Specificity. *Angewandte Chemie International Edition* **2011,** 50, (52), 12487-12490.

92. Wegman, D. W.; Ghasemi, F.; Khorshidi, A.; Yang, B. B.; Liu, S. K.; Yousef, G. M.; Krylov, S. N., Highly-Sensitive Amplification-Free Analysis of Multiple miRNAs by Capillary Electrophoresis. *Analytical Chemistry* **2015,** 87, (2), 1404-1410.
93. Wang, L.; Yang, C. J.; Medley, C. D.; Benner, S. A.; Tan, W., Locked Nucleic Acid Molecular Beacons. *Journal of the American Chemical Society* **2005,** 127, (45), 15664-15665.
94. Jørgensen, S.; Baker, A.; Møller, S.; Nielsen, B. S., Robust one-day in situ hybridization protocol for detection of microRNAs in paraffin samples using LNA probes. *Methods* **2010,** 52, (4), 375-381.
95. Hjertén, S., Zone broadening in electrophoresis with special reference to high-performance electrophoresis in capillaries: An interplay between theory and practice. *Electrophoresis* **1990,** 11, (9), 665-690.
96. Labib, M.; Khan, N.; Ghobadloo, S. M.; Cheng, J.; Pezacki, J. P.; Berezovski, M. V., Three-Mode Electrochemical Sensing of Ultralow MicroRNA Levels. *Journal of the American Chemical Society* **2013,** 135, (8), 3027-3038.
97. Natsume, T.; Ishikawa, Y.; Dedachi, K.; Tsukamoto, T.; Kurita, N., Effect of base mismatch on the electronic properties of DNA-DNA and LNA-DNA double strands: Density-functional theoretical calculations. *Chemical physics letters* **2007,** 446, (1), 151-158.
98. Wegman, D. W.; Cherney, L. T.; Yousef, G. M.; Krylov, S. N., Universal Drag Tag for Direct Quantitative Analysis of Multiple MicroRNAs. *Analytical Chemistry* **2013,** 85, (13), 6518-6523.
99. Ghasemi, F.; Wegman, D. W.; Kanoatov, M.; Yang, B. B.; Liu, S. K.; Yousef, G. M.; Krylov, S. N., Improvements to Direct Quantitative Analysis of Multiple MicroRNAs Facilitating Faster Analysis. *Analytical Chemistry* **2013,** 85, (21), 10062-10066.
100. Wark, A. W.; Lee, H. J.; Corn, R. M., Multiplexed Detection Methods for Profiling MicroRNA Expression in Biological Samples. *Angewandte Chemie International Edition* **2008,** 47, (4), 644-652.